Collaborateurs humains et robots humanoïdes : contagions motrices et prise en charge de l'ensemble du corps

Ashesh Vasalya

THÈSE

Pour obtenir le grade de

Docteur

Délivrée par **l'Université de Montpellier**

Préparée au sein de l'école doctorale I2S - Information, Structure, Systèmes
Et de l'unité de recherche CNRS-AIST UMI2318/JRL

Spécialité : **SYAM - Systèmes Automatiques et Microélectroniques**

Présentée par : **Ashesh VASALYA**

Human and humanoid robot co-workers: motor contagions and whole-body handover

Soutenue le 6 Décembre 2019 devant le jury composé de

Damien CHABLAT	Directeur de Recherche, CNRS	Rapporteur
Erhan ÖZTOP	Professor, Özyegin University	Rapporteur
Rachid ALAMI	Directeur de Recherche, CNRS	Examinateur (President)
Sébastien COURTOIS	Head Mechatronics, Softbank Robotics Eu	Examinateur
Ganesh GOWRISHANKAR	Chargé de Researcher, CNRS	Codirecteur de thèse
Abderrahmane KHEDDAR	Directeur de Recherche, CNRS	Directeur de thèse

Acknowledgements

Foremost, I would like to express my sincere gratitude to my supervisors Professor Abderrahmane Kheddar, and Dr Gowrishankar Ganesh, for having me offered this opportunity and for their continuous guidance and support throughout this endeavour.

I would like to thank Damien Chablat and Erhan Öztop for taking the time to review this manuscript, and Rachid Alami, Sébastien Courtois for examining this thesis.

I would like to thank Kazuhito Yokoi, Eiichi Yoshida and Ryusuke Sagawa for welcoming me in their laboratory. Sakai Naoko for her precious help with Japanese administration.

I would like to thank Ko Ayusawa, Yumeko Imamura, Yusuke Yoshiyasu, Adrien Escande for their timely assistance throughout my stay at JRL.

I would like to thank Mitsuharu Morisawa, Shuuji Kajita and Kenji Kaneko for their support and assistance during the breakdowns of our favourite robot HRP-2Kai and Pierre Gergondet for software related issues.

I thank my fellow colleagues: Takahiro, Antony, Kai, Kevin, Daphne. My PhD student life in Japan would not have been comfortable without their invaluable assistance.

I would like to thank my family, my cousins and my friends for believing in me and supporting me throughout my life.

Last but not least, I would like to express my deepest love and gratitude to my dear Arisa for her support and everyday motivation for the past three years, without you, my life in Japan would not be pleasant.

Résumé de la thèse

L'interaction homme-robot est un domaine émergent qui couvre plusieurs aspects des sciences humaines et d'ingénierie robotique [45]. Le travail effectué dans cette thèse porte sur les interactions entre l'homme et un robot humanoïde vu comme un collaborateur dans des scénarios plutôt industriels. Dans ce contexte, les études que nous avons menées dans la première partie de cette thèse ont examiné l'influence que peuvent avoir une certaine façon de programmer les tâches d'un robot humanoïde sur le comportement de partenaires humains. Nous avons choisi un paradigme de tâches d'inspiration industrielle : *Pick-n-Place*. Dans le contexte des interactions homme-robot (pHRI), nous avons développé un nouveau framework de transfert d'objets bi-manuel utilisant le contrôle corps complet, et la locomotion d'un robot dans la 2ème partie de cette thèse.

Distinct motor contagions

Lorsqu'un agent humain ou robotique effectue une action suivie de l'observation de cette action par une personne tièrce, des effets comportementaux implicites tels que des *contagions motrices* font que certaines caractéristiques (paramètres cinématiques, but ou résultat) de cette action deviennent semblables à l'action observée. Cependant, des études antérieures sur les contagions motrices ont examiné les effets induits soit pendant l'observation de l'action, soit après, mais jamais ensemble. C'est pourquoi il n'est pas établi si ces effets sont distincts les uns des autres, et en quoi ils sont different.

Dans le chapitre 2, au cours du paradigme de tâche de mouvement répétitif *Pick-n-Place*, nous avons examiné l'effet des contagions motrices induites chez les participants pendant (contagions *en-ligne*) et après (contagions *hors-ligne*). Les mêmes mouvements en question sont effectués soit par une personne ou par un robot humanoïde, le répétiteur par contre est toujours une autre personne. Nous avons examiné en particulier les trois questions suivantes :

1. Les contagions en-ligne et hors-ligne résultant de l'observation d'un même mouvement peuvent-elles affecter différentes caractéristiques de mouvement du participant humain ?

2. Comment les forces des contagions en-ligne et hors-ligne varient-elles selon la nature de l'agent qui les réalise (c.-à-d. s'il s'agit d'un humain ou d'un robot) et leur implication sur la personne qui les observe et les réalise de son côté aussi ?

3. Les contagions en-ligne et hors-ligne sont-elles différentes ou constituent-elles le même effet observé à différents moments ?

Nos résultats et conclusions suggèrent que les contagions *en-ligne* affectent la fréquence de mouvement du participant tandis que les contagions *hors-ligne* affectent leur vitesse de mouvement. De plus, les contagions motrices *hors-ligne* étaient principalement notables après l'observation d'une personne. Les effets des contagions *en-ligne* étaient les mêmes que celles des personnes et des robots humanoïdes. Par conséquent, la contagion *hors-ligne* est peut-être plus sensible à la nature de l'agent observé. Ces deux contagions ont également été observées comme étant sensibles aux caractéristiques comportementales de deux personnes, mais avec les robots, ces contagions motrices n'ont été induites que lorsque les mouvements du robot étaient une copie du mouvement biologique. Enfin, les observations générales faites dans ce chapitre mettent l'accent sur notre hypothèse que des contagions motrices distinctes sont induites chez une personne qui observe une autre personne (contagions *en-ligne* et *hors-ligne*).

Motor contagion influences human co-worker performance

La présence d'un agent humanoïde influence-t-elle la performance des personnes qui l'entourent ? Alors que les études passées ont examiné comment les effets des contagions motrices induites par l'observation des mouvements de l'homme et du robot ont affecté soit la vitesse de mouvement de l'agent humain, soit la variance du mouvement, mais jamais les deux ensemble. Par conséquent, nous soutenons que puisque la précision dans les mouvements avec la vitesse est importante dans la plupart des tâches industrielles, il est nécessaire de considérer à la fois la précision et la vitesse de la tâche pour mesurer précisément la performance dans une tâche.

Dans le Chapitre 3, sous le même paradigme de tâche répétitive et avec l'ajout de quelques conditions supplémentaires, nous avons systématiquement varié le comportement du robot, et observé comment la performance d'un observateur humain est affectée par la présence d'un agent humanoïde. Nous avons également étudié l'effet de la forme physique du robot humanoïde où le torse et la tête étaient couverts, et où seul le bras était visible pour les participants humains. Plus tard, nous avons comparé ces comportements avec ceux d'une personne et examiné comment le comportement observé change avec l'expérience des robots.

Nos résultats suggèrent que la présence d'un agent humanoïde ou d'une personne peut influencer les fréquences de performance des participants humains. Nous avons observé que les participants deviennent plus lents avec un partenaire observé plus lent, mais aussi plus rapide avec un partenaire observé plus rapide. Nous avons également soutenu que le rendement doit être mesuré en considérant la vitesse (ou la fréquence) et l'exactitude des tâches ensemble. Nous avons montré comment la précision du toucher des participants a changé en même temps que les contagions.

Nous avons également étudié les effets de la forme physique, en ajoutant deux conditions dans lesquelles la tête et le torse de l'homme et du robot étaient couverts, et les participants humains ne pouvaient voir que le bras mobile visible

de leur collègue. Nos résultats suggèrent que la présence d'un collègue humanoïde peut affecter la performance humaine, mais seulement lorsque sa forme humanoïde est visible. De plus, cet effet a été supposément accru par le fait que les participants humains avaient déjà fait l'expérience d'un robot. Enfin, nos résultats montrent que la fréquence des tâches humaines, mais non la précision des tâches, est affectée par l'observation d'un robot humanoïde, à condition que la tête et le torse du robot soient visibles et que les mouvements d'inspiration biologique du robot soient réalisés.

Bi-manual and locomotion synchronized bi-directional object handover

Dans le chapitre 4, nous avons conçu un framework pour le transfert d'un objet entre un homme et un robot humanoïde dans un contexte d'interaction physique. Nous avons concentré nos efforts sur l'élaboration d'un framework de transfert simple mais robuste et efficace. Nous avons introduit un transfert bidirectionnel intuitif d'objets entre utilisant le contrôle corps complet en synchronization avec la locomotion. Tout au long de ce chapitre, le problème du transfert bidirectionnel d'objets entre une personne et un humanoïde a été traité avec la perspective d'atteindre un mouvement fluide continu et ponctuel. Au départ, nous avons commencé par concevoir un framework général dans lequel nous avons développé des modèles pour prédire la position de la main humaine convergeant au point de transfert, ainsi que pour estimer la configuration de saisie de l'objet et de la main humaine active pendant le transfert. Nous avons également conçu un modèle pour minimiser les forces d'interaction lors de la phase de remise d'un objet de masse inconnu ainsi que pour minimiser la durée totale de la remise d'un objet. Nous avons conçu ces modèles pour répondre à trois questions importantes liées à la remise d'objet robot humain —**quand** (*timing*), **où** (*position cartesienne*) et **comment** (*orientation et forces d'interaction*) pendant un transfert.

Dans ce framework de transfert, en utilisant le robot humanoïde HRP-2Kai, nous avons d'abord testé et confirmé la faisabilité de ces modèles dans le scénario où les collaborateurs humains et robotiques utilisent toujours leur 'main' droite et gauche respectivement. Par la suite, un framework généralisé a été présenté et testé où les deux collaborateurs ont pu choisir arbitrairement quelle main utiliser. De plus, grâce au contrôleur natif de bas niveau de notre robot HRP-2Kai, nous avons pu étendre notre framework de transfert, ce qui a permis au robot d'utiliser les deux mains (bi-manuel) simultanément pendant le transfert des objets.

De plus, pour un transfert proactif d'un objet entre l'homme et le robot, nous avons pensé qu'il était important d'envisager la possibilité que le robot fasse un pas pour transférer ou échanger un objet avec une personne. Notamment, dans les scénarios où un déplacement sur une courte distance est nécessaire. Nous avons donc exploré toutes les capacités d'un robot humanoïde bipède et ajouté un scénario où le robot doit prendre quelques mesures proactives pour transférer ou

échanger l'objet avec des personnes. Ce scénario a été mis en œuvre sur HRP-2Kai et testé avec différentes taxonomie de transfert.

Conclusion

Pour conclure cette thèse, les résultats que nous avons obtenus ont contribué au domaine des interactions homme-robot humanoïde, notamment lors d'une interaction humain-robot sans contact (HRI) et d'une interaction physique (pHRI) respectivement. Le travail effectué dans cette thèse est d'inspiration industrielle, mais nous pensons qu'il pourrait aussi s'appliquer aux problèmes de services domotiques impliquant un robot humanoïde. Nous avons commencé avec le scénario d'interaction homme-robot non physique basé sur un exemple de tâche d'inspiration industrielle *Pick-n-Place*, puis nous avons avancé vers les interactions physiques homme-robot avec un exemple de transfert d'objet bidirectionnel entre un humanoïde et une personne.

Dans le chapitre 2 and 3, nous avons examiné une tâche industrielle empirique répétitive dans laquelle un participant humain et un robot humanoïde collaborent l'un près de l'autre. Nous avons principalement choisi la tâche cyclique et répétitive *pick-n-place* pour les expériences car nous voulions une tâche qui soit simple mais riche et qui puisse représenter plusieurs scénarios industriels. Nous avons constaté qu'il s'agit d'une des tâches les plus courantes dans les sites de production industriels où les robots sont utilisés. Notez que cette étude n'a pas tenu compte des effets de facteurs tels que l'âge, les caractéristiques physiques ou comportementales du partenaire humain. Ils ont peut-être indirectement affecté ces deux contagions motrices, c'est peut-être un sujet de discussion intéressant et il faudra l'explorer dans des recherches futures.

Dans l'ensemble, les résultats mentionnés et discutés dans les chapitres 2 et 3 mettent en évidence plusieurs nouvelles caractéristiques de contagions motrices, mais ouvrent aussi de nouvelles questions pour des recherches futures. On peut exploiter ces résultats pour personnaliser la conception des robots collaborateurs dans l'industrie et le sport. Si l'éthique le permet, ces contagions pourraient être utilisées pour améliorer la performance de travailleurs humains, et par conséquent, leur productivité.

Enfin, nous concluons le chapitre 4 par un essai préliminaire du framework de transfert complet sous les scénarios mentionnés ci-dessus, y compris la locomotion. Nous confirmons que notre framework bidirectionnel de transfert d'objets est intuitif et adaptable à plusieurs objets aux propriétés physiques distinctes (forme, taille et masse), y compris les outils industriels. Il n'a besoin que des informations sur la forme et la taille de l'objet remis, bien que la connaissance de la masse de l'objet ne soit pas importante au début. Nous avons confirmé la faisabilité de notre framework de transfert sous plusieurs objets dont la masse varie de$[0,17$ à $1,1]$ kg, selon les scénarios mentionnés ci-dessus. Cependant, au cours de plusieurs essais de transfert, nous signalons que la masse calculée de l'objet n'est pas exacte et a une erreur marginale de $\pm 10\%$ par rapport à la masse réelle de l'objet et doit encore être améliorée pour mieux estimer les forces inertielles en jeu ou pour trouver de meilleurs moyens afin de

supprimer les décalages des capteurs de force. Bien que cela n'ait pas affecté le seuil optimal qui est important au moment de la remise de l'objet du robot à une personne.

Bien que dans l'ensemble notre méthode nous permette de ne pas arrêter le mouvement de l'effecteur final tout en étant capable de transférer l'objet (dans les deux sens), si le transfert a lieu alors que les effecteurs finaux humains et robotiques sont en mouvement, ce problème de transfert serait étendu au problème de la collaboration et de la manipulation des objets, qui est déjà largement étudié dans notre groupe de recherche. Nous nous sommes donc concentrés uniquement sur le problème de transfert bidirectionnel proactif et avons donc décidé de réduire la vitesse des effecteurs finaux (${}^{ef}v \simeq 0$) au moment du transfert.

En ajoutant une dimension liée à la locomotion, nous ne nous sommes pas concentrés sur le problème de la planification du mouvement ou de la navigation dans un environnement encombré, mais nous avons plutôt concentré nos efforts pour résoudre et optimiser le problème de transfert d'objets qui exige des efforts partagés immédiats entre la paire homme-robot dans un petit espace où peu de pas sont nécessaires et suffisants pour un transfert réussi des objets. La méthode que nous proposons est simple mais efficace pour tirer profit des robots humanoïdes bipèdes et traiter le problème du transfert bidirectionnel bidirectionnel d'objets en utilisant le contrôle du corps entier et la locomotion du robot.

Abstract

The work done in this thesis is about the interactions between human and humanoid robot HRP-2Kai as co-workers in the industrial scenarios. By interactions, we started with the non-physical human-robot interaction scenario based on an industrially inspired *Pick-n-Place* task example and then advanced towards the physical human-robot interactions with an example of human, humanoid robot dual-arm bi-directional object handover. The research topics in the thesis are divided into two categories. In the context of *non-physical* human-robot interactions, the studies conducted in the 1st part of this thesis are mostly motivated by social interactions between human and humanoid robot co-workers, which deal with the implicit behavioural and cognitive aspects of interactions. While in the context of *physical* human-robot interactions, the 2nd part of this thesis is motivated by the physical manipulations during object handover between human and humanoid robot co-workers in close proximity using humanoid robot whole-body control framework and locomotion.

When an individual (human and robot) performs an action followed by the observation of someone's action, implicit behavioural effects such as motor contagions causes certain features (kinematics parameters, goal or outcome) of that action to become similar to the observed action. However, previous studies have examined the effects of motor contagions induced either during the observation of action or after but never together; therefore, it remains unclear whether and how these effects are distinct from each other.

We designed a paradigm and a repetitive task inspired by the industrial *Pick-n-Place* movement task, in first HRI study, we examine the effect of motor contagions induced in participants during (we call it *on-line* contagions) and after (*off-line* contagions) the observation of the same movements performed by a human, or a humanoid robot co-worker.

The results from this study have suggested that *off-line* contagions affects participant's movement velocity while *on-line* contagions affect their movement frequency. Interestingly, our findings suggest that the nature of the co-worker, (human or a robot), *tend* to influence the *off-line* contagions significantly more than the *on-line* contagions.

Moreover, while the past studies have examined how the effects of induced motor contagions due to the observation of human and robot movements have affected either human co-worker's movement velocity or how it affected movement variance but never both together. Therefore we argue that since precision in movements along with speed is the key in most industrial tasks, hence it is necessary to consider both task accuracy and task speed to measure the performance in a task accurately.

Therefore in second HRI study, under the same paradigm and repetitive industrial task, we systematically varied the robot behaviour and observed

whether and how the performance of a human participant is affected by the presence of the humanoid robot. We also investigated the effect of physical form of humanoid robot co-worker where the torso and head were covered, and only the moving arm was visible to the human participants. Later, we compared these behaviours with a human co-worker and examined how the observed behavioural effects scale with experience of robots.

Our results show that the human and humanoid robot co-workers have been able to affect the performance frequencies of the participants, while their task accuracy remained undisturbed and unaffected. However, with the robot co-worker, this is true only when the robot head and torso were visible, and a robot made biological movements.

Next, in pHRI study, we designed an intuitive bi-directional object handover routine between human and biped humanoid robot co-worker using whole-body control and locomotion, we designed models to predict and estimate the handover position in advance along with estimating the grasp configuration of an object and active human hand during handover trials. We also designed a model to minimize the interaction forces during the handover of an unknown mass object along with the timing of the object handover routine.

We mainly focused on three important key features during the human humanoid robot object handover routine —the *timing*(s) of handover, the *pose* of handover and the *magnitude* of the interaction forces between human hand(s) and humanoid robot end-effector(s). Basically we answer the following questions, —**when**(*timing*), **where** (*position in space*), **how**(*orientation and interaction forces*) of the handover.

Later, we present a generalized handover controller, where both human and the robot is capable of selecting either of their hand to handover and exchange the object. Furthermore, by utilizing a whole-body control configuration, our handover controller is able to allow the robot to use both hands simultaneously during the object handover. Depending upon the shape and size of the object that needs to be transferred.

Finally, we explored the full capabilities of a biped humanoid robot and added a scenario where the robot needs to proactively take few steps in order to handover or exchange the object between its human co-worker. We have tested this scenario on real humanoid robot HRP-2Kai during both when human-robot dyad uses either single or both hands simultaneously.

Keywords: Robotics, Humanoid robot co-worker, Behavior, Robotic behavior, Human performance, Motor contagion, Human-robot interaction, Physical human-robot interaction

Discipline : Systèmes Avancés et Microélectronique

Laboratoire d'Informatique, de Robotique et de Microélectronique de Montpellier
UMR 5506 CNRS/Université de Montpellier
Bâtiment 5 - 860 rue de Saint Priest

Contents

List of Figures

List of Tables

Introduction

Humanoid robots are amazing yet complex systems; therefore, during human-robot interaction, it is crucial to understand what makes the behaviour of humanoid robot human-alike and the sense of trust that comes with it. In today's industry, there is a strong need for collaboration between humans and robots. These robots are required to move around the human co-worker, interact with them, understand their need and collaborate with them if need be either in a close shared workspace or in a large cluttered environment. The core value behind these human-robot interactions is the *safety* of both human and robot co-workers. As suggested by the author *Isaac Asimov* in his 'Three Laws of Robotics'.

1. "Law 1: A robot may not injure a human being or, through inaction, allow a human being to come to harm."

2. "Law 2: A robot must obey the orders given it by human beings except where such orders would conflict with the First Law."

3. "Law 3: A robot must protect its own existence as long as such protection does not conflict with the First or Second Law."

The question that we try to answer here is what kind of behavioural and algorithmic improvements that we could bring for the better acceptance of a humanoid robot in industrial scenarios as co-workers? Whether bringing changes in their appearance or improving their control algorithms would enable them to act more human-alike during an interaction with a human co-worker?

This thesis contributes in the broad field of human-robot interactions (especially with the humanoid robot) both at a safer distance and nearby, namely during a human-robot interaction (HRI) and physical human-robot interaction (pHRI) respectively. The work done in this thesis is about the interactions between human and humanoid robot as co-workers in the industrial scenarios. By interactions, we started with the non-physical human-robot interaction scenario based on an industrially inspired *Pick-n-Place* task example and then advanced towards the

physical human-robot interactions with an example of human-humanoid robot dual-arm bi-directional object handover.

This thesis has two parts. In the context of *non-physical* human-robot interactions, the studies conducted in the 1st part of this thesis are inspired by social interactions between human and humanoid robot co-workers, which deal with the implicit behavioural and cognitive aspects of interactions. While in the context of *physical* human-robot interactions, the 2nd part of this thesis is inspired by the physical manipulations and handover of the object between human and humanoid robot co-workers nearby using robot whole-body control and locomotion.

Thesis Outline : In an empirical industrial co-worker setting, in one HRI study (Chapter 2), we examine the effect of motor contagions induced in participants during and after the observation of the same movements performed by a human, or a humanoid robot co-worker. While in (Chapter 3), we systematically varied the robot behavior and observed whether and how the performance of a human participant is affected by the presence of the humanoid robot. We also investigated the effect of the physical form of humanoid robot co-worker where the torso and head were covered, and only the moving arm was visible to the human participants. Later, we compared these behaviours with a human co-worker and examined how the observed behavioural effects scale with experience of robots. Finally, in the pHRI study (Chapter 4), we designed an intuitive bi-directional object handover framework between a human and a biped humanoid robot co-worker using whole-body control and locomotion. We predicted and estimated the handover position and relative orientation of an object or human hand during a handover and examined the interaction forces during the handover of an unknown mass object along with the overall duration of object handover routine.

Next in Chapter 1, we start with the in-depth review of previous works in the related fields.

Chapter 1

State of the art

Robotic platforms with a floating base and whose overall shape and configuration resemble that of a human body (child or adult) is called humanoid robots. A humanoid robot (such as Russian space robot 'Fedor', 'iCub' from RobotCub, 'Nao' from Aldebaran, Boston Dynamics's 'Atlas' or domestic helper HRP series robots by Kawada industries) generally consists of a head, two arms, a torso and *two legs*.

Humanoid robotics design takes inspiration directly from human capabilities. Previous human-robot interaction studies [27, 54, 97, 101], have shown that the human acceptance of the robot co-worker during a task increases when the robot appears and behaves human-like during an interactive task.

In all of our studies, we used *biped* humanoid robot HRP-2Kai [61] as the robot co-worker who has two arms and two legs, a head and a torso. HRP-2Kai is a life-size biped humanoid robot which is 154 cm tall, has 32 degree-of-freedoms and weighs about 58 kg. It was designed and manufactured by the Kawada Industries, Inc in collaboration with AIST under Humanoid Robotics Project (HRP).

1.1 Human-robot interaction (HRI)

Human-robot interaction is an emerging field which deals with the study and research of interactions between humans and robots. HRI research studies aim to model and design robotic platforms, including improvements of algorithms and control systems based on human partners' expectations during interactions such as remote assistance or collaborative work among co-workers. These interactions can be divided into two general categories depending on the distance between human and robot [45]. Interactions that often carry out at a safer distance and without a need of physical touch (direct or indirect via an object) between humans and robots are termed as *non-physical* HRI, while interactions that often require humans and robots to be in proximity such as during a physical

manipulative event(s) with a goal of achieving a task together, that may involve touch or contact, transfer, assistance or collaborations are termed as *physical* HRI or pHRI. These interactions can also be further distinguished based on the applications that require social interactions [27, 104] or physical manipulations during a task. The studies conducted in the 1st part of this thesis are mostly motivated by social interactions between human and humanoid robot co-workers, which deal with the implicit behavioural and cognitive aspects of interactions. While the 2nd part of this thesis is motivated by the physical manipulations of an object between human and humanoid robot co-workers nearby. Human-robot social interaction is a vast field in itself; therefore we will not be discussing it in detail here, rather our focus lies on one particular behavioural aspect of social interaction, i.e. 'motor contagion'.

1.1.1 Motor contagion

When an individual performs an action followed by the observation of someone's action, implicit behavioural effects such as motor contagions causes certain features (kinematics parameters, goal or outcome) of that action to become similar to the observed action. Past two decades of several studies in sports and psychology have examined and reported various cases of motor contagions in human behaviours, most of which are induced by the observation of other humans and in fact robots as well [10, 14, 28, 32, 35, 43, 46, 52, 88, 94]. Due to increasing usage of robots as co-workers in today's industries, it is of uttermost importance to understand the effects of robots on nearby working human co-workers. In these industrial scenarios where human-robot dyad would eventually share a workspace and possibly collaborate during a task, by understanding how the robot behaviour could affect human behaviour can be proven crucial and beneficial in optimizing and designing robot control to ensure that robot would be perceived well and won't cause harm or disturbance to the human co-workers. While where ethically valid, robots may also be useful to modulate human co-worker behaviour/performance for the productivity of the task.

In our studies, specifically in Chapter 2, we divided motor contagions into two categories depending on *when* they are induced relative to the observation of the action performed. We called motor contagions as *on-line* contagions, that are induced *during* the observation of actions performed by another human or robot

co-worker. One example of *on-line* contagions would be the study performed by [66], where they analyzed human participant movements variance when he/she observed spatially congruent or in-congruent movements made by another human or robot. Their findings suggest that *on-line* contagions are induced only during the observation of human but not with a robot when it made non-biological movements.

While on the other hand, *off-line* contagions effects are induced *after* the observation of action either by human or robot. One example of this kind of contagions would be the study by [13], where they analyzed the change in participant's hand movements velocity in a task performed with and without an object, *after* observing the same movement being performed by a human or a humanoid robot. The results of this study suggest that the participant's hand velocity was subsequently affected after the human and humanoid robot (biological) movement observation.

However, both *on-line* contagions [19, 27, 69, 70, 84, 87] and *off-line* contagions [12, 51, 55, 56, 65, 82] have been largely studied, but in all these previous studies, researchers have focused on either type of motor contagions and never examined or analyzed them together. Hence, it is still unclear, if and how *on-line* and *off-line* motor contagions are different from each other in terms of the human movement behavioral features they affect and the magnitude of these effects.

To address this issue, in Chapter 2, we designed a paradigm inspired by the industrial co-worker setting and examined the differences between the induced *on-line* and *off-line* contagions in participants by the observation of the same movements performed by both human and humanoid robot co-worker. In our empirical repetitive industrial task, we carefully varied the behaviour of the co-worker (human and humanoid robot) and analyzed the induced *on-line* and *off-line* motor contagions in human participant's behaviour.

1.1.2 Motor contagion: a social influencer

While the studies of the human-robot interaction on motor contagions are sparse, the results from them suggest that motor contagions due to observation of robots affect human movement velocity [12, 13, 65, 82], or the human movement variance [19, 69, 70, 87], but latter studies have reported changes in

arguably abstract tasks. Also, former studies which showed changes in movement velocity have not examined how participant movement variance changes with the change in movement velocity. On the other hand, precision in movements along with speed is the key in most industrial tasks; hence it is necessary to consider both task accuracy and task speed (or rather say frequency in case of a repetitive task) to accurately measure the performance in a task. Therefore it is interesting to examine how both of these parameters (speed and variance) of human movements could be affected by observing a humanoid robot co-worker and whether it is possible to quantify the affected *performance* of human co-worker due to motor contagions.

Furthermore, some studies in the past highlight contradictory evidence that robot co-worker physical form does [27] or does not [70] affect the human movement's variance. Though it is unclear regarding the movement speed and hence performance, finally, it remains to be seen whether and how these effect of motor contagions on the task performance are to be modulated due to the prior human experience with robots in general. This issue with performance `Vs` experience could be proven crucial in understanding how the continued exposure of robot co-worker would be on human performance.

We addressed these issues, by further extending our work from Chapter 2 and by exploiting the behavioral effects of motor contagions on human participant's movement speed (frequency) and as well as their task accuracy, after the observation of same movement by a humanoid robot co-worker and report these findings in detail in Chapter 3. We also reported our findings on the effect of the physical form of humanoid robots as well as the magnitude of these effects with human participants prior experience with robots.

1.2 Physical human-robot interaction (pHRI)

Interactions that often require humans and robots to be in close proximity such as during a physical manipulative event(s) to achieve a task together that may involve touch or contact, transfer, assistance or collaborations are considered as *physical* human-robot interactions or just pHRI. As mentioned earlier, 2nd part of this thesis is motivated by the physical manipulations of the object between human and humanoid robot co-workers nearby.

The usage of robots in personal as well as in commercial sectors have evolved significantly in recent years. Moreover, robot working and sharing a workspace with humans as co-workers in these sectors can often lead to opportunities where human and robot have to work together and collaborate within a confined space. One of the most often tasks that occurs during this human-robot collaborative interaction is the handing-over or exchange of an object such as tools in industrial scenarios or a glass of water in personal scenarios from either robot to human or vice-versa. This problem of object handover is a complex collaborative task that occurs seamlessly and effortlessly during the physical interaction between the human dyads, often without any explicit communication. Some well-known object handover examples such as "handing over a glass of water to a patient by the caregiver", "sharing a tool to a mechanic", "handing a business card to a client" and many more are often fundamental in our society. These natural yet simple physical interactive tasks occur flawlessly multiple times between the human dyads daily and under several scenarios in space and time. Although handovers are fluent phase-less natural events between human-human interactions, during the human-robot dyad interactions, the handover of an object is a challenging task and often regarded as unnatural (non-biological) behaviour.

This unnatural behaviour mainly arises due to the lack of responsiveness and unreliability of the robot co-worker, and the safety issues of the human co-worker during the interaction. In the previous human-robot interaction studies [54, 97, 101] and also in our work Chapter 3, we have shown that the human acceptance of the robot co-worker during a task increases when the robot appears and behaves human-like, especially during a collaborative, interactive task. Therefore again in our next study, we primarily chose to consider humanoid robot HRP-2Kai as the robot co-worker. In Chapter 4, we mainly focused on solving the problem of intuitive and proactive bi-directional object handover between human and a biped humanoid robot dyad using robot Whole-Body Control (WBC) [15, 17, 95, 106]. We formulated our handover problem by taking inspiration and insights from the previous works in the field of object handover between human-human and human-robot dyads in general. We will now discuss some of those significant previous research works.

1.2.1 Previous handover studies

Overview: Object handover being the most common interactive task and knowing its significance in daily life; it is evident that object handovers have been widely studied by the researchers both during the interactions of human-human and human-robot dyads. These past studies related to object handovers can be categorized under three main research topics. The prediction and estimation of human motion towards the handover location and concurrent robot motion planning towards that location [53, 67, 71, 73, 74, 105, 112]. To understand and codify the interaction forces that is applied on the object between the dyads during the handover [29, 30, 76, 79, 90]. To effectively minimizing the overall handover duration between the dyads [24, 54, 80, 81].

Studies on handover motion: In order for the human-robot object handovers to be proactively intuitive, the robot must be able to predict and estimate the human motion in advance. Instead of simply waiting for the object to be presented by the human at the handover location, the robot must proactively plan its motion by observing and predicting next human motion and arrive at the human chosen handover location approximately at the same time. [71] have compared several mathematical position prediction models where human is always *giver* and robot is always *receiver*. Thanks to these models, their preliminary results show an overall reduction in handover duration period. While [68, 86, 96, 110] have developed human hand motion prediction model by gaining insights learned from the human-human object handover studies. However, since specifically developing alone position prediction model is not the main focus of our study; therefore, we primarily decided to accommodate a simple method to predict the human hand motion using *constant velocity* based model. We have further discussed this in detail in Chapter 4.

Studies on handover configuration: Although predicting handover location is not enough, the robot must also be able to find the most appropriate configuration to grasp (as *receiver*) or release (as *giver*) the object, based on the comfort and requirement of the human co-worker. Therefore for an intuitive and smooth handover of an object, the robot should relatively orient its hand (in our case gripper as the end-effector) and configure accordingly. Though there are several possible configurations to handover an object, the robot must determine the correct configuration of its end-effector during the handover which is suitable and natural for the human. Moreover, according to to [23], we humans prefer

handover of an object in its default orientation. [6] work suggests that robot takes human comfort and convenience under consideration to find the appropriate orientation during the handover, which they gave a higher score based on the appropriateness and safety. [111] Showcased human-robot object handover using imitation learning based on human-human demonstration. The robot relies on the posture of the human participant to determine the pose of object handover. [67] proposed object handover and grasp planning method that incorporates cultural etiquette (one-hand, two-hand, two-hand mid-air) based on the object's function, object shape and safety of both human and robot. While [77, 98, 109] estimated the appropriate handover orientation using a 3D image of the object and by tracking human hand. [72] Introduced a simulated model planner to grasp the unknown objects during the interactive manipulative tasks. However even though the handover motion can be planned or optimized online but it is still essential for the robot to promptly adapt to changes in the handover location during the interaction, especially at the time of handover or exchange of the object.

Studies on interaction forces: Previous studies on the forces during these handover interactions analyzed the relationship between grip force (applied on the object by the human) and the load force (object weight shared by the robot). [75] findings suggest a gradual change in the grip force while the human dyad implicitly share the load force during the transfer of the object. [29] Investigated the grip forces applied on an object while it is being exchanged between the human-human dyad during a handover. They found a linear relationship between these forces, suggesting that the *giver* is responsible for safety of object during the transfer and *receiver* is responsible for the timing of handover. [79] demonstrated a grasping system based on the 6DOF wrench (force and torque) feedback that first acknowledges the stable and secure grasp on the object by the human, only after that the object is released by the robot. [76] Learned from the insights during the human dyad handovers and developed a dynamic force controller which significantly reduces the internal forces between the human-robot dyad compared to the traditional threshold-based controller. Inspired by the human object grasping, [90] designed a robotic grasping controller with minimal normal forces while grasping an object to make sure it does not slip. [85] proposed object re-grasping controller in case of false grasping. [68] presented a dynamic object handover controller based on the contextual policy search, where the robot learns about the object handover while interacting

with the human and dynamically adapts to the motion of the human. [30] Designed a controller to estimate the applied grip force and load force by measuring the joint position/angle errors on a compliant underactuated humanoid hand. However, in most of these studies, knowledge of object mass is a prerequisite. In our approach, knowing object mass in advance is optional as it can be calculated during the handover routine, but we do rely on knowing the object physical, structural properties.

Studies on robot motion planning: Majority of studies related to human-robot object handovers were carried out in the past with traditional robotic arm manipulators attached to either a stationary-base or to a wheeled-base mobile robotic system [23, 53, 68, 76, 111] and latter studies are often related to the robot motion planning and navigation in an ample space and lacks proactive behaviour using 'biped' locomotion of a humanoid robot which is capable of walking as human does. To the best of our knowledge, bi-directional object handover with biped walking has not been considered in the previous works on the human-robot dyad object handover. However [30, 109] have utilized biped walking capable humanoid robots in their studies but without considering locomotion. Therefore for the robot to be sufficiently proactive, we believe it is crucial to consider the possibility of the robot taking a step to handover or exchange an object with the human co-worker, in scenarios where short-distance travel is required. We do not focus on the problem of motion planning or navigation in a large cluttered environment [67, 74, 105]. However, instead, we concentrated our efforts to solve and optimize object handover problem which requires immediate shared efforts between human-robot dyad in a small space where few steps are necessary and enough for a comfortable and convenient object handover. We proposed simple but effective methods to take advantage of a biped humanoid robot and deal with the problem of bi-directional object handover using robot whole-body control. Though there are many state-of-the-art methods available to generate walking patterns for a biped humanoid robot, however, the study done in Chapter 4 primarily adopted the walking pattern generator (WPG) which was designed and tested in our group [25, 59] along with its native stabilizer [26, 60].

1.2.2 Proactive handover formulation

We concentrated our efforts towards developing a simple yet robust and efficient handover controller for bi-directional object exchange and transfer between the

human and the robot co-workers using robot Whole-Body Control (WBC). WBC allows simultaneous execution of several tasks at once, for example, a humanoid robot capable of using and configuring either single or both hands during the handover and manipulation of the object and at the same time, being proactive and capable of taking few steps or more during the exchange and transfer of the object. WBC exploits the full potential of the entire floating based robot body and allows interaction with the environment using multi-contact strategies [1] [106]. Several previous studies such as [54, 101] have treated object handover routine as a non-continuous entity and analyzed the routine of handover individually into three main sub-tasks — approach, deliver and retreat. However, we take a similar approach as one mentioned in the [76, 81] and treat the object handover between human and humanoid robot co-worker as one-shot continuous fluid motion.

[105, 109] and [67] have adapted object handover and manipulation using dual-arm motion planning but did not consider robot locomotion. Also, in previous studies, dual-arm manipulation is limited between robot arms only without involving human co-worker. Our handover controller, however, enables both human and robot to utilize either single or both hands simultaneously during the object handover routine.

We initially formulate our handover problem under the scenario of human-robot bi-directional object handover using human right hand and robot left end-effector. We mainly focus on three important key features during the human humanoid robot object handover routine —the *timing*(s) of handover, the *pose* of handover and the *magnitude* of the interaction forces between human hand(s) and humanoid robot end-effector(s). Basically we answer the following questions in Chapter 4, —**when** (*timing*), **where** (*position in space*), **how** (*orientation and interaction forces*) of the handover.

Later, we present a generalized handover controller, where both human and the robot is capable of selecting either of their hand to handover and exchange the object. Furthermore, by utilizing the WBC configuration, our handover controller can allow the robot to use both hands (bi-manual) simultaneously during the object handover, depending upon the shape and size of the object that needs to be transferred. Our bi-directional handover controller is intuitive; also, it is adaptable to several objects of distinguishable physical properties (shape, size and mass). Our handover controller only needs the pertinent information of the environment

[1] as explained by the IEEE Technical Committee on Whole-Body Control

(object), mainly the object's shape and size information, though knowing the mass of the object is not essential in the beginning.

Finally, we explored the full capabilities of a biped humanoid robot and added a scenario where the robot needs to proactively take a few steps to handover or exchange the object between its human co-worker. We have tested this scenario during both when human-robot dyad uses either single or both hands simultaneously. Note that by proactive nature of robot, we meant that our approach did not require a robot to be trained from the human operator, rather robot behaviour should be able to meet the human co-worker's expectations.

Chapter 2

Distinct motor contagions

Several studies in the past have demonstrated that just by observing an action performed by human or robot can affect the movements of an observing human; an effect widely known as motor contagion. Although, these previous studies have either analyzed the motor contagions induced during (which we call *on-line* contagions), or induced after (*off-line* contagions) the observation of the robot, but never together. Therefore, it is still unclear whether and how these two motor contagions differ from each other. In this Chapter, we designed a paradigm inspired by the industrial co-worker setting and examined the differences between the induced *on-line* and *off-line* contagions in participants by the observation of the same movements performed by both human and humanoid robot co-worker. We specifically examined three questions:

1. Can on-line and off-line contagions from the observation of the same movement affect different movement features of the human participant?

2. How do the strengths of the on-line and off-line contagions vary with the nature of the co-worker (i.e. if human or robot) and the behaviour of the co-worker?

3. Consequently, are the on-line and off-line contagions different, or do they constitute the same effect observed in different instances?

2.1 Materials and methods

2.1.1 Participants

In total, 45 healthy adults participated in our study. Three participants (2 males and a female of 3 nationalities, 29.6±5, mean±SD, aged 25-35) worked as volunteer models for capturing the human arm motion data. A total of 42 participants (22

females, 20 males of 11 nationalities, age between 20-39, mean±SD, 25.9±4.35) participated as 'co-worker' in the main study. All human participants had normal or corrected to normal vision. However, according to the *Edinburgh Handedness Inventory* [89], three of them were left-handed. We had received prior approval from the local ethics committee at the National Institute of Advanced Industrial Science and Technology (AIST) in Tsukuba, Japan, to conduct these experiments.

Before beginning the experiment, all participants were carefully instructed and informed regarding the experiment and task procedure. All of the participants agreed and gave their written consent to participate in this study. However, participants were unaware of the motives of the experiment as they were not told what aspect of their behaviour we will be analyzing later. This naïve nature of the participants were crucial as to avoid biasing in the results, since we were mainly interested in the implicit effects of motor contagions. Each participant was awarded with 2021 Japanese Yen for their valuable contribution.

Participants for the study were recruited through an advertisement via a local event forum, Facebook page of our experiment and via word of mouth in the Tsukuba University, Tsukuba, Japan. There were no restrictions, apart from participants needed to be at least 18 years old to participate in this experiment.

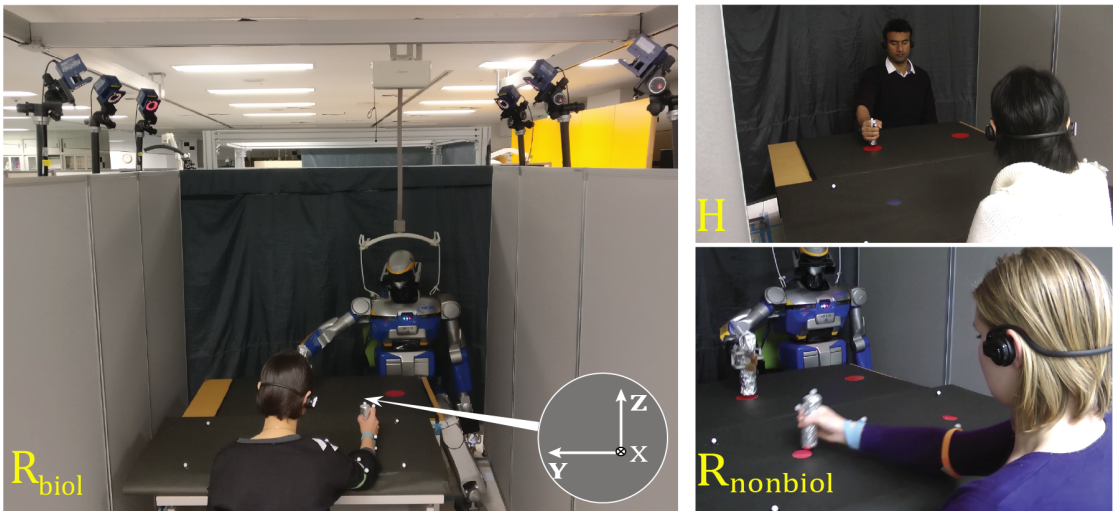

FIGURE 2.1: Experimental setup: The participants in our experiment worked in three conditions; (i) with a robot co-worker performing *biological* movements (R_{biol}), (ii) a human co-worker (H), and (iii) a robot co-worker performing *non-biological* movements (R_{nonbiol}). The coordinate axis defining the movement setup is indicated in white and fixed on the participant's table.

2.1.2 Setup

The experimental setup is shown in (Fig. 2.1). Initially, participants were requested to sit comfortably on a chair in front of a large table. While the 'co-worker' was sitting on the other side of the same table. The 'co-worker' was either a humanoid robot or a human experimenter. A touchscreen was placed horizontally underneath the table. Both co-worker and participant were presented with a unique pair of red circles on their respective side of the table. Each circle for participants had a diameter ⊘5cm and the circles for co-worker had a diameter ⊘9cm. Also, each pair of circles were at a distance of 50cm from each other. We had enclosed the experimental setup by movable panels and covered the panel behind the co-worker with a dark grey curtain.

We placed ten passive reflective markers on the hands, arms, elbows and shoulders of the participants and co-worker. We used six kestrel infra-red cameras (`Motion Analysis Co.,`) at 200Hz to track the position of these markers.

A biped humanoid robot HRP-2Kai (154cm tall, 58kg, 32DOF) was used as robot co-worker [61]. A male, trained experimenter (age: 37) was assigned to act as a human co-worker. During the experiment, both co-workers used their right hand.

2.1.3 Experimental task and conditions

The task to carry out in our experiment was inspired by the industrial *pick-n-place* part-assembly task. Participants were required to touch the red circles repeatedly on the touchscreen with a stylus in their right hand. The same task was performed by the co-worker (Human or the HRP-2Kai) in front of the participants. The participants worked in a series of 50 seconds *trials* with the co-worker. In each trial, they initially performed alone for 10 seconds (participant-alone period), performed with the co-worker for the next 20 seconds (together period), and then relaxed while watching the co-worker performs its/his task for the last 20 seconds (co-worker-alone period) (Fig. 2.2A).

We instructed the participants to "*always hold the stylus like a stamp and touch alternatively inside each red circle on the touchscreen with continuous and smooth hand movements at a comfortable speed*". Participants were not instructed regarding the movement or speed of their hand trajectories. All participants wore

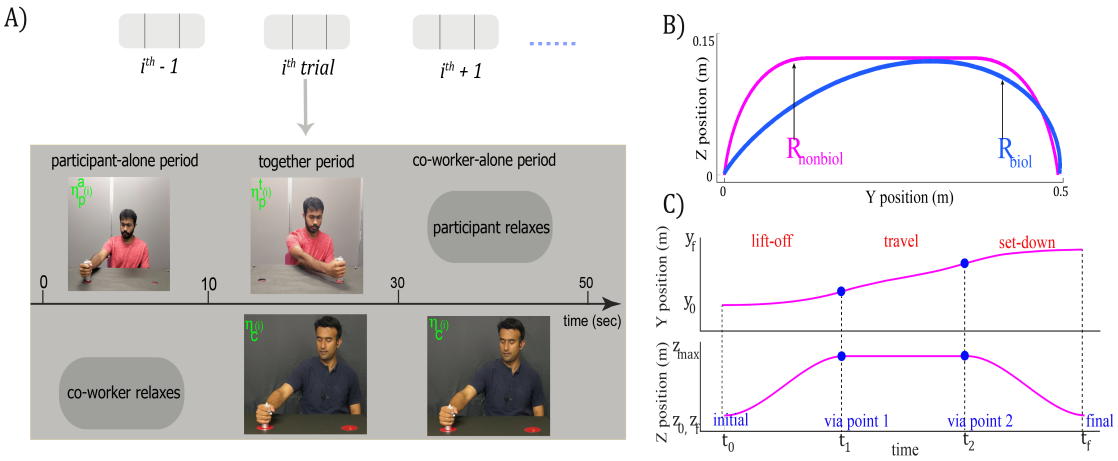

FIGURE 2.2: A) Trial protocol: The participants worked in repeated trials with either a robot or human co-worker (the figure shows the trial with a human co-worker). Each trial consisted of a period when the participant worked alone and co-worker relaxed (participant-alone period), both worked together (together period), and the co-worker worked alone (co-worker-alone period). The notation of the kinematic and time variables (represented in general by $\boldsymbol{\eta}$) in each period are shown in the figure. B) The trajectories made by the robot co-worker in the R_{biol} and R_{nonbiol} conditions. C) The time trajectories followed by the robot co-worker in the R_{nonbiol} condition in the Y and Z dimension, and the via-points (blue circles) used to generate the trajectory.

headphones (through which white noise was sent) and had no audio feedback of the noise from the moving robot (confirmed in the post-experiment questionnaire). They were explicitly told to "*focus on your own task and ignore the co-worker when he/it starts after them*".

In total, participants behaviour was tested in six experimental conditions. In each condition, co-worker's behaviour, such as physical appearance or movement trajectory, was changed. In this chapter we only discuss our findings and present results from three conditions relevant for distinguishing the *on-line* and *off-line* contagions. Whereas in the next Chapter (More than just co-workers), we have discussed the effect of physical features of the co-worker on the participant's behaviour.

In the beginning, the participants worked with a human co-worker in the Human (H) condition. The HRP-2Kai robot acted as the robot co-worker in the Robot biological (R_{biol}) condition and played back (biological) hand movements. These biological movements of a human volunteer (blue plot in Fig. 2.2B), were recorded in a preliminary experiment (also see section 2.1.4). Finally, the participants worked again with the HRP-2Kai robot as the co-worker, in the Robot non-biological (R_{nonbiol}) condition, where the robot now performed a

non-biological movement profile. This profile was roughly trapezoidal in shape and velocity profile (magenta plot in Fig. 2.2B).

Each participant worked in three conditions. Our experiment consists of six *condition combination groups*, such that each participant in a combination group worked in the R_{biol} condition, and two out of five remaining conditions. This provided us with the opportunity to compare participant's behaviour in any condition and against his/her behaviour in the R_{biol} condition. Since each of our experimental condition lasted over 20 minutes, which made the total time of experiment over an hour. Therefore to avoid participants being tired, we did not allow them to experience all the conditions. Note that the order of conditions was chosen randomly across the participants. In this Chapter we discuss our results from the participants in R_{nonbiol} and/or H conditions, in addition to the behaviour of the same participant's R_{biol} condition.

The participant worked in a series of 10 trials in each condition. The co-worker performed at a pseudo-randomly selected constant yet unique frequency (in the range of 0.16 to 1.1Hz) in each trial. This pseudo-random nature of the co-worker performance was critical to avoid contamination by behavioural drifts across trials. A metronome using headphones were provided to the human co-worker (like in [13]), to cue him/her of the required movement frequency, and to assist in keeping and maintaining the particular movement frequency.

2.1.4 HRP-2Kai movement trajectories

We played back recorded human hand movement as the arm movements of HRP-2Kai in the R_{biol} condition. In a preliminary experiment, we recorded the hand movements of three volunteers (a female and two males). *Motion Analysis Co.,* motion tracking system was used to record their hand movements, while at the same time, volunteers were cued by an audio metronome to help maintain their hand movement frequency. These movements were acquired at several frequencies between 0.16 to 1.1Hz. Interestingly these three volunteers movements were found statistically similar in the x, y and z velocity profiles ($p > 0.05$), and showed similar fashion in movement height with movement frequency, `i.e.`, trajectory height consistently decreased with the increase of movement frequency. Therefore in this experiment, we chose to only use the recorded movements from one of the male volunteers. In order to maintain the trajectory shape and also the characteristic

variance of human trajectories, we purposely decided that it is better than taking an average of trajectories by the three volunteers.

In our task, the human movements were distinguished by smooth velocity changes but did not exhibit any direction changes (via points). Therefore for the R_{nonbiol} condition, we designed a via-points based robot trajectory. Inspired by the industrial manipulators trajectories of constant velocity phase and trapezoidal shape during *pick-n-place* task and keeping in mind our HRP-2Kai joint constraints during fast movements, we redesigned a trapezoidal shape trajectory for this condition with smooth curves between the acceleration and deceleration transition phases. Our task required humans to make movements mainly in the YZ plane. Hence we also designed the robot arm trajectory in the YZ plane. Using two temporal via-points [11], we designed a smooth piece-wise polynomial trajectory in position-time using the third-order polynomial segments. The boundary conditions restricted the slope (velocity) to zero at the start, the end and the via-points (see Fig. 2.2C). The initial (y_0) and final (y_f) positions in `Y` were set to zero and 50 cm respectively, as per the movements required by the participants. To give a non-biological behaviour, we set the maximum `Z` height (z_{max}) for the robot in the R_{nonbiol} condition to 13 cm one way and 8cm the other.

2.2 Data analysis

2.2.1 Variables

Our analysis is based on the position data of the markers placed on the participant's and co-worker's stylus. In order to bring out the possible behavioural differences between the movements towards and back between the touches on the touchscreen, we analyzed behavioural variables across each movement between the red circles on the touchscreen, which we call as *iterations* (such that two consecutive iterations constituted a movement cycle). The participants and co-workers made non-stop continuous movements between the touches, and hence we could extract individual iterations by a participant or co-worker by examining the directional changes of their y-velocity in the recorded motion capture data. In this chapter, we focused our efforts on the kinematic variables along the `Y` and `Z` axes inside each iteration and analyzed the maximum movement length (y_{max}), maximum movement height (z_{max}),

maximum absolute velocities ($\max|\dot{y}|$, $\max|\dot{z}|$), mean absolute velocities ($|\bar{\dot{y}}|$, $|\bar{\dot{z}}|$), maximum accelerations ($\max(\ddot{y})$, $\max(\ddot{z})$), and minimum accelerations ($\min(\ddot{y})$, $\min(\ddot{z})$), by the participants and co-workers to understand whether and how the co-worker behaviour were affected by the *on-line* and *off-line* contagions. In addition to the kinematic variables, we analyzed time between the touches in each iteration, which we will refer to as the half-time period or (*htp*).

2.2.2 Participant sample size

We initially conducted our experiment with the sample size of 35 participants such that all of them participated in the R_{biol} condition and 14 participants in each of the five other conditions. We call it as *participant group*, where participants performed in R_{biol} condition along with one of the five other condition. Thus a total of five *participant group*s. Note that these groups are different from the previously mentioned six *condition combination group*s. The number '14' also represents the participant numbers in similar previous studies [12, 13] and this participant number '14' also corresponds to the G* power analysis [33] using two-way one sample T-test ($\alpha = 0.05$, $\beta = 0.85$, $d = 0.9$) [108] for the biological experiments. We discovered notable motor contagions in the *htp*s in the R_{biol} condition (median = 0.014, Z(31) = 3.14, $p = 0.0016$, 3 participants with slopes beyond the 95% confidence interval were removed as outliers). We thus believed that a positive *htp* slope in R_{biol} condition as true, and checked the *htp* values in the R_{biol} conditions in each participant group. But with these participants numbers, the *htp* slopes in the R_{biol} condition were not significant across the participant groups ($p < 0.05$, one-way ANOVA). The *htp* slope during R_{biol} condition were observed to be significant with two participant groups ($p = 0.022$, $p = 0.038$), marginally significant with other two participant groups ($p = 0.07$, $p = 0.08$) and not significant in one participant group ($p = 0.36$). Hence, we later proposed and decided to add 7 participants (50%) across these groups, making a total of 42 participants. This addition of participants ensured that the *htp* slopes across the participant groups become similar ($P = 0.99$; one-way Kruskal-Wallis H-test). After removal of three outliers, this gave us participants numbers of 13 in the H condition, 18 in the R_{nonbiol}, and 39 in total for the R_{biol} condition.

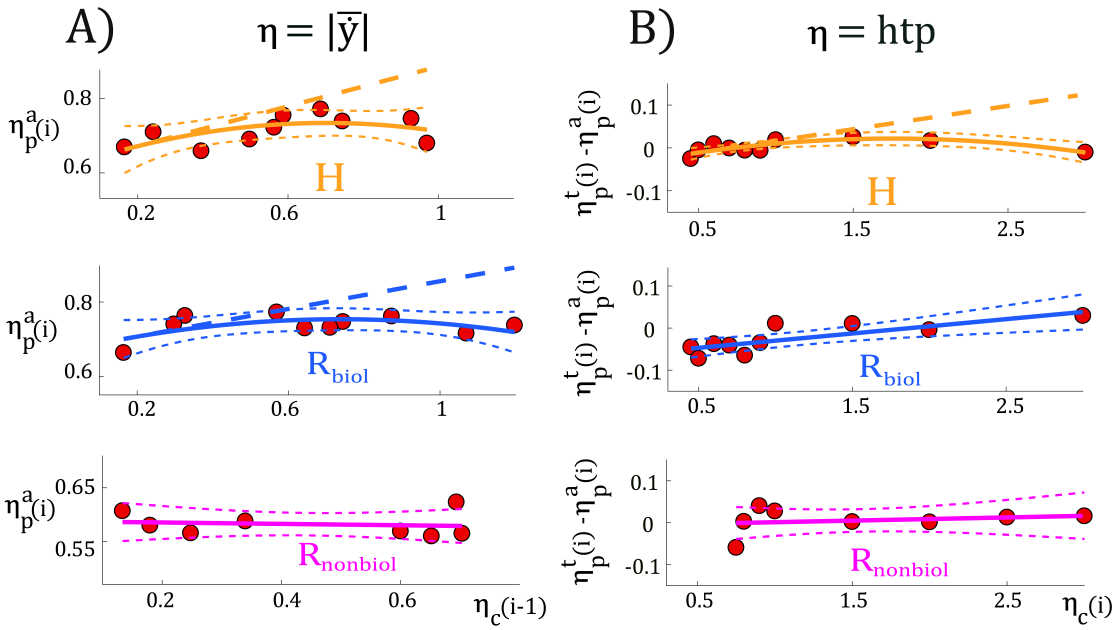

FIGURE 2.3: Examples of linear regression fits obtained in the H (orange), R_{biol} (blue), R_{nonbiol} (magenta) conditions: A) *off-line* contagions in the participant's $|\bar{\dot{\boldsymbol{y}}}|$ (**y**-axis) as a function of co-worker's $|\bar{\dot{\boldsymbol{y}}}|$ (**x**-axis); B) *On-line* contagions in the participant's *htp*s (**y**-axis) as a function of co-worker's *htp*s (**x**-axis). We used the AIC to choose either a first or second order model to fit the data for each participant. The lines represent the tangent slopes at the minimal co-worker feature value.

2.2.3 Quantifying the *off-line* contagions

After observing the co-worker, we quantified the participant's change in behaviour by analyzing how the average value of a given kinematic or time variable η_p by a participant during the participant-alone period in trial i ($\eta_p^a(i)$) has changed, compared with that of the co-worker in the co-worker-alone period of the previous trial ($\eta_c(i-1)$). We later used the first-order or second-order regression model to explain the data and performed the regression using MATLAB's `fitlm` function. The first or second-order regression models were chosen based on the Akaike Information Criteria, or AIC [5]. Some examples of fittings are illustrated in (Fig. 2.3A). We then gathered the slope at the minimum co-worker variable value ($\min[\eta_c(i)]$) across participants. The gathered slope data for each variable and condition was then checked for normality using the *Shapiro-Wilk* test and further analyzed for a difference from zero either using a one-sample T-test or a *Signed Rank* test based on whether the distribution was normal or not, respectively. (Fig. 2.4A) illustrate the data plots of $|\bar{\dot{y}}|$ from the three reported conditions.

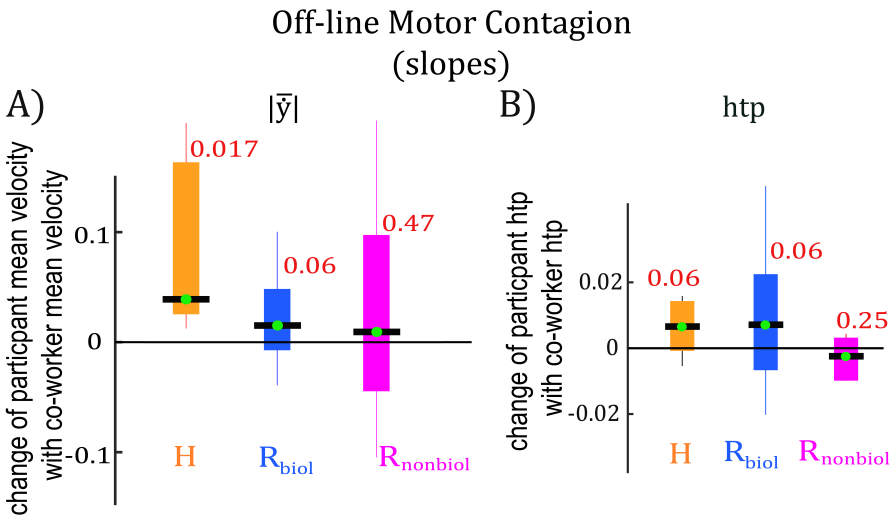

FIGURE 2.4: The *off-line* contagions: Observed changes in the participant's $|\bar{\boldsymbol{y}}|$ and *htp* in the H (orange plots), R_{biol} (blue plots), R_{nonbiol} (magenta plots) conditions. All p values are Bonferroni corrected.

2.2.4 Quantifying the *on-line* contagions

To quantify the effects due to the *on-line* contagions, we now looked again at the average value of all analyzed kinematic or time variable η_p but this time in together period. Note that in order to remove any persistent *off-line* contagions in this period, we regressed the *change* in the participant's behaviour, between the together period and alone-period in a trial $(\eta_p^t(i) - \eta_p^a(i))$, and the corresponding value of the same variable in the co-worker behaviour in the same trial $\eta_c(i)$. A first-order or second-order regression model was chosen again using AIC for each participant, and similarly with the *off-line* contagion analysis, the slope of tangent at the minimum co-worker variable value $(\min[\eta_c(i)])$ was gathered across participants, then checked for normality using the *Shapiro-Wilk*, and finally analyzed for difference from zero using a one-sample T-test or a *Signed Rank* test. The (Fig. 2.3B) illustrates the fitting of *htp* in representative participants in the three reported conditions and the collection of slopes are in shown in (Fig. 2.5B).

2.2.5 Statistical correction

As mentioned earlier, every participant in this study performed in three conditions: the R_{biol} condition, and two of the remaining five conditions. therefore we make two comparisons for each participant, between R_{biol} and the two other conditions.

Correspondingly, in our comparisons in (Fig. 2.5), we use a Bonferroni correction of (3 conditions − 1) 2, and hence all p values below 0.05 were multiplied by 2.

2.2.6 Movement congruency analysis

Moreover, during the *on-line* contagions, we also investigated if movement congruency between the participant and the co-worker influenced the *on-line* contagions in $|\bar{y}|$ and *htp* of participants. In every iteration, we compared the velocity of the participant to the velocity of the co-worker and classified it as a congruent iteration if the co-worker moved in the same direction as the participant for more than 50% of the iteration time, or otherwise as an incongruent iteration. We then performed the same regression analysis as described above to obtain two slopes for each participant, taking either their congruent or incongruent iterations. Later, we averaged the difference between the two slopes across the participants to analyze whether congruency affected the *on-line* contagions. The plots of the difference of $|\bar{y}|$ and *htp* between the congruent and incongruent iterations are shown in (Fig. 2.6).

2.3 Results

2.3.1 *Off-line* contagions affect mean velocities but not htps

Our findings agree with the results of recent studies in the past [65, 82], which have shown that *off-line* motor contagions affect the hand movement velocity of participants. We observed (Fig. 2.4A) a significant positive slope between the mean absolute y-velocity ($|\bar{y}|$) of participants and the human co-worker in the H condition (median = 0.040, p = 0.017, orange plot in Fig. 2.4A). In the R_{biol} condition, where the robot co-worker HRP-2Kai made the biological movements, the slope leaned to significance for the $|\bar{y}|$ velocity (median = 0.017, Z(38) = 1.86, $p = 0.063$, blue plot in Fig. 2.4A). Finally in the R_{nonbiol} condition, when the robot movement was not biological, the results again agreed with previous works and the slope between the $|\bar{y}|$ of participants relative to the $|\bar{y}|$ of the robot was zero ($p = 0.47$, magenta plot in Fig. 2.4A).

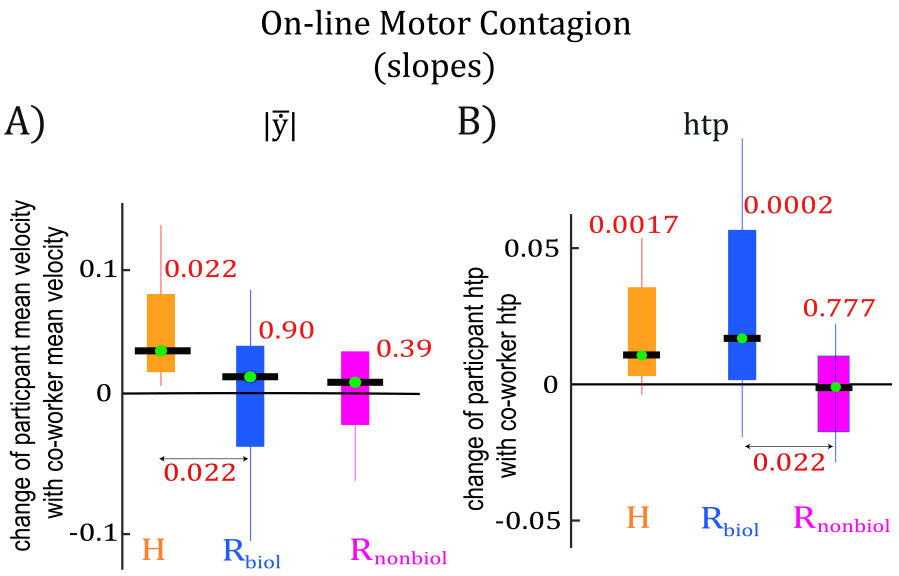

FIGURE 2.5: The *on-line* contagions: Observed changes in the participant's $|\dot{\bar{y}}|$ and *htp* in the H (orange plots), R_{biol} (blue plots), R_{nonbiol} (magenta plots) conditions. All p values are Bonferroni corrected.

Also a positive slope has been observed between the maximum absolute y-velocities ($\max|\dot{y}|$) of the participants and of the human co-worker in the H condition (median = 0.54, $p = 0.017$), however this was not present in the robot co-worker conditions (R_{biol}: $p = 0.18$; R_{nonbiol}: $p = 0.29$). Overall, these observations agree and support previous results which showed that the mean velocity of human participants are affected by *off-line* contagions after seeing a human or robot co-worker, although only when the robot co-worker performs biological movements.

Interestingly, the participant's *htp*s due to *off-line* contagions remain unaffected, no significant effect was observed. The *htp* slopes were observed to be insignificant with human co-worker in the H condition (median = 0.006, $p = 0.06$), as well as the robot co-workers R_{biol}: (median = 0.007, Z(38) = 1.89, $p = 0.06$); R_{nonbiol}: (median = -0.002, Z(17) = -0.18, $p = 0.25$). The p values were marginally insignificant, as illustrate in (Fig. 2.4B).

Note that in our task, it is entirely reasonable to observe a strong positive slope in the $|\dot{\bar{y}}|$, but not in the corresponding *htp*s. This is because in our task the participant movements were mainly in the YZ plane, and hence the *htp*, which is measured when the participant touches on the touchscreen, and it depends not only on the y-velocity, but also the z-velocities of the participant. While on the contrary, due to the same reason, any effect induced in the $|\dot{\bar{y}}|$ would partly show

up in the *htp*s, and this was probably the reason behind the marginal insignificance observed in the participant *htp*s.

Finally, we found no effect ($p > 0.1$) on any of the remaining analyzed kinematic variables (maximum movement length ($y_{\max}$), maximum movement height ($z_{\max}$), maximum absolute velocities ($\max|\dot{y}|$, $\max|\dot{z}|$), mean absolute velocity ($|\bar{\dot{z}}|$), maximum accelerations ($\max(\ddot{y})$, $\max(\ddot{z})$), and minimum accelerations ($\min(\ddot{y})$, $\min(\ddot{z})$)) due to the *off-line* contagions, in all three conditions H, R_{biol} and R_{nonbiol}.

2.3.2 *On-line* contagions affect htps and not mean velocities

Our findings strongly suggest that the *on-line* motor contagions are distinct from *off-line* motor contagions. Firstly, we measured a significant effect on the *htp* of participants when they worked in parallel with the co-worker, unlike *off-line* contagions. The slope of *htp*s was strongly significant both when the participants worked with the robot co-worker who made biological movements (median = 0.017, $Z(38) = 3.70$, $p = 0.0002$, blue plot in Fig. 2.5B) in the R_{biol} condition, as well as when they worked with a human co-worker (median = 0.014, $p = 0.0017$, orange plot in Fig. 2.5B) in H condition. As expected, when the robot co-worker's movement were non-biological in nature, no effects were observed in R_{nonbiol} ($p = 0.777$, magenta plot in Fig. 2.5B).

However, in the H condition, we found an effect on the mean absolute y-velocity ($|\bar{\dot{y}}|$) of the human participants (median = 0.034, $p = 0.022$, orange plot in Fig. 2.5A), but we didn't find this effect in the R_{biol} condition (median = 0.013, $Z(38) = 0.13$, $p = 0.90$, blue plot in Fig. 2.5A), nor in the R_{nonbiol} condition ($p = 0.39$, magenta plot in Fig. 2.5A). Suggesting that this effect was overall absent with the robot co-worker. At last, again with human co-worker, we noticed some effects in the $\max(\ddot{y})$ and $\max(\ddot{z})$, but it was completely absent in both of the robot co-worker conditions.

Our findings in the R_{biol} condition favors the notion that *off-line* contagions affect a participant's *htp* but not a participant's $|\bar{\dot{y}}|$. On the other hand, in the H condition, the effects on both *htp* and $|\bar{\dot{y}}|$ were observed. Therefore to settle this conflict, we consequently measured if the results in the H condition were coupled; `i.e.`, whether the $|\bar{\dot{y}}|$ was indeed affected in the H condition, or

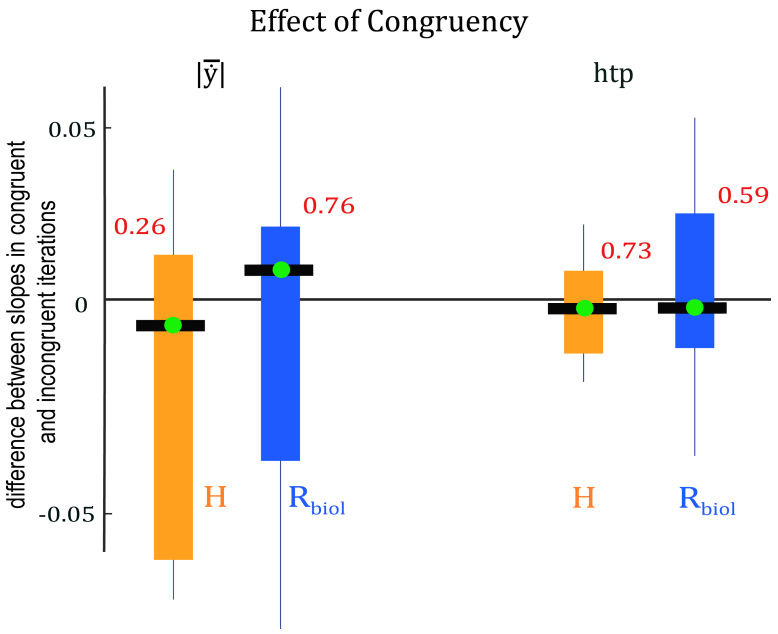

FIGURE 2.6: Effect of congruency on *on-line* contagions: the difference in slopes, between the velocity congruent and incongruent iterations across participants, was zero for both the $|\bar{y}|$ and *htp*s of participants during the observation of the human (H, orange plot) condition and robot co-worker (R_{biol}, blue plot) condition. The lack of effect difference suggests that the *on-line* contagion does not affect the movement velocities in our study.

whether it was a consequence of the effect on the *htp*. In the H conditions, we separated and collected the movement iterations depending on whether the participant's movement was predominantly congruent (*cong* iterations), or incongruent (*in-cong* iterations) with an observed (co-worker's) movement (see subsection Movement congruency analysis for details), and compared the *on-line* contagions in these two types of iterations separately. By *cong* iterations we mean, when the co-worker's movement direction corresponds to that of the participant, and the *in-cong* iterations, when the movements direction do not correspond. In accordance with the previous studies [12, 65, 82], we hypothesized that if the *on-line* contagions affect the $|\bar{y}|$, then the contagion strength (`i.e.` the signed slope), would be significantly different between the *cong* iterations and the *in-cong* iterations. Otherwise, if the *on-line* contagions are in the *htp*, which is a time unit, the congruency of the observed movement (relative to the participant's own movement) should not change the strength of the contagions.

Our data analysis and results stipulate no difference in the $|\bar{y}|$ and *htp* slopes in the *cong* and *in-cong* iterations of the H condition ($p = 0.26$ and $p = 0.73$, orange plots in Fig. 2.6 respectively). Likewise, no such difference was either observed between the slopes of $|\bar{y}|$ and *htp* in the *cong* and *in-cong* iterations of the R_{biol}

condition ($p = 0.76$ and $p = 0.59$, blue plots in Fig. 2.6 respectively). Therefore, these results strongly emphasize that the *on-line* contagions predominantly affect the participant's *htp*s but not velocity.

2.4 Discussion

We initially asked three particular questions at the beginning of this Chapter, regarding the effects of a human or humanoid robot co-worker's action observation on one's behaviour, during and after the same action observations. Our findings agree with the previous works on *off-line* motor contagion and show similar results that the mean absolute velocity of human participants in the predominant movement direction (`Y` direction, in this study) are implicitly affected after observing a co-worker (both human and robot). However, with the robot co-worker, this effect was present only when the robot made biological movements (Fig. 2.2B, blue plot). On the contrary, due to *off-line* contagions, we found minimal effects on the participant's *htp*s (Fig. 2.4B). While due to the *on-line* contagions, we primarily observed the effects in the participant *htp*s during both, when working with a human or robot co-worker, however with robot co-worker, again only when the robot made biological movements (Fig. 2.5B). We also observed an effect on the mean absolute y-velocity of participants when they worked with human co-workers (Fig. 2.5A), but on the contrary, the *iteration*s congruency analysis (section Movement congruency analysis) strongly emphasizes that this effect was in fact a residual effect on the *htp*. To summarize, our results suggest that both *on-line* and *off-line* contagions affect distinct movement features of the human participant from the observation of the same movement. The *on-line* contagions are more frequent in the frequency or rhythm (quantified by *htp*) of the movements, while the *off-line* contagions mostly affect velocity.

In this study, we quantified the *on-line* contagions as the relation (slope) between the *difference* of the human participant's movement feature when working with the co-worker compared to working alone, and the co-workers feature. This difference extracts the *off-line* effects in the participant behaviour, which arises due to the observation of previous and different co-worker movements. Therefore it is essential to note that the insufficiency to obtain a particular effect in the *on-line* contagions analysis, does not necessarily mean that the effect is absent during these observations of the co-worker. Instead, here,

the analysis of *on-line* contagions represents particularly the effects that changed when working alone, in compared to when working parallel to a co-worker.

Interestingly, our findings suggests that the nature of the co-worker, (human or a robot), *tend* to influence the *off-line* contagions significantly more than the *on-line* contagions. While with the human co-worker, strong *off-line* contagions were measured in the participant's $|\overline{\dot{y}}|$ ($p = 0.017$, Fig. 2.4A), but with the robot co-worker, this effect seemed diminished ($p = 0.063$, Fig. 2.4A). Although the difference of these effects between the two conditions ($p = 0.34$) weren't significant enough to conclude definitely. However, the effect on the participant's *htp*s was clearly visible due to *on-line* contagions, both with the human co-worker ($p = 0.0017$, Fig. 2.5B) and robot co-worker ($p = 0.0002$, Fig. 2.5B), and as well these affects were not different from each other ($p = 0.62$).

Finally, the overall observations made in this Chapter emphasize on our hypothesis that distinct motor contagions are induced in human participant's *during* the observation of a co-worker (*on-line* contagions) and as well as *after* the observations of a co-worker (*off-line* contagions). These observed distinctions in the affected movement features and the sensitivity of these effects to the nature of the co-worker provide a better understanding on how human movements may be influenced by the robot co-workers working near them. These insights could be crucial to the physical and behavioural design of robots working near humans.

In the next chapter, we further explored the topic of motor contagions between human and humanoid robot co-workers and our findings suggest that by exploiting motor contagions, one can influence the performance of human co-worker and while where ethically valid, these motor contagions may also be used to improve worker performance speed and hence productivity in an industrial task.[1]

[1]The video of this study is available at https://youtu.be/eq4UOeJx3cY

Chapter 3

More than just co-workers

In the previous chapter, we explored distinct motor contagions induced in the human co-worker during (*on-line*) and after (*off-line*) the observation of action by either the human or robot co-worker. Here, under the same experimental setup and the task, we focused on exploiting the induced motor contagions in the human co-worker. We primarily asked one specific question in this Chapter —Does the presence of a humanoid robot co-worker influence the performance of humans around it?

During the human-robot interactions, previous studies on motor contagions have either analyzed the effects of robot co-worker movement observation on human's movement velocity or the effects on their movement variance, but never both together. We argue here that the performance has to be measured considering together, both the task speed (or frequency) as well as task accuracy. Therefore in the same experimental task, as discussed in the previous Chapter section (2.1), along with the addition of three new conditions, by coherently varying the robot behaviour, we observed how the performance of a human participant co-worker is affected by the presence of the humanoid robot co-worker. Where in two new conditions, we investigated the effect of physical form, by covering the head and torso of the human and robot co-workers in the human covered and robot covered respective conditions and only the moving robot arm was visible to the participants. While in the third new condition (robot non-biol), we investigated the effects of robot movement velocity profile with the velocity-phases of both industrial and biological trajectories. Finally, as ground truth, we compared these behaviours with a human co-worker, and also examined how these observed behavioural effects vary on the scale with the

experience of robots.

3.1 Materials and methods

The arrangement of experimental setup and task are the same as mentioned in the Chapter 2. However, the total number of conditions and features analyzed are different here. To explain clearly and avoid confusion, we have renamed the conditions as can be seen in (Fig. 3.1) and mentioned some essential details again in the below subsection.

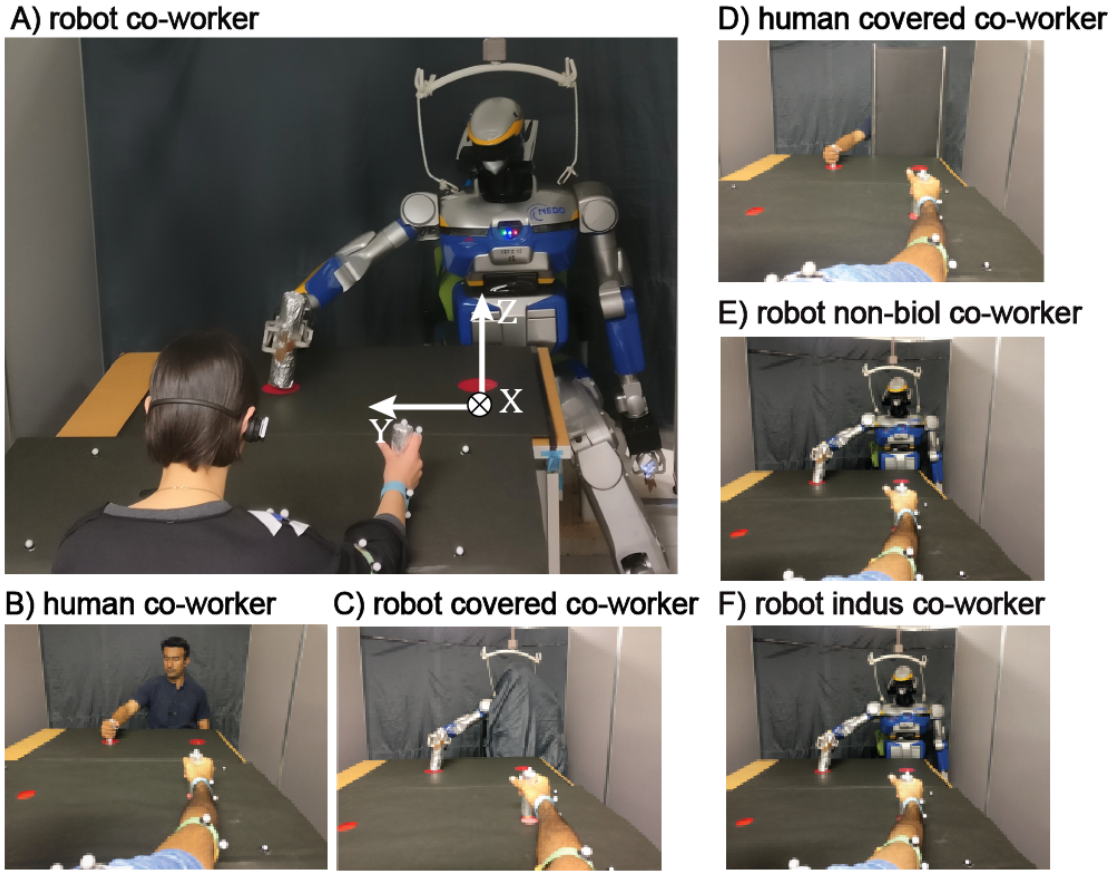

FIGURE 3.1: The participants in our experiment worked in six conditions; with a robot performing *biological* movements in A) robot co-worker condition; B) human co-worker condition; to check relevance of human form in C) robot covered co-worker condition; and D) human covered co-worker condition; E) a robot co-worker performing *non-biological* movements in robot non-biol co-worker condition; F) a robot co-worker performing industrial movements. The coordinate axis defining the movement setup is indicated in white (A).

3.1.1 Experimental task and conditions

As mentioned in the previous Chapter, our task was motivated by the industrial *pick-n-place* part assembly task, which required the participants to touch repeatedly inside two static red circles on the touchscreen with a hand stylus. The participants were only instructed to touch inside each circle consecutively. However, they were free to touch anywhere inside each circle. During a preliminary experiment, we discover that the participant's touches had less than 1 cm standard deviation, both in the x and y movement directions. Therefore, on purpose, we chose to keep the radius of the touch circles more than `2x` times larger than their standard deviation in the main experiment. Hence the target size of touch circles was 5 cm in diameter. This increase in the size of touch circles was crucial to us since the participants were asked to touch the circle in each trial, but they were free to touch anywhere on the circle. This enabled us to observe and measure the variance along with standard deviation in the participant's touch position (that may result in contagion in their speed) across our experiment.

A co-worker being the human experimenter or HRP-2Kai humanoid robot worked on the same task in front of the participants. Again the participants were asked to perform their task at their own chosen 'comfortable' frequency, and ignore the co-worker. The trial protocol was the same, as mentioned in the previous Chapter. The participants worked in a series of 50 seconds trials with the co-worker. In a trial, participants initially performed alone for 10 seconds (participant-alone period), performed with the co-worker for next 20 seconds (together period) and then relaxed while watching the co-worker performs the task for the last 20 seconds (co-worker-alone period) (Fig. 3.2).

All participants wore earbuds and headphones, which enabled them to hear only white noise and had no external audio feedback; it was later confirmed in the post-experiment questionnaire, Q6. All participants were instructed to "*always hold the stylus like a stamp and touch alternatively inside each red circle on the touchscreen with continuous and smooth hand movements at a comfortable speed*". While they were explicitly told to "*focus on your own task and ignore the co-worker when he/it starts after them*". No other instructions were given regarding their hand speed and trajectory.

Unlike Chapter 2, here we have studied and analyzed data from all six experimental conditions. In four conditions, the participants worked with an

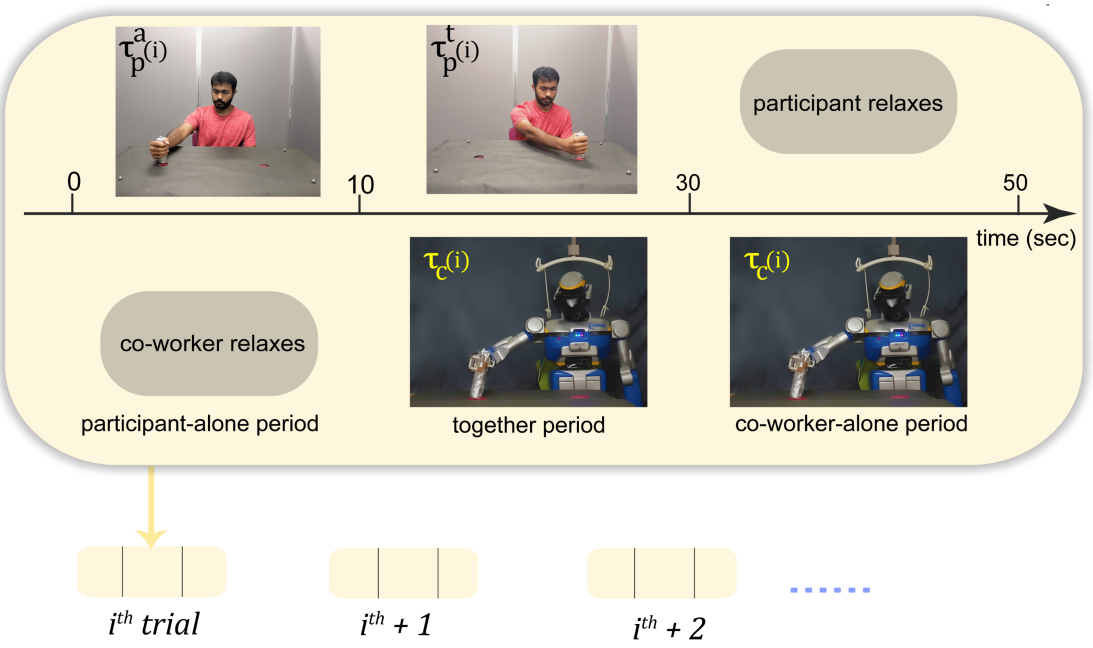

FIGURE 3.2: The participants worked in repeated trials with either a robot or human co-worker (the figure shows the trial with a robot co-worker). Each trial consisted of period when the participant worked alone and co-worker relaxed (participant-alone period), both worked together (together period), and the co-worker worked alone (co-worker-alone period). The notation of the time variable (represented in general by τ) in each period are shown.

HRP-2Kai humanoid robot co-worker, specifically in (a) *robot co-worker* in which the robot played back biological movements, and the whole robot was visible to the participant (b) *robot covered co-worker*, in which the robot played back biological movements. However, its head and torso were covered, and the participant could only see the robot's moving arm. (c) *robot non-biol co-worker*, in which a fully visible robot performed *non-biological* arm movements, (d) *robot indus co-worker*, in which a fully visible robot performed *industrial* arm movements. While in the remaining two conditions, participants worked with a trained human experimenter in, (e) *human co-worker* and (f) *human covered co-worker*, where the head and torso of the human experimenter were covered (see Fig. 3.1).

In the experiment, all participants worked over ten trials in each condition, and there were three conditions per experiment. We had six *condition combination* groups, see (Table 3.1), and each participant was assigned to one of that group. Each participant worked in the robot co-worker condition (as a primary condition), and in addition to two out of five other remaining conditions. The order of the conditions was balanced across the combination groups. This

allowed us to compare the behaviour of the same participants in each condition in a combination group, with their behaviour in the robot co-worker condition.

TABLE 3.1: condition combination groups (G)

HRP-2Kai in robot co-worker (RV), robot covered co-worker (RC), robot non-biol co-worker (RN), robot indus co-worker (RI) conditions and Human experimenter in human co-worker (HV), human covered co-worker (HC) conditions. The order of conditions in a combination group were randomized across participants.

Sessions/Groups	**G1**	**G2**	**G3**	**G4**	**G5**	**G6**
Session 1	RI	RC	HV	RC	RN	RC
Session 2	RV	RI	RV	HC	HV	RN
Session 3	RN	RV	HC	RV	RV	RV

In the robot co-worker conditions, robot movements were a playback of the human recorded movements of a previous human volunteer (see subsection HRP-2Kai movement trajectories for details). In this study, we quantified the participant performance in the trials by their half time periods or *htp* (the average time between two consecutive alternate touches, measured using motion capture system), and the variance of their press location (measured as a change of mean and standard deviation of their touchscreen presses in the `X-Y` plane).

3.1.2 HRP-2Kai movement trajectories

The biological movements that were played on HRP-2Kai in robot co-worker and robot covered co-worker conditions were a playback of the human arm movements (Fig. 3.3, blue plot). We have already discussed this in detail in the subsection of the previous Chapter (2.1.4).

It is well known that human movements can be characterized by a bell-shaped velocity profile [40]. Generally, when the movements are governed goal-oriented, (when the end positions of the goal are fixed). In such cases, it is possible to see a peak of the bell-shaped profile to be shifted forward (in the direction of goal target) in time when the precision is required near the end of the motion. A similar case is also valid in our task where the participants were required to touch inside circles, within a given target region. However, the velocity profiles of human movements are typically characterized by a single peak. Therefore, to formulate and design a 'non-biological' movement profile for the robot non-biol

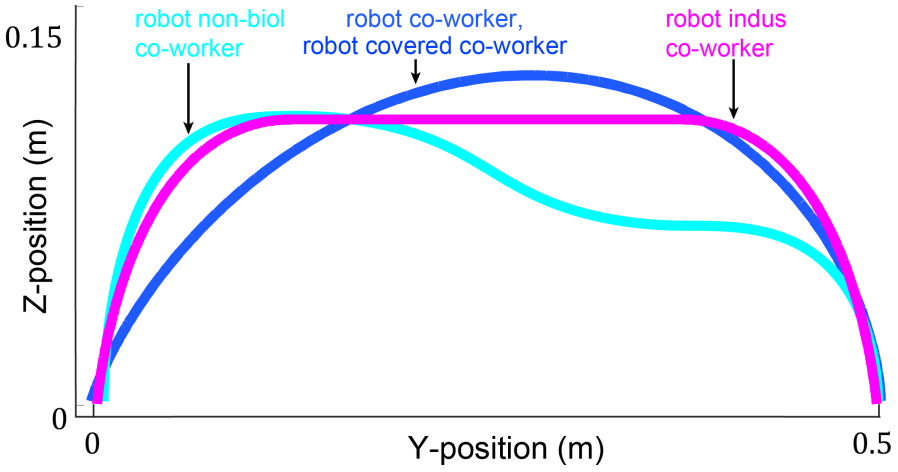

FIGURE 3.3: The trajectories played by the robot in robot co-worker, robot covered co-worker, robot non-biol co-worker and robot indus co-worker conditions.

co-worker condition, which consists of essence from both biological and industrial movements, we developed a new movement profile with multiple velocity peaks. This movement profile was developed in position-time (cyan plots in Fig. 3.3) profile using segments of fifth and third-order polynomials during the lift-off, carry, set-down phases [11] (see cyan plots in Fig. 3.4). Again, our observations suggested that human volunteers made movements predominantly in the `Y-Z` plane. Therefore, this piece-wise polynomial trajectory for the robot non-biol co-worker condition was also designed over the y (horizontal) and z (vertical) dimensions, while x was always kept at constant zero.

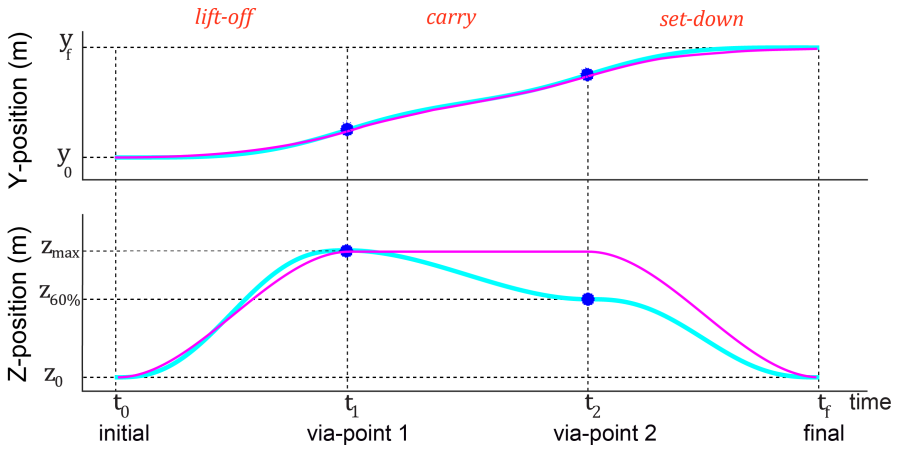

FIGURE 3.4: The time trajectories in the Y and Z axis by the HRP-2Kai in the robot non-biol co-worker and robot indus co-worker condition, and the via-points (blue circles) used to generate both trajectories.

A constant velocity phase characterized the industrial trajectory. Note that this trajectory is the same as the trajectory in R_{nonbiol} condition, which was mentioned in the previous Chapter. We have only changed the name of the trajectory to robot indus co-worker (magenta plots in Figs. 3.3 and 3.4), again to avoid confusion with the results of the previous Chapter.

3.2 Data analysis

3.2.1 Variables

Here again, our analysis is based on the position data of both the participant's and co-worker's stylus markers. Precisely here, we analyzed the 'time' behavioural variable across each movement between the red circles on the touchscreen. In this study, we were interested in the task performance of participants. Therefore we primarily concentrated on the 'time' between alternate touches in each *iteration* (a movement between two consecutive alternate touches), which we referred as the half-time period (*htp*) or τ, and the location of their touches on the touchscreen (in the `X-Y` plane). It is worth mentioning again that both participants and co-workers were instructed to make non-stop continuous movements between touches at their comfortable speed. Therefore we were able to tease out the individual *iteration*s of participants and co-workers by focusing on the changes in the direction of `y`-velocity in their recorded motion capture data. We have already analyzed and discussed the various measures of kinematic parameters such as position, velocity and acceleration along the `Y` (horizontal) and `Z` (vertical) axes over each iteration in the Chapter 2.

We quantified the motor contagion in a participant' *htp* (the average time between two consecutive alternate touches) by analyzing the change of participant's *htp* between the together period and alone-period (see Fig. 3.2) in a trial ($\tau_p^t(i) - \tau_p^a(i)$), relative to the *htp* of the co-worker behaviour in the same trial ($\tau_c(i) - Av(\tau_p^a)$), where $Av(\tau_p^a)$ represents the average undisturbed *htp* by a participants across his/her participant-alone periods. We later regressed the data obtained on each participant with either a first or second-order regression model. The regression model was chosen based on the Akaike Information Criteria (AIC) [5] and using `fitlm` function of `MATLAB`. Across participants, we collected the slope of the tangent at the minimum abscissa value of data ($\min[\tau_c(i) - Av(\tau_p^a)]$). These slopes were then checked for normality using

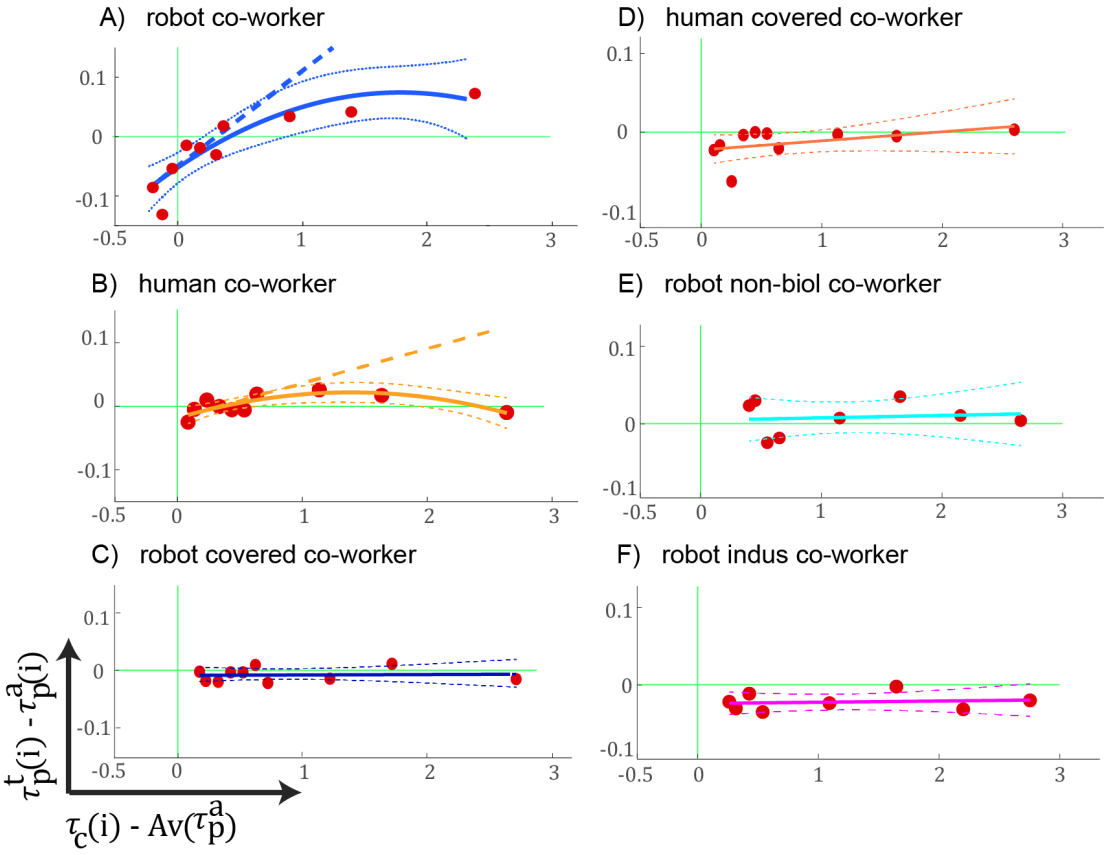

FIGURE 3.5: The change of participant's *htp* (the average time between two consecutive alternate touches) between the together period and alone-period ($\tau^t_p(i) - \tau^a_p(i)$), relative to the *htp* of the co-worker behaviour in the same trial ($\tau_c(i) - Av(\tau^a_p)$), where $Av(\tau^a_p)$ represents the average undisturbed *htp* by a participant across all his/her participant-alone periods. Note that the (robot or human) co-worker *htp* was random across trials, and the data in plots here are the ensemble of the participant behaviours arranged in increasing co-worker's *htp* on the abscissa. Each plot represent a condition, A) robot co-worker (blue); B) human co-worker (orange); C) robot covered co-worker (dark blue); D) human covered co-worker (dark orange); E) robot non-biol co-worker (cyan); F) robot indus co-worker (magenta) conditions. We used the AIC to choose either a first or second order model to fit the data for each participant. The lines represent the tangent slopes at the minimal data abscissa value.

Shapiro-Wilk test. Finally, data were analyzed for the difference from zero using a one-sample T-test in case of a normal distribution, otherwise using a Signed Rank test. (Fig. 3.5), shows the one sample fitting [1] of *htp* of randomly chosen participant in each of the six reported condition and the collection of slopes comparison across six conditions are plotted in (Fig. 3.6). We applied a similar procedure to analyze the change in average `X` and average `Y` press locations of participants touches, along with the standard deviation of `X` and `Y` press locations relative to the *htp* of the co-worker behaviour in the same trial ($\tau_c(i) - Av(\tau_p^a)$). (Fig. 3.7) shows the analysis of these slopes.

Next, we examine the significance of the human form; we further extended this study by adding two more conditions, specifically robot covered co-worker and human covered co-worker conditions, where we completely covered (hidden) the head and torso of the co-worker. However, only the moving arm was visible to the participants (see Fig. 3.1C, D or inset photos in Fig. 3.6) while we kept the experimental settings and analysis in these two new conditions exactly same as in the robot co-worker and human co-worker conditions.

3.2.2 Participant sample size

As mentioned earlier in the subsection (Participant sample size) of the previous Chapter, that we initially recruited 35 participants, all of them participated in the main robot co-worker condition and two out of remaining five other conditions, to enable an intra-participant one sample T-test between the robot co-worker and each of the remaining conditions. These five remaining conditions namely are human co-worker, robot covered co-worker, human covered co-worker, robot non-biol co-worker and robot indus co-worker. Thus giving us five *participant group*, such that randomly selected 14 participants performed in robot co-worker condition along with one of the five other conditions. The number '14' also represents the participant numbers in similar previous studies [12, 13] and this participant number '14' also corresponds to the G* power analysis [33] using two-way one sample T-test ($\alpha = 0.05$, $\beta = 0.85$, $d = 0.9$) [108] for the biological experiments. However, with these participant numbers, we found that the slopes in the same robot co-worker condition were not similar among the participant groups ($p < 0.05$, one-way ANOVA). The *htp* slopes of robot co-worker condition were significantly different from zero with

[1] see (Appendix: Motor contagion) for all participants *htp* fitting figures in all conditions.

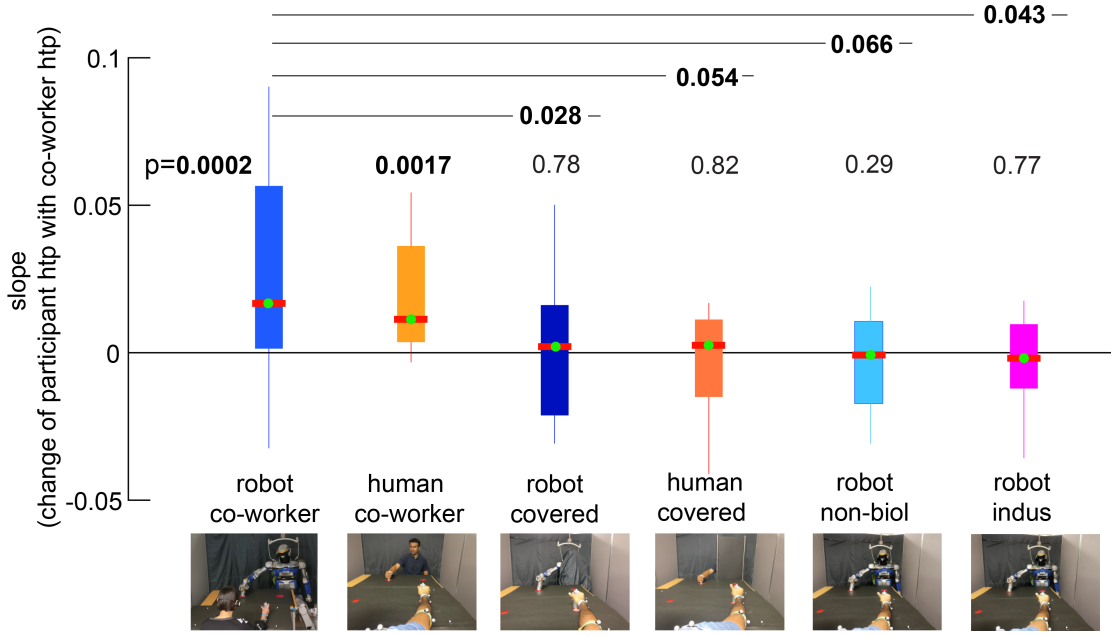

FIGURE 3.6: The plot of the collection of slopes which is obtained in (Fig. 3.5 and A.2 to A.6) supplementary figures. The condition-wise comparison of the change of participants *htp* with co-worker *htp*. P-values are Bonferroni corrected where required. The tangent slope at the minimum data abscissa value ($\min[\tau_c(i) - Av(\tau_p^a)]$) was collected across participants (as shown in Fig. 3.5), checked for normality using the Shapiro-Wilk test and then analyzed for difference from zero using a one sample T-test (in case the distribution was normal) or a Signed Rank test.

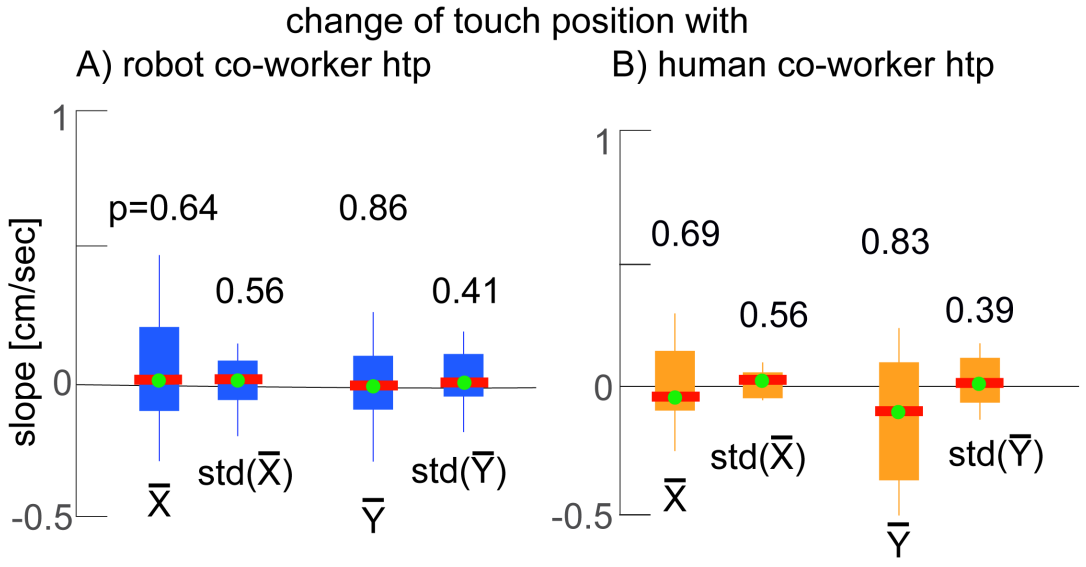

FIGURE 3.7: Change of participant touch position with A) robot co-worker *htp*; B) human co-worker *htp*. A similar procedure which was used to quantify *htp* was also used here (see subsection Data analysis) to analyze the change in a participant's average X press location, average Y press location, standard deviation of X press location, and standard deviation of Y press locations relative to the *htp* of the co-worker behaviour in the same trial.

two participant groups (p=0.022, and p=0.038), marginally significant in two participant group (p=0.07, and p=0.08) and not significant in one participant group (p=0.36). As a majority of the values tended to be significant, hence we later proposed and decided to add 7 participants (50%) across these groups (robot covered co-worker, robot non-biol co-worker and robot indus co-worker conditions), making a total of 42 participants. This addition of participants ensured that the *htp* slopes across the participant groups become similar ($P = 0.99$; one-way Kruskal-Wallis H-test). After removal of three outliers, this gave us participants numbers of 13 (human co-worker condition), 13 (human covered co-worker), 17 (robot covered co-worker), 17 (robot non-biol co-worker), 18 (robot indus co-worker), and 39 in total for the robot co-worker condition, see (Table 3.2).

TABLE 3.2: Participant sample size

condition	**sample size**
robot co-worker	39
human co-worker	13
robot covered co-worker	17
human covered co-worker	13
robot non-biol co-worker	17
robot indus co-worker	18

3.2.3 Questionnaire

3.2.3.1 Perception and fatigue

All participants in our experiment had to answer a short six-question post-experiment questionnaire. A 7 point Likert scale was used to measure the participants' response on each of these questions. Participants were requested to choose a score between 0 to 7, where 0 (Not at all), 7 (very strongly). These questionnaires were presented after every session they participated in:

Q1. My movements were affected when the agent was working with me.

Q2. My movement speed was changed when the agent was working with me.

Q3. I was tired during the experiment.

Q4. I could maintain the movement speed that I wanted even when the robot was performing its task.

Q5. I found it difficult to do my task when the agent was working with me.

Q6. I could hear noises from the co-worker during the experiment.

Q1, Q2, Q4 and Q5 were designed to access whether the participants cognitively realized the effects on their behaviour due to the co-worker. A score close to one in Q1, Q2 and Q5 (and a score close to 7 in Q4) indicates that they did not consciously realize the effects. Therefore we considered the Q4 scores by subtracting the reported values from 7.

3.2.3.2 Robot exposure questionnaire

Soon after the end of our data collection, we noted that it is vital to measure the participant's robot experienced and exposure to robots. Therefore further questionnaire of four questions was sent to participants:

RQ1. How many hours do you see and/or read about robots on average per week (include robots on TV)?

RQ2. If you work with robots currently, how many hours do you work with robots (or on robotics related topics) per week?

RQ3. If you have worked with robots, but do not work anymore, how many hours have you worked on them?

RQ4. How will you rate your knowledge of robots?

For each question, the participant had to answer in hours and chose between '0', 'less than 5', '5-10' '10-15', '15-20', '20-25', '25-30', 'more than 30'.

3.3 Results

3.3.1 Robot behaviour influences human movement frequency

(Fig. 3.5) shows the change of participant's *htp* (the average time between two consecutive alternate touches) between the together period and alone-period

$(\tau_p^t(i) - \tau_p^a(i))$, relative to the *htp* of the co-worker behaviour in the same trial $(\tau_c(i) - Av(\tau_p^a))$, where $Av(\tau_p^a)$ represents the average undisturbed *htp* by a participants across all his/her participant-alone periods. Note that the *htp* of both co-workers (robot and human) was random across trials, and the data of the participant behaviours are grouped and arranged in increasing order of co-worker's *htp* on the abscissa in (Fig. 3.5). Later the slope of the polynomial at the lowest data abscissa was collected as a measure of how the participant *htp* was affected by the co-worker *htp*. We found that the slope distribution was not normal across the participants in the robot co-worker condition ($p<0.05$, Shapiro-Wilk test, median=0.017) and distribution was significantly positive across participants (median=0.017, $Z(38)=3.70$, $p=0.0002$, Signed Rank test). The robot performance *htp* (hence frequency) has influenced the human participants, as can be seen by the positive slopes (light blue data) in (Fig. 3.6). Primarily, the longer *htp* of the robot has caused the human participant's *htp* to increase (see first quadrants of Fig. 3.5A) but for many participants, this increase had a threshold after which the participant's *htp* decreased. Therefore because of this behaviour, we found a second-order fit to explain the data better with many participants using AIC. On the other hand, the shorter *htp* of the robot (only in robot co-worker condition) has also caused the participant's *htp* to decrease (3rd quadrants of Fig. 3.5A), emphasizing that a faster robot made the participants' frequency higher. Not surprisingly, the *htp* results were similar to the human co-worker. The positive slopes (orange data) in (Fig. 3.6) illustrates that the human participants' performance (median=0.012, $p=0.0017$, Signed Rank test) was influenced by the human co-worker's performance *htp* (frequency).

3.3.2 Press accuracy in the human not affected by robot co-worker

We next analyze and measure the task performance of a human co-worker (participants) as means of whether and how their touch accuracy has changed alongside the contagions in their *htp*. It is important to remember that the provided target circles to the participants were large enough in diameter (5 cm diameter) and the participants were free of constraints as to where inside the target circle they should be touching. Hence the positions of participant's touches were susceptible to change and could cause an increase in variance (touch positions) due to their movement speed, without violating the task.

Although, interestingly, we found that while the participants' movement frequency or *htp* has changed, but we did not find any trend in the participants' touch accuracy during the task.

Across all participants and when they worked alone in the participant-alone period, we found the mean touch positions were ($\overline{X}$=0.95 cm; $\overline{Y}$=1.17 cm), and the mean standard deviations were (std(X)=0.23 cm; std(Y)=0.79 cm) from the centre of the circle. It is very crucial to note that the participants were also able to maintain the same touch positions (there was no change of mean touch positions $\overline{X}$: p=0.64; $\overline{Y}$: p=0.86) and mean standard deviations (change of std(X): p=0.56; std(Y): p=0.41) between when they worked alone and when they worked with the robot co-worker (Fig. 3.7A), suggesting that the robot did not affect participants task accuracies.

Similarly in the human co-worker condition in which the participants worked with another (unfamiliar) human experimenter, we found constant press accuracy, with no observed changes in the mean touch positions ($\overline{X}$: p=0.69; $\overline{Y}$: p=0.83; Fig. 3.7B) and mean standard deviations (std(X): p=0.56; std(Y): p=0.39; Fig. 3.7B). Remember that the provided target circles to the participants were large enough in diameter (5 cm diameter), and the participants were free of constraints as to where inside the target circle they should be touching. Although the participants could have changed their touch position and variance while still satisfying the required task, however, but we do not observe this trend.

In this experiment, together, the lack of change in task accuracy alongside the change in movement frequency, shows that robot, as well as human co-workers, were able to influence the participant task performance.

3.3.3 Human form matters

Interestingly, in the robot covered co-worker condition and human covered co-worker condition, covering the head and torso eliminated the contagions in the participant's *htp*. The participant's *htp*s were no longer affected in the robot covered co-worker (T(16)=-0.3, p=0.78; dark blue data in Fig. 3.6) and the human covered co-worker (T(12)=0.24, p=0.82; dark orange data in Fig. 3.6). These effects were significantly lower than the effects induced in the same participants in the robot co-worker condition (T(16)=2.74, p=0.028, Bonferroni corrected, one

sample T-test between robot co-worker and robot covered co-worker; T(12)=2.50, p=0.054, Bonferroni corrected, one sample T-test between robot co-worker and human covered co-worker). These results emphasize that the human form is crucial for the induction of performance changes.

Finally, previous studies have shown that motor contagions are not present when the robot movements are not biologically inspired or non-biological (industrial) in nature [13, 66]. Therefore we added another two conditions (robot non-biol and robot indus) with robot co-worker (see subsection HRP-2Kai movement trajectories), in which the participants could see the robot whole upper body. However, in robot indus condition, robot movements were inspired from the traditional trapezoidal shape velocity profile trajectory while in the robot non-biological condition, robot movements were designed by gaining insights from both the biological and industrial trajectories. Agreeing with previous studies, we did not find any significant change in *htp*s in this condition (Z(16)=-1.07, p=0.29 (cyan data); Z(17)=-0.28, p=0.77 (magenta data) in Fig. 3.6), and these values were different (tending to significance) compared to the robot co-worker condition of the same participants (robot non-biol condition: T(16)=2.32, p=0.066, Bonferroni corrected, one sample T-test) and (robot indus condition: T(17)=2.53, p=0.043, Bonferroni corrected, one sample T-test).

3.3.4 The performance effect were implicit

To further analyze the post-experiment questionnaire across the participants, we took an average of the scores from Q1, Q2, Q5 and Q4 (value subtracted from 7) and found the score to be equal to (mean±SD, 1.90±0.18) for the robot co-worker condition, and (mean±SD, 1.65±0.24) for the human co-worker condition respectively. The participants did not consciously realize the effects on their behaviour as suggested by these low scores. The participants were not tired during the task in each condition, as confirmed by the Q3, the obtained scores of (mean±SD, 0.96±0.18) across the participants in the robot co-worker condition, and (mean±SD, 0.75±0.22) in the human co-worker condition. Finally, the participants did not hear any external audio cues from either the robot's joints in the robot co-worker conditions (mean±SD, 0.5±1.25) nor the human co-worker's touches in the human co-worker conditions (mean±SD, 0.58±1.36) as confirmed by Q6.

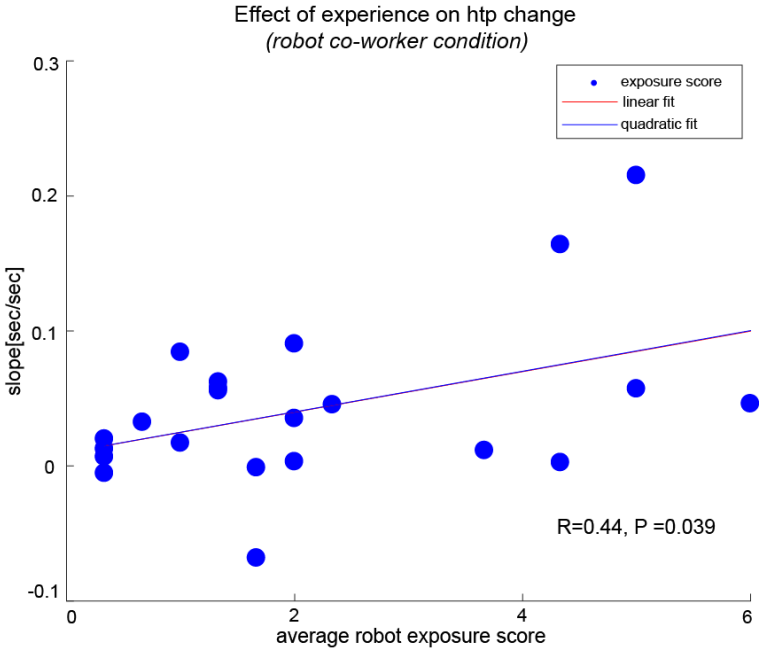

FIGURE 3.8: The plot of the change of participant *htp*, with respect to their prior robot exposure and experience (self-scored by participants) showed a significant correlation between the two.

3.3.4.1 Contagion increases with robot exposure

During the 2^{nd} questionnaire, which we had sent out at the end of our experiment and data collection. Twenty-three participants had answered on our robot exposure questionnaire. One participant out of these 23 who rated scored '0' for all questions was removed. We then took the average scores (taking either one from RQ2 and RQ3, as they were equivalent) for the others and plotted it against their *htp* slope in the robot co-worker condition in (Fig. 3.8). Interestingly, we found a significant positive correlation (Pearson's R=0.44, p=0.039) effect, suggesting that the strength of this effect on the participants is directly proportional to more exposure and experience with robots. This result also agrees with a recent report where participants with more experience with robots show higher adaptation to it, see [107].

3.4 Discussion

To summarize the study mentioned in this Chapter, primarily, our findings suggest that the presence of a humanoid robot co-worker (or a human co-worker) can influence the performance frequencies of human participants. We observed that

participants become slower with a slower co-worker, but also faster with faster co-workers. In this study, we focused on measuring and then examining the change of participant behaviour 'relative' to the robot behaviour. Therefore, to quantify the motor contagion, we examined the ratio and analyzed the change in participant's *htp* between the together period and alone-period in a trial and relative to the *htp* of the co-worker behaviour in the same trial. The negative numerator term $(\tau_p^t(i) - \tau_p^a(i))$ suggests that participants get faster from their initial participant-alone period *htp* (movement speed) and vice versa. It is important to note that the removal (subtraction) in the denominator of $Av(\tau_p^a)$ is a constant, which only shifts the curve in the negative abscissa and does not affect the slope.

Note that the results we obtain here are specific to cyclic or repetitive tasks since we found that robots are generally employed in industries where typical *pick-n-place* tasks are the most common. Although, it has been shown that cyclic and discrete tasks may be very different in terms of neural processes [92], and further studies are required to verify whether the effects that we observe here are also valid for discrete movements. Further studies are also required to understand whether and how the contagions we observed here are related to *Motor entertainment*, which is a phenomenon predominantly defined for rhythmic auditory stimuli [93, 103]. In our task we provided participants with white noise feedback to avoid hearing noise or audio cues from the moving robot, having said that, it may be possible the effect we observed here could be a type of *visual* Motor entertainment. Though at the moment, nothing can be said more concretely on this topic.

Our results show that the human and humanoid robot co-workers have been able to affect the performance frequencies of the participants, while their task accuracy (touch press) remained undisturbed and unaffected (Fig. 3.7). However, with the robot co-worker, this is true only when the robot head and torso were visible, and a robot made biological movements. A slower robot co-worker was able to reduce human performance (in terms of speed and accuracy), while a faster robot co-worker improves it. Recent studies have pointed out that some specialized robots can have an impact on both human performance and motivation during physical [102] and cognitive [36] interactions. However, here in our results, we show that the mere presence of humanoid robots can instigate effects in human performance.

Interestingly, among all six conditions that we examined, we only observed the effect on the movement frequency when the head and torso of the co-worker (both human and robot) was visible to the participants (Fig. 3.6), Mainly in

human co-worker condition and robot co-worker condition, suggesting that the human form plays a determining role for these effects over the biological nature of the movements made. Instead of using a traditional robotic manipulator, we primarily investigated the effect of the human form by covering the head and torso of the humanoid robot due to two main reasons. Firstly, this allowed us to test the identical physical appearance of the robotic arm and its movement between the conditions robot co-worker and robot covered co-worker. Therefore we ruled out the possibility of not having this effect in robot covered co-worker condition is mere because of two different robots were used. Secondly, this also allowed us to clarify that induction of motor contagions, and its effect is not influenced by the *presence of a humanoid co-worker* or that participants were aware of it, but rather by the visibility of head and torso of the humanoid robot co-worker. By using a traditional manipulator, both of these issues would have been remained unclear. However, these results gave us and other new opportunities for several new questions to be researched in the near future. First, we now know that the visibility of the head and torso of a humanoid modulates the motor contagions in the human co-worker, but the reasons behind this are still unclear. We could argue that this effect is probably related to aspects of saliency as the torso not only occupies a more substantial visual field but (especially the head and the eyes) also probably attract participant attention when present. Second, we examined the conditions when the head and torso remained static in our task while the robot co-worker made predominantly arm movements. At this point, it remains to clarify how the torso movements would affect contagions. While we believe, if the torso moves in a task, then the effect of the torso's visibility should increase as well. Finally, here both the participants and co-workers (human and humanoid robot HRP-2Kai) performed the same task and we analyzed their behaviour in it, although this would be very interesting to examine how the contagions manifest in settings where the co-workers and participants work on different tasks, including non-industrial task that is explicitly collaborative, or competitive.

Quantitatively speaking, our observed trends were highly significant but not substantial. However, these trends were noticeable to increase within our participants, especially with their participant's robot experience (Fig. 3.8). This suggests that they can prevail over a long time and are thus may important in scenarios involving long time robot-human interactions.

In order to moderate or exploit the contagions induced by the humanoid robot co-worker, one can find these results useful for customizing the design of

robot co-workers in industries and sports in future studies. Motor contagions related to body postures or undesirable competitions could affect worker health and psychology in prolong duration but may be minimized by controlling the physical appearance and/or kinematics of robot co-workers, while where ethically valid, contagions may also be used to improve worker performance speed and hence productivity.[2]

[2]The video of this study is available at https://youtu.be/O5ChMWlzZx8

Chapter 4

Proactive whole-body object handover

In previous human-robot interaction studies [54, 97, 101] and also in our work in Chapter 3, we have shown that the human acceptance of the robot co-worker during a task increases when both the appearance and behaviour (motion) of the robot are similar to that of humans; especially during an interactive task. In this study, we also use HRP-2Kai as the robot co-worker.

We discussed our findings in *non-physical* human-robot interaction. Here we introduced a framework particularly focused on intuitive and proactive bi-directional object handover between a human-humanoid dyad using Whole-Body Control (WBC). This study concerns *physical* human-robot interaction (pHRI). We enhance our whole-body motion controller [17] with tasks to achieve bi-directional object handover between human and humanoid robot co-workers. We took inspiration and insights from existing state-of-the-art works in object handover between human-human and human-robot dyads and extended some ideas to bi-manual and locomotion synchronized handovers.

4.1 Handover routine

We take similar approach as [76, 81] and treat the continuous process of object handover between human and humanoid as *sequence*, such that object handover from human to humanoid is one *sequence* and return of object to human is another *sequence*. These two handover *sequence*s make one handover *routine*. An overview of handover *sequence* is illustrated in (Fig. 4.2).

Within the handover routine, both human and robot always start from a standing posture (see Fig. 4.1). The robot standing posture has a Center of Mass CoM(z) height 0.87 meters. We assume that human is ready with the intention to handover the object if he/she is holding the object in his/her hand. The only

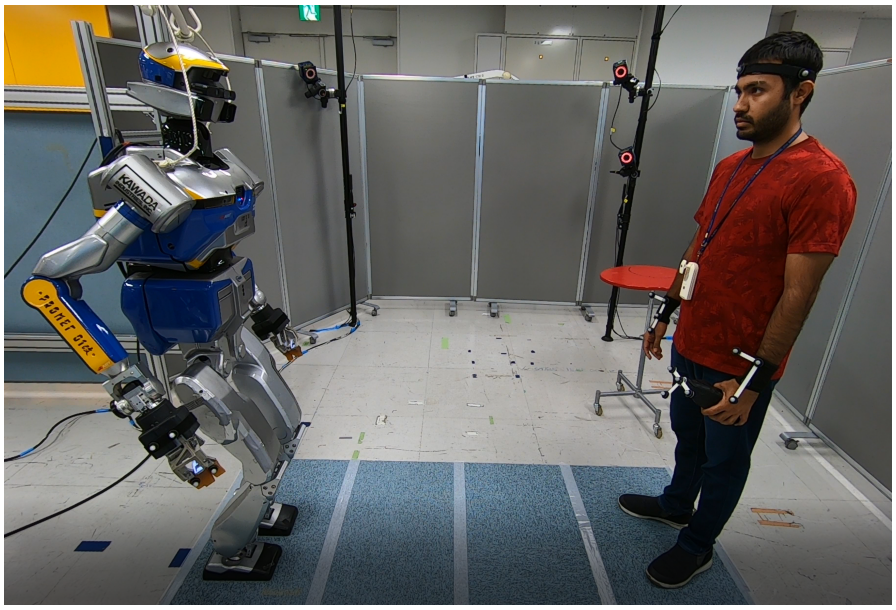

FIGURE 4.1: Human and humanoid starting posture.

predefined condition is that human must seriously exchange the object with a robot in one continuous shot. The human can choose his/her hand configuration, speed, trajectory and the handover location but within the robot's reachable workspace.

During 1st *sequence* of handover *routine*, the human carries the object to different handover locations with distinguishable orientations of the object carrying hand and tries to give the object to the robot. Similarly, during 2nd *sequence* of handover, human approaches somewhere in the robot reachable workspace to receive the object from robot using his/her choice of hand orientation and preferred handover location. The robot end-effectors reachable workspace is given by equation (4.1), object handover can occur as long as estimated handover location is within this region.

$$1 = \begin{cases} X_{\text{min}} <= {}^{h}\mathcal{P}_{\text{ef}}(x) <= X_{\text{max}} \\ Y_{\text{min}} < {}^{h}\mathcal{P}_{\text{ef}}(y) <= Y_{\text{max}} \\ {}^{h}\mathcal{P}_{\text{ef}}(z) >= CoM(z) \end{cases} \tag{4.1}$$

where, ${}^{h}\mathcal{P}_{\text{ef}}$ is the relative 3D position of active human hand `w.r.t` robot end-effector. The default values of X_{min} and X_{max} are 0.1 and 0.8 meters respectively, for robot left end-effector Y_{min} and Y_{max} are 0.15 and 0.75 meters respectively, while for robot right end-effector Y_{min} and Y_{max} are -0.75 and 0.15 meters respectively.

Just like during human-human object handover, another thing that we incorporated in our handover *routine* is to give visual tracking like behaviour to HRP-2Kai by following an object or active human hand using robot's head, depending on the handover *sequence*. Using a `gaze` task (QP tasks), HRP-2Kai follows object during 1st *sequence* of handover and follows active human hand which is approaching to retrieve the object during 2nd *sequence*.

Hereafter and until section (Either hand generalized handover) we will formulate the handover *routine* using human right hand and robot left end-effector; afterwards we will generalize our one-handed handover *routine* for four possible handover combination scenarios:

- **human right hand $\longleftrightarrow$ robot left end-effector**
- human left hand $\longleftrightarrow$ robot left end-effector
- human left hand $\longleftrightarrow$ robot right end-effector
- human right hand $\longleftrightarrow$ robot right end-effector

4.2 Experimental setup

Our experiment setup is shown in (Fig. 4.1). Initially, we started by having a human co-worker and robot co-worker standing comfortably in front of each other at a distance of 1.2 meters from each other. This distance is known to be the social distance in human proxemics [47]. Movable panels partially enclosed the whole setup.

4.2.1 Robot

We used an HRP-2Kai robot [61] as the co-worker. The human and humanoid are free to use their both hands, end-effectors respectively in handing over the objects.

4.2.2 Mocap

We used motion capture (in short *mocap*) system manufactured by (*Motion Analysis Co.,*), to track and get the position data of the passive reflective

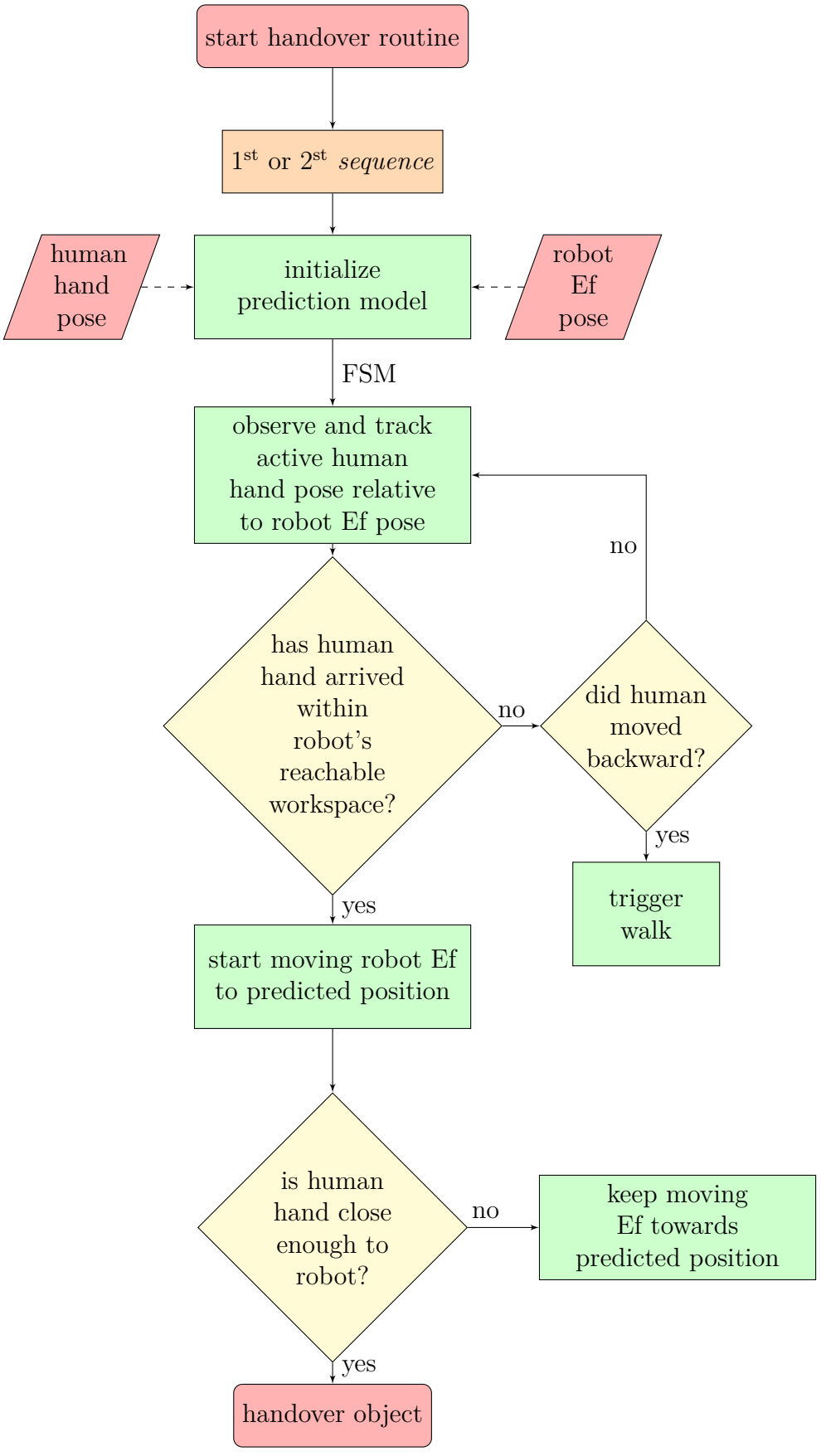

FIGURE 4.2: General overview of human humanoid handover *sequence*. 1st (human has object) or 2nd (robot has object).

markers. We used twenty passive reflective markers in several handover scenarios. We placed four markers on each end-effectors, three markers were placed on the head of the human co-worker to get his/her position in mocap frame, three markers were placed on each of the hands of a human co-worker and also on the object itself. The markers on the human hands and object were utilized to get their respective position, and orientation in the mocap frame and we used makers on the robot end-effectors during object handover and release-return of object from the robot grippers to human co-worker as a substitute to lack of haptic feedback, see section (Interaction forces model) for more details. These passive markers were tracked using ten kestrel infra-red cameras, each at 200 Hz. These mocap markers position data was utilized using a real-time interface between mocap system (`cortex`) and `ROS` called *ros-cortex-bridge*, which was designed to transmit this position data to the robot controller in real-time.

4.2.3 Handover object(s)

As shown in (Fig. 4.3), we used three easily distinguishable objects during the one-handed handover between the human-humanoid dyad. The mass of objects varies from 0.22 kg to 1.1 kg.

FIGURE 4.3: Distinguishable shape and mass objects used during one-handed handover between human and humanoid co-worker.

4.3 Robot QP controller

We used our research group's native multi-objective Quadratic Programming (QP) [106] based low-level Whole-Body Control (WBC) to govern and optimize the motion of HRP-2Kai. "WBC exploits the full potential of the entire floating based robot body and allows interaction with the environment using multi-contact strategies". It also allows concurrent execution of several tasks at once, for example using WBC, the humanoid can utilize one or both of its end-effector(s) to grasp and manipulate the object while at the same time takes a step forward or backward, allowing itself to reach the handover location.

To realize human, humanoid bi-directional object/tool handover, we introduced several tasks and formulated them in a quadratic fashion, so it conforms with QP based controller. The QP enables whole-body control of our HRP2-Kai while respecting both internal and external constraints. Few such constraints encompass joints limits, force and torque limits, contact constraints, stability constraints such as keeping the centre of mass (CoM) inside the support polygon along with self-collision constraints with the environment and itself while generating optimal joint trajectories. Below we mentioned some significant constraints that a robot must satisfy at each time step during human-robot object handover.

4.3.1 QP constraints

The QP controller's objective is to compute an acceleration of $\ddot{q}$, where q is the robot configuration vector at each time step (dt) to achieve a set of targets or tasks. At each dt, the QP is formulated and solved by the LSSOL solver [44]. The tasks are formulated either linear constraints or quadratic costs [106]. However, we want to solve these tasks in a best possible manner as a linearization of some tasks may not be feasible or maybe conflicting, therefore using least-square approximation, the quadratic cost c corresponding to a task $\mathscr{T}_i = 0$ is given by:

$$c_i(q, \dot{q}, \ddot{q}) = \frac{1}{2}\left\| J_i\ddot{q} + \dot{J}_i\dot{q} - \ddot{\mathscr{T}}_i \right\|^2 \tag{4.2}$$

where J_i the Jacobian matrix of $\mathscr{T}_i$, and the quadratic objective function of QP controller would be,

$$\min_{\ddot{q},\tau,f} \sum_{i \in O} \omega_i c_i(q, \dot{q}, \ddot{q}) + \omega_f \|f\|^2 \tag{4.3}$$

which is subject to constraint on equation of motion, as well as other below mentioned constraints,

$$M(q)\ddot{q} + N(q, \dot{q}) = J_c^T f \tag{4.4}$$

where f is the set of contact forces, M denotes the inertial matrix of the robot, N accounts for Coriolis and gravity effects, J_c is the Jacobian matrix of all points of contact.

The QP objective function in equation (4.3) is made of two terms and the tasks $\mathscr{T}_i$ mentioned in next subsection (QP tasks) are weighted against each other by weight w_i based on their relative importance and priority. While the damping weight w_f ensures the smoothness and uniqueness of solution by keeping Hessian matrix positive definite.

1. Static equilibrium:

   $\underline{\tau} \leq J^i(q_i)^T f_i - g^i(q_i) \leq \overline{\tau}$

   where sub-script or super-script i is the i-th robot, q_i is the i-th robot configuration vector, f_i is the set of contact forces vector of i-th robot, J is the Jacobian matrix of all points of contact forces, and $\overline{\tau}$ and $\underline{\tau}$ are the maximum and minimum steady state torque limits respectively, and g be the gravity constant.

2. Joint limits:

   $\underline{q_i} \leq q_i \leq \overline{q_i}$

   $\underline{q_i}$ and $\overline{q_i}$ are the lower and upper limits for robot joints.

3. Self collisions:

   $\delta(X_j^i(q_i), X_k^i(q_i)) > \epsilon_{jk} \qquad \forall (j,k) \in \mathscr{I}^i_{\text{self collision}}$

   δ is the function of distance, $X_j^i(q_i)$ is the occupied volume by j-th body of robot in configuration q_i, ϵ_{jk} is the pair of user select minimum distances (j,k) and $\mathscr{I}^i_{\text{self collision}}$ is the robot sets of self collision pairs.

4. Environment collision:

   $\delta(X_j^i(q_i), X_k) > \epsilon_{jk} \qquad \forall (j,k) \in \mathscr{I}^i_{\text{robot environment}}$

   $\mathscr{I}^i_{\text{robot environment}}$ is the set of robot environment (object) collision pairs.

5. Contact Constraint: $\mathscr{I}_{\text{contact}} = J_i(q)(\dot{q}_{s(k)} - \dot{q}_{p(k)}) = 0$
   The objective of this constraint is to maintain a null velocity [83] between the joints of bodies in contact, where $p(k)$ and $s(k)$ are the predecessor and successor bodies of a robot(s) in contact that imposes a constraint [38].

4.3.2 QP tasks

As mentioned earlier, below, we introduced the following outlined tasks to the multi-objective QP controller to achieve safe and reliable human-robot object handover. Let function $\mathscr{T}_i(q)$ denote the geometric objectives (task error) that we require to regulate to zero or maintain above zero, i.e. $\mathscr{T}_i(q) = 0$ and $\mathscr{T}_i(q) \geq 0$.

1. Posture task: $\mathscr{T}_{\text{posture}} = q_d - q = 0$
   Posture task is the first task that is added to the QP controller, it allows the robot to maintain an initial posture.

2. Com task: $\mathscr{T}_{\text{CoM}} = \text{CoM}_d - \text{CoM}(q) = 0$
   Com task is used in conjunction with the stability constraint to all time maintain the CoM position inside the support polygon.

3. Joint limit task: $\mathscr{T}_{\text{jlim}} = \underline{q_i} \leq q_i \leq \overline{q_i}$
   This task is used occasionally whenever there is a need to limit certain joint movements.

4. Position task at body k: $\mathscr{T}_{\text{pos}} = r_k^d - r_k(q) = 0$
   Where, r_k and r_k^d are the current and desired position of i-th robot k-th body. Robot end-effector position task is used to reach the desired handover location [106].

5. Orientation task at body k: $\mathscr{T}_{\text{ori}} = Err((E_k^d), E_k(q))$
   Where, E_k is the orientation of i-th robot body to world. Robot end-effector orientation task is used to compute orientation relative to human hand orientation.

6. Gaze task : $\mathscr{T}_{\text{gaze}} = u_{\text{target}} - u = 0$
   Where, u_{target} and u are the target vector in world and body vector that needs to be oriented respectively. We used gaze task to orient the head joints of HRP-2Kai towards the active human hand position in the world;

more details can be found in [91]. Note that by active human hand we meant by either object carrying human hand during human-to-robot handover trial or by the hand which is approaching to grasp the object during robot-to-human handover trial.

4.4 Notations

Let $\mathcal{M}$ (Mocap) and $\mathcal{R}$ (Robot) be the two fixed frames with the same orientation that represent both Cartesian coordinate systems and Plücker coordinate systems denoted by X in the Euclidean space. Both $\mathcal{M}$ and $\mathcal{R}$ are defined by their position and orientation of a Cartesian frame, such that ${}^{M}X_{R}$ denotes the Plücker coordinate transform which depends only on the position and orientation of frame $\mathcal{M}$ relative to frame $\mathcal{R}$ (see Fig 4.4).

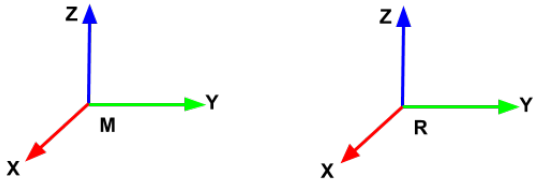

FIGURE 4.4: $\mathcal{M}$ and $\mathcal{R}$ Cartesian coordinate systems.

- We used 6D spatial vectors to express the pose of human hands and robot end-effectors as well as objects. We, therefore, adopt a 6D notation based on spatial vectors, which was explained in Chapter 2 of [38].

- One can receive and control the robot end-effector current orientation ${}^{\text{ef}}\mathcal{O}_{R} \in \mathbb{R}^{3\times3}$ and current position ${}^{\text{ef}}\mathcal{P}_{R} \in \mathbb{R}^{3}$ respectively in the $\mathcal{R}$ frame, by using QP's `Orientation` task and `Position` task (see subsection QP tasks), therefore,

$$ {}^{\text{ef}}X_{R} = \begin{bmatrix} {}^{\text{ef}}\mathcal{O}_{R} & {}^{\text{ef}}\mathcal{P}_{R} \end{bmatrix} \tag{4.5} $$

- Likewise, ${}^{h}\mathcal{O}_{M} \in \mathbb{R}^{3\times3}$ and ${}^{h}\mathcal{P}_{M} \in \mathbb{R}^{3}$, denotes the human hand h orientation and position respectively in the $\mathcal{M}$ frame, obtained from the **L** shape body (see Fig. 4.5), which is later further explained in section (Grasp configuration

model),

$$ {}^{h}X_{M} = \begin{bmatrix} {}^{h}\mathcal{O}_{M} & {}^{h}\mathcal{P}_{M} \end{bmatrix} \tag{4.6} $$

- ${}^{h}\mathcal{O}_{\text{ef}} \in \mathbb{R}^{3\times3}$ and ${}^{h}\mathcal{P}_{\text{ef}} \in \mathbb{R}^{3}$ respectively, denotes the human hand h orientation and position relative to robot end-effector,

$$ {}^{h}X_{\text{ef}} = \begin{bmatrix} {}^{h}\mathcal{O}_{\text{ef}} & {}^{h}\mathcal{P}_{\text{ef}} \end{bmatrix} \tag{4.7} $$

- Let ${}^{o}\mathcal{O}_{M} \in \mathbb{R}^{3\times3}$ and ${}^{o}\mathcal{P}_{M} \in \mathbb{R}^{3}$, denotes the object orientation and position respectively in the $\mathcal{M}$ frame, obtained from another **L** shape body (see Fig. 4.5) attached on the object.

$$ {}^{o}X_{M} = \begin{bmatrix} {}^{o}\mathcal{O}_{M} & {}^{o}\mathcal{P}_{M} \end{bmatrix} \tag{4.8} $$

- For convenience, we formulated the problem with a common origin O, such that $\mathcal{R} \equiv M$ (both frames are located between the feet of robot HRP-2Kai), therefore, we can get human hand pose `w.r.t.` or relative to robot end-effector

$$ {}^{h}X_{\text{ef}} = {}^{h}X_{M}\,{}^{\text{ef}}X_{R}{}^{-1} \tag{4.9} $$

- otherwise, when $\mathcal{R} \neq M$, using Plücker transform ${}^{M}X_{R}$,

$$ {}^{h}X_{\text{ef}} = {}^{h}X_{M}\,{}^{\mathbf{M}}\mathbf{X}_{\mathbf{R}}\,{}^{\text{ef}}X_{R}{}^{-1} \tag{4.10} $$

Note that, the mathematical notations in the following sections follow ISO guidelines. The Euclidean distance is represented in meters. The time unit is set in seconds or mentioned otherwise.

4.5 Position prediction model

In case of object handover and when the human co-worker is ready with the intention to handover the object, instead of merely waiting for the object to be presented by the human at the handover location, the robot must proactively plan its own movements by observing past and predicting near-future human hand movements so that it could arrive at the human chosen handover location

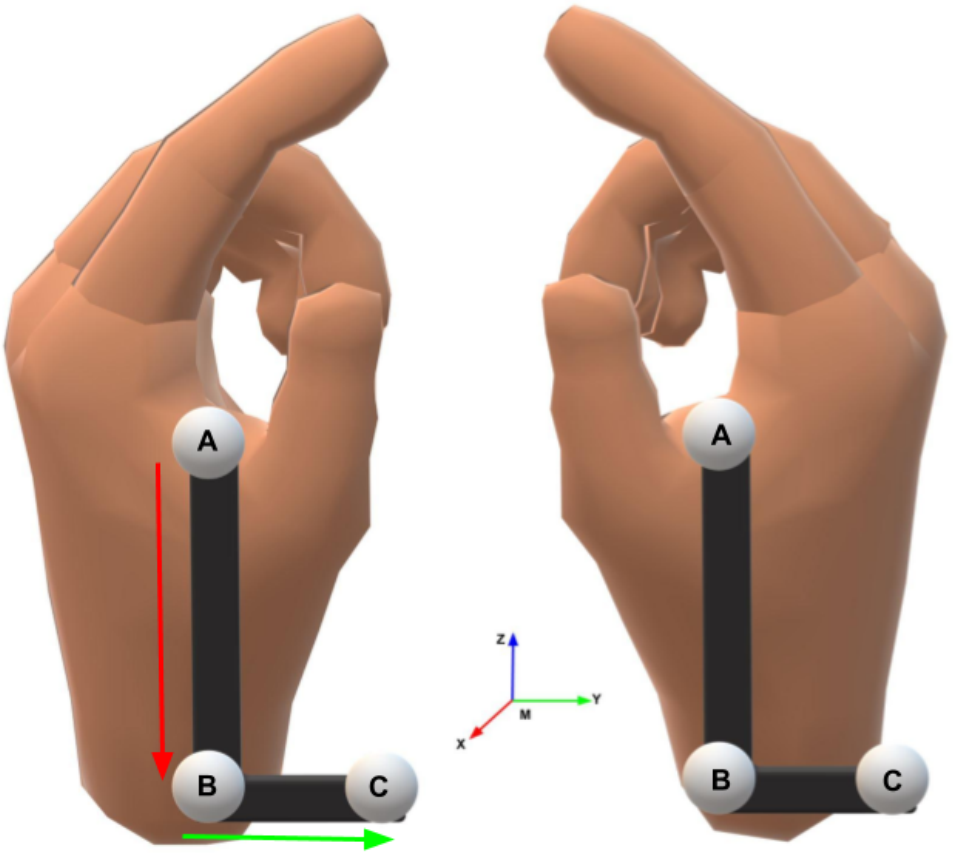

FIGURE 4.5: **L** shape rigid body on the human hand(s)

approximately at same time —either to receive or return the object. Therefore, the estimation of handover time, as well as the approximation of handover location, must be realized early during the handover *sequence*. Note that this proactive nature of the robot co-worker should also be available when the human co-worker requests for the object.

Here we designed a prediction model, with robot left end-effector pose ${}^{\text{ef}}X_R$ (4.5) and human hand mocap marker position ${}^{h}\mathcal{P}_M$ (4.6) as inputs. Note that for simplicity, we formulated the problem with a common origin O, such that frame $\mathcal{R} \equiv M$. To get the position and orientation of the human hand, we placed a rigid body with a shape similar to an alphabet **L** on the wrist of a human hand(s) and on the object as shown in (Fig. 4.5). The three mocap markers A, B and C make up the three vertices of **L** shape body. Note that from onward by ${}^{h}\mathcal{P}_M$ we would mean the position of point A on the **L** shape body as the human hand marker position (Fig. 4.5).

The prediction model behaviour can be tuned by two initially required constant sample size, i_{observe} —a predefined sample size required to observe the motion of

the human hand and i_{predict} —required to predict the human hand position in advance.

In order for the handover between human and humanoid to be smooth and intuitive, the robot needs to proactively estimate the near future position of human hand in advance, during both *sequence*s when robot act as receiver (1^{st} *sequence*) or when robot acts as giver (2^{nd} *sequence*) of a handover *routine*. Therefore we formulate the movements of the human hand as a constant velocity based linear motion model to predict his/her hand (hence handover) position continuously. The robot observes human hand movements for a predefined sample size i_{observe} along with the average velocity of his/her hand during that time and then predicts the near future human hand movement direction and position using equations (4.11) and (4.12) for the predefined i_{predict} sample size.

$$ {}^{h}\bar{\mathcal{V}}_{M} = \frac{1}{i_{\text{observe}}} \sum_{j=1}^{j=i_{\text{observe}}} ({}^{h}\mathcal{P}_{M}(j) - {}^{h}\mathcal{P}_{M}(j-1))/dt \tag{4.11} $$

$$ {}^{h}\mathcal{P}_{M}(i_{\text{predict}}) = {}^{h}\bar{\mathcal{V}}_{M} \cdot (i_{\text{predict}} - i_{\text{observe}}) \cdot dt + {}^{h}\mathcal{P}_{M}(i_{\text{observe}}) \tag{4.12} $$

where dt is controller run-time, in our case it is 5ms as mentioned earlier in the section (Robot QP controller). j in equation (4.11) is sample index. ${}^{h}\bar{\mathcal{V}}_{M}$ is the average human hand movement velocity during i_{observe} sample size. ${}^{h}\mathcal{P}_{M}(i_{\text{predict}})$ is the predicted position of human hand at i_{predict}. The prediction model updates and converges itself over time and in doing so updates the robot end-effector position towards the active human hand, upon condition if predicted position is within the robot end-effector's reachable workspace.

Recalling equation (4.9) or (4.10), the updated translation component of plücker transformation ${}^{h}X_{\text{ef}}$, which provides the predicted position of human hand with respect to robot end-effector in the robot coordinate system is given by (4.13).

$$ {}^{h}X_{\text{ef}}(i_{\text{predict}}) = {}^{h}X_{M}\,{}^{M}X_{R}\,{}^{\text{ef}}X_{R}{}^{-1} \tag{4.13} $$

where, ${}^{M}X_{R}$ is the Plücker coordinate transform frame $\mathcal{M}$ relative to frame $\mathcal{R}$, if $\mathcal{R} \neq M$.

Finally, the handover location is estimated based on the human hand predicted position when the following conditions satisfy (4.14), that is when the human hand velocity is minimum and robot end-effector is closest to the human hand.

$$\begin{cases} \left\| {}^{h}\bar{\mathcal{V}}_{M} \right\| & <= 1e^{-2} \\ \left\| ({}^{h}\mathcal{P}_{M}(i_{\text{predict}}) - {}^{\text{ef}}\mathcal{P}_{R}) \right\| & <= 2e^{-2} \end{cases} \tag{4.14}$$

where, ${}^{h}\mathcal{P}_{M}(i_{\text{predict}})$ is the desired position for robot end-effector to reach and ${}^{\text{ef}}\mathcal{P}_{R}$ is the actual current position of robot end-effector and also both positions are in same frame or transformed otherwise. We have also explained the procedure of predicting human hand position and estimating handover location in Algorithm (1) of (Appendix: Handover).

In this section, we presented how to predict and estimate the handover location, though just by knowing the handover location in space is not enough for an optimal smooth handover of an object. Therefore in next section (Grasp configuration model), we will present the orientation component of ${}^{h}X_{\text{ef}}$ which gives the graspable relative orientation of robot end-effector `w.r.t` human hand or object orientation during handover.

4.6 Grasp configuration model

To take into account comfort and requirement of the human co-worker, it is pivotal for the robot to be able to find the most appropriate configuration to grasp (as *receiver*) or release (as *giver*) the object [6, 23]. Therefore for an intuitive and smooth handover of an object, the robot should relatively orient it's end-effector and configure according to the orientation of either object (1^{st} *sequence*) or human hand (2^{nd} *sequence*) during the handover *routine*. Though there are several possible configurations to handover an object, the robot must determine the correct configuration of its end-effector during the handover which is suitable and comfortable enough for the human and could be perceived natural in the eyes of a human co-worker. Note that in this study, we mainly chose to handover the object in which it is most commonly being grasped (default configuration) hence natural to the eyes of the human, one example would be holding an object such as a water bottle when its cap is in the upright position during the handover.

We propose a simple method to get the desired object grasping orientation of robot end-effector either by considering the relative orientation of the active human hand or the object itself. This handover grasp configuration model consists of two

sub-models, in first sub-model, we determine the orientation of the active human hand or object itself. In the second sub-model, we utilize the first sub-model to continuously get the desired relative orientation of the robot end-effector during the handover *routine*.

To determine the object or active human hand orientation, as mentioned in previous section we placed an **L** shape rigid body on the wrist of the human hand(s) and a similar one on the object as well such that during the object handover scenario, vector $\vec{AB}$ along the longer side and vector $\vec{BC}$ along the shorter side of the **L** shape are set to be parallel with the X-axis and Y-axis of the mocap frame $\mathcal{M}$ respectively, as well as orthogonal to each other (as shown in Fig. 4.5). For simplicity, let us consider $\hat{x}$ be the unit vector, which is parallel and along the X-axis and likewise a unit vector $\hat{y}$ is parallel and along the Y-axis of the mocap frame $\mathcal{M}$, such that

$$\hat{x} = \frac{\vec{AB}}{\left\|\vec{AB}\right\|}$$

$$\hat{y} = \frac{\vec{BC}}{\left\|\vec{BC}\right\|}$$

Let ${}^{h}\mathcal{O}_{M}$ in equation (4.6) be the rotation matrix representing the orientation of human hand (or object) in the mocap frame $\mathcal{M}$ and since $\hat{x} \in \mathbb{R}^3$ and $\hat{y} \in \mathbb{R}^3$ are the two orthogonal unit vectors of an **L** shape body on each human hand (Fig. 4.5), therefore a cross product of them would result in another unit vector $\hat{z} \in \mathbb{R}^3$ which is also orthogonal to both $\hat{x}$ and $\hat{y}$. Also using right-hand rule, one can easily get the direction of the unit vector $\hat{z}$ by given equation (4.15).

$$\hat{z} = \hat{x} \times \hat{y} \tag{4.15}$$

Furthermore, to represent the orientation of human hand in $\mathbb{R}^{3\times3}$, we used these unit vectors $\hat{x}, \hat{y}$ and $\hat{z}$ as columns of the rotation matrix ${}^{h}\mathcal{O}_{M}$ [7, 34, 57] in equation (4.16), such that these unit vectors $\hat{x}, \hat{y}$ and $\hat{z}$ represent human hand (or object) orientation around the $roll - pitch - yaw$ axes, respectively.

$${}^{h}\mathcal{O}_{M} = \begin{Bmatrix} \hat{x}.x & \hat{y}.x & \hat{z}.x \\ \hat{x}.y & \hat{y}.y & \hat{z}.y \\ \hat{x}.z & \hat{y}.z & \hat{z}.z \end{Bmatrix}_{3\times3} \tag{4.16}$$

Therefore, the pose (4.6) of active human hand or object can be determined using equations (4.12, translation) and (4.16, orientation). Recalling again that active human hand is the one that carries the object during 1st *sequence* or the hand which is approaching to grasp the object during 2nd *sequence* of a handover *routine*.

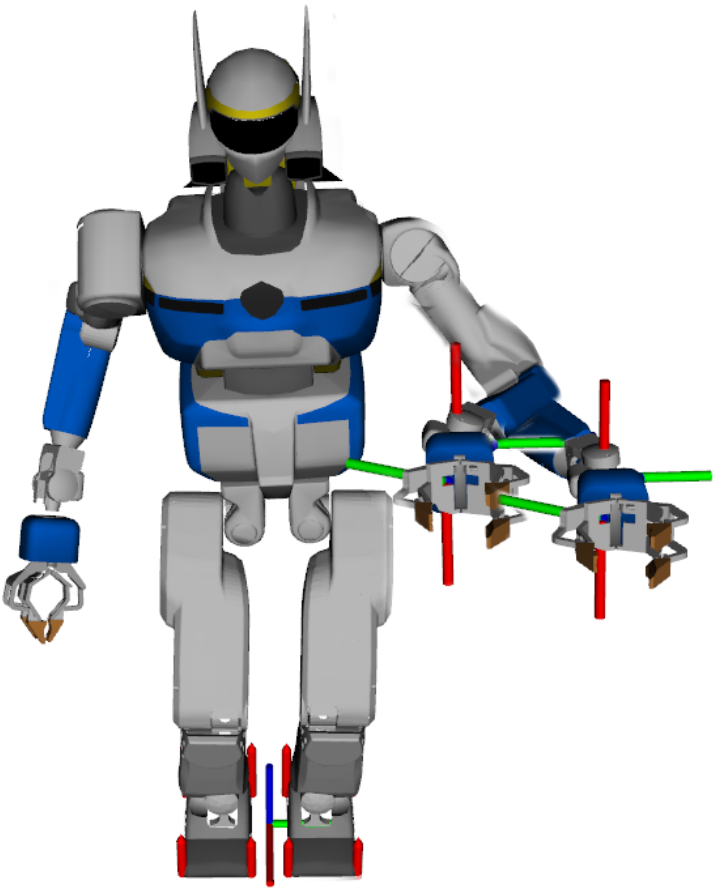

FIGURE 4.6: Some possible fixed orientation of HRP-2Kai (left end-effector) during the handover trials in the robot frame $\mathcal{R}$

HRP-2Kai lacks conventional anthropomorphic hands, but instead it has gripper (Fig. 4.6) alike hands [62, 100] mainly to increase the manipulability. In this second sub-model, to continuously determine the desired grasping configuration of robot end-effector during the handover, we were first required to know the fixed initial orientation (default) of the robot end-effector and active human hand, in which object handover is feasible between human and robot co-workers.

Consequently we considered a initial possible scenario where the robot end-effector and active human hand orientations are fixed throughout the handover *routine*, irrespective of the handover *sequence* where robot is a giver or receiver.

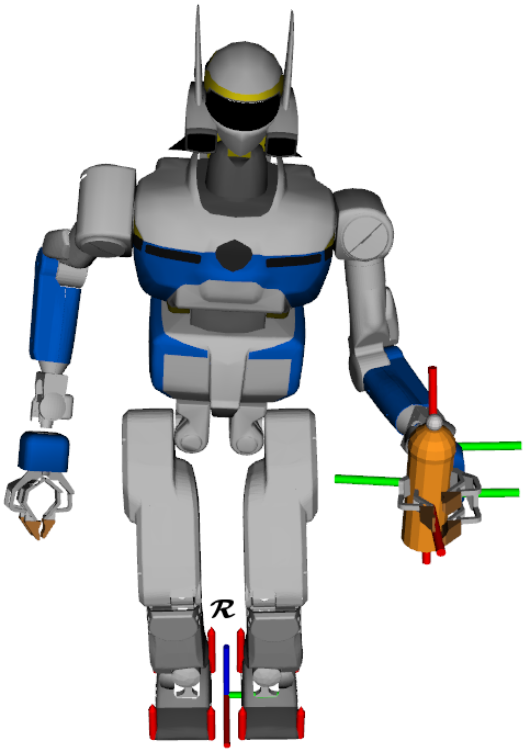

FIGURE 4.7: HRP-2Kai (left end-effector) holding object with fixed orientation during handover in the robot frame $\mathcal{R}$

Let ${}^{\text{efInit}}\mathcal{O}_R$ denote the initial and fixed orientation of the robot end-effector in the robot frame $\mathcal{R}$ as shown in (Fig. 4.6, and Fig. 4.7). Whereas, let ${}^{\text{hInit}}\mathcal{O}_M$ be the fixed grasping configuration of human hand determine by the equation (4.16), such that both,

$$\begin{cases} {}^{\text{efInit}}\mathcal{O}_R \subset {}^{\text{ef}}\mathcal{O}_R \\ {}^{\text{hInit}}\mathcal{O}_R \subset {}^{h}\mathcal{O}_M \end{cases} \tag{4.17}$$

Note that both of these fixed subsets in equation (4.17) of handover grasping configuration for human and robot co-workers are selected before the handover *routine* based on the known physical, structural properties of the object. Since by knowing the object shape, it is possible to determine how a human co-worker would initially grasp the object in its default configuration, assuming that particular grasp is what seemed natural and comfortable to the human co-worker. Also as the active human hand (which grasps the object) has **L** shape body on the wrist, therefore prior to initiating the handover *routine* when human co-worker grasps the object, one can find the ${}^{\text{efInit}}\mathcal{O}_R$ by aligning the vector $\vec{AB}$ and $\vec{BC}$ of active human hand **L** shape with the global X-axis and Y-axis respectively.

Now, during the handover *routine* to correctly transform desired human hand orientation into robot end-effector frame, we further utilize the equation (4.13). Using QP's `Orientation` task [78, 106] (see subsection QP tasks) and compute the task error Err between *current* human hand orientation ${}^{h}\mathcal{O}_{M}$ obtained using equation (4.16) and *fixed* robot end-effector orientation ${}^{\text{efInit}}\mathcal{O}_{R}$, the resulting orientation from the `Orientation` task is the desired robot end-effector orientation relative to the human hand orientation (see Fig. 4.8, for few of many possible orientations).

Therefore using fixed orientation component ${}^{\text{efInit}}\mathcal{O}_{R}$ and current human hand orientation ${}^{h}\mathcal{O}_{M}$ from equation (4.16) derived in first sub-model, we further modify equation (4.13) to get the desired orientation ${}^{h}\mathcal{O}_{\text{ef}}$ of robot end-effector during the handover *routine*.

$$\begin{bmatrix} {}^{\mathbf{h}}\mathcal{O}_{\text{ef}} & {}^{h}\mathcal{P}_{\text{ef}} \end{bmatrix} = \begin{bmatrix} {}^{\mathbf{h}}\mathcal{O}_{\mathbf{M}} & {}^{h}\mathcal{P}_{M} \end{bmatrix} \begin{bmatrix} {}^{M}\mathcal{O}_{R} & {}^{M}\mathcal{P}_{R} \end{bmatrix} \begin{bmatrix} {}^{\text{efInit}}\mathcal{O}_{\mathbf{R}} & {}^{\text{ef}}\mathcal{P}_{R} \end{bmatrix}^{-1} \tag{4.18}$$

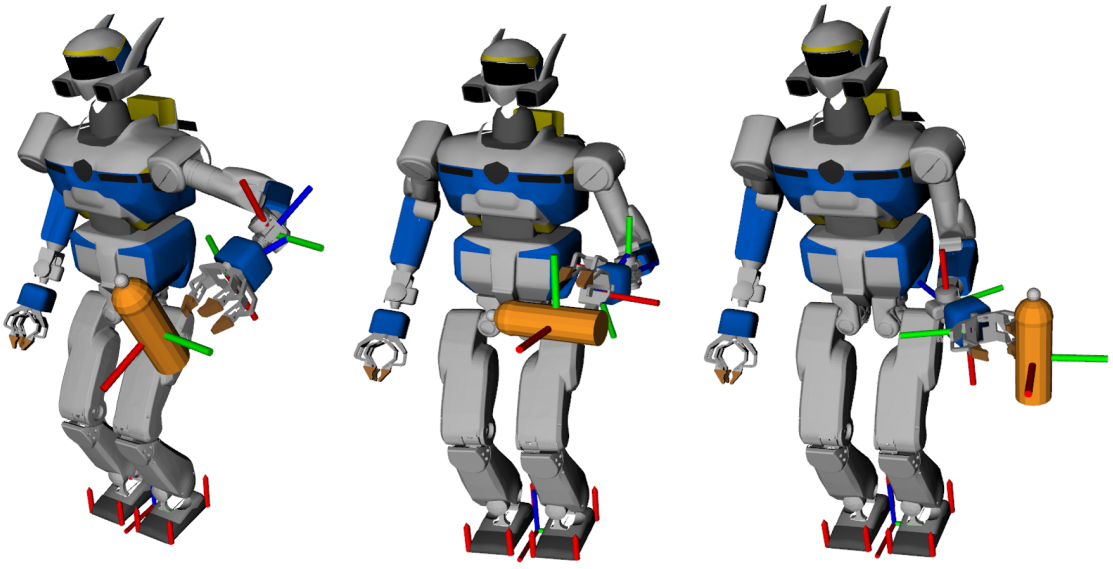

FIGURE 4.8: Robot HRP-2Kai (left end-effector) multiple possible object grasping configurations during the handover trials in the robot frame $\mathcal{R}$.

Finally, one can get the pose of the handover location by using the translation component of ${}^{h}X_{\text{ef}}$ in the equation (4.7) which is updated based on the predicted position of active human hand (see section Position prediction model) while the orientation component is updated based on the relative orientation of object during 1^{st} *sequence* and active human hand during 2^{nd} *sequence* of a handover *routine*.

4.7 Interaction forces model

Another problem that we focused here is related to the *timing* of grasping and releasing the object and minimizing the forces during such interactions. The *timing* at which the robot should close its gripper(s) to grasp the object, if robot tries to close too early to grasp the object when a human co-worker is not ready it can lead to a collision resulting in an accident or if robot waits too long then it may lead to unreliable behaviour. Along with the previously mentioned problem we also address here another issue related with the *magnitude* of interaction forces between human co-worker hand(s) and robot co-worker end-effector(s) holding the object during the release of object in the 2^{nd} *sequence* of handover i.e. when robot returns the object to the human.

We had to find the equilibrium for the robot to know the appropriate *timing* at which the handover should occur, which would be intuitive and can be perceived natural to the eyes of human (keeping in mind that HRP-2Kai does not have anthropomorphic hands but rather manipulative grippers). At the same time, we needed to come up with a solution to keep the *magnitude* of interaction forces at a minimum. We came up with two methods to tackle this problem, one highlights the simplicity and other highlights efficiency, but when used together, we get a reliable and safest solution possible under such a scenario.

HRP-2Kai is equipped with 6-axis *wrist* force sensor on both hands, capable of precisely sensing interaction forces and torques with the environment along x, y, z axes of the sensor local coordinate frame (let us call it s). We designed a model of interaction forces which enable the robot end-effector to interact with the object independent of the knowledge of the object's mass in advance.

4.7.1 Method 1: mocap markers

Without actual haptic sensor feedback information from the robot end-effector, we had to rely on the wrist force sensor and mocap markers data of the robot end-effector (see Fig. 4.9), therefore we used mocap makers in conjunction with the force feedback from the wrist sensor of HRP-2Kai to know whether the object is within its vicinity to grasp or not. Mocap makers on the robot end-effector were crucial to know the relative position of the object from the active human hand holding it and the robot end-effector. We placed four passive infra-red markers on the robot end-effector(s) in rectangular-shaped configuration as shown in (Fig. 4.9,

4.10 and 4.11). Two of the markers were placed parallel and along the local x-axis of force sensor on the wrist of robot end-effector and rest two markers were placed on the gripper tips as shown in (Fig. 4.9).

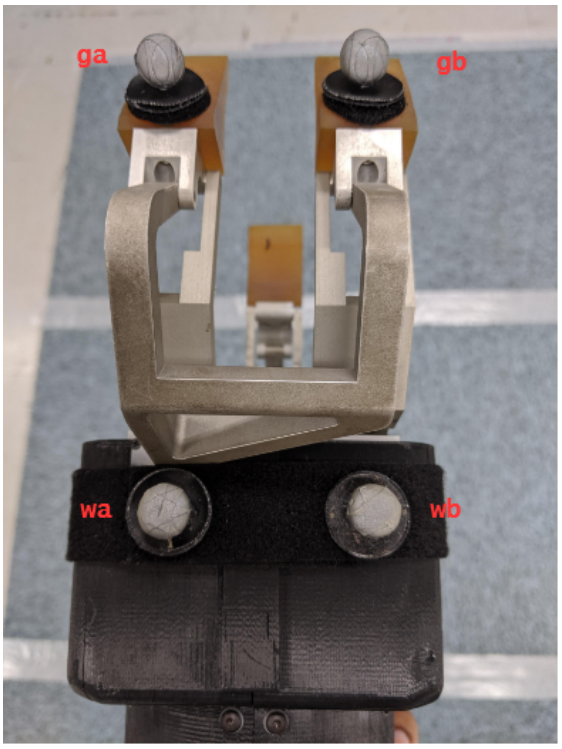

FIGURE 4.9: Passive IR markers on the robot HRP-2Kai right end-effector.

Let $\{{}^{\text{wa}}\vec{P}, {}^{\text{wb}}\vec{P}, {}^{\text{ga}}\vec{P}, {}^{\text{gb}}\vec{P}\} \in \mathbb{R}^3$ be the four position vectors of the mocap markers that are placed on the robot end-effector wrist and gripper tips respectively, also let ${}^{\text{obj}}\vec{P} \in \mathbb{R}^3$ be the position vector of mocap marker that placed on the object as shown in the (Fig. 4.7 and Fig. 4.8). To get the relative position of object and active human hand with respect to robot end-effector, assuming human has the object and is ready with the intent to handover the object. We utilized basic linear algebra and vector products [8, 18, 31] to get the area of triangles $\triangle {}^{\text{wa}}P{}^{\text{wb}}P{}^{\text{ga}}P$, $\triangle {}^{\text{wa}}P{}^{\text{wb}}P{}^{\text{gb}}P$ and $\triangle {}^{\text{wa}}P{}^{\text{wb}}P{}^{\text{obj}}P$ using equation (4.19) such that upon the satisfaction of following conditions in equation (4.21) would give us the relative position of object. Basically we were interested in the output of function $f({}^{\text{obj}}\vec{P})$, this function measures the area of triangles formed by the markers on robot end-effector and the object marker. The positive output means that object is within the graspable reach of robot end-effector and that the robot now is ready to close the gripper.

$$\triangle ABC = \frac{\left\| \vec{AB} \times \vec{AC} \right\|}{2} \tag{4.19}$$

where $\vec{A}$, $\vec{B}$, $\vec{C}$ are the three coordinate vectors of a triangle $\triangle ABC$,

$$f({}^{\text{obj}}\vec{P}) = \begin{cases} (\triangle {}^{\text{wa}}P^{\text{wb}}P^{\text{ga}}P - \triangle {}^{\text{wa}}P^{\text{wb}}P^{\text{obj}}P) > 0 \\ (\triangle {}^{\text{wa}}P^{\text{wb}}P^{\text{gb}}P - \triangle {}^{\text{wa}}P^{\text{wb}}P^{\text{obj}}P) > 0 \end{cases} \tag{4.20}$$

$$if \begin{cases} f({}^{\text{obj}}\vec{P}) == 1, & \text{within graspable reach} \\ f({}^{\text{obj}}\vec{P}) == 0, & \text{object outside gripper} \end{cases} \tag{4.21}$$

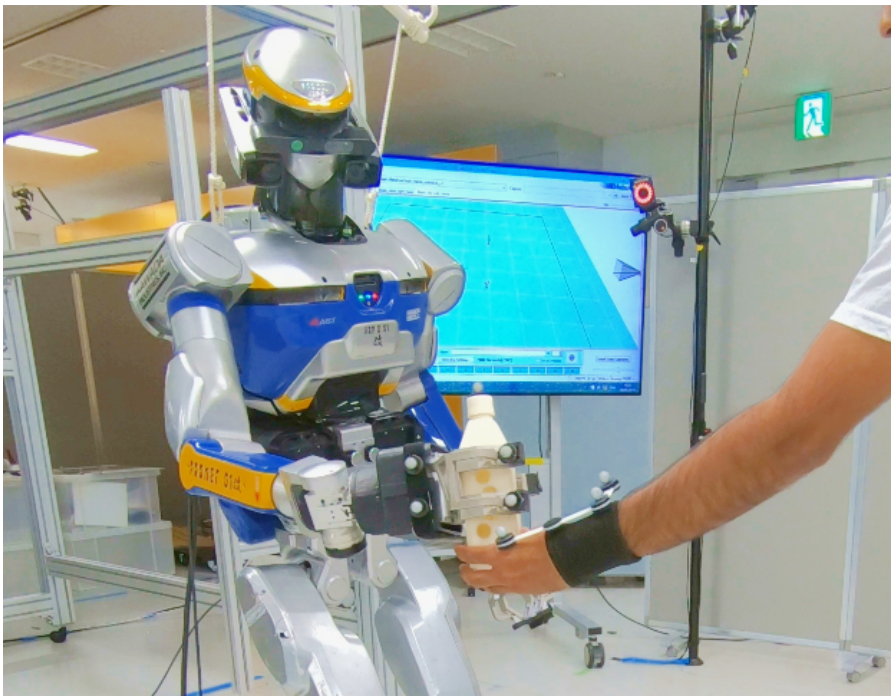

FIGURE 4.10: Passive IR markers on the robot HRP-2Kai right end-effector, human right hand and object during handover.

We explained further in detail in the subsection (Finite state machine), but before that, we mention another (Method 2: surface wrench) that we also utilize for closing gripper when the object is in the vicinity.

4.7.2 Method 2: surface wrench

Just by knowing the relative position of the object `w.r.t` the robot, end-effector gripper is not enough for safe and reliable object handover. As the lack of anthropomorphic hands and the visual features of the manipulative gripper can be intimidating to some humans. Therefore in conjunction to the mocap marker-based method mentioned earlier we also computed ${}^{\text{surf}}\vec{f}$, the *gravity-free*

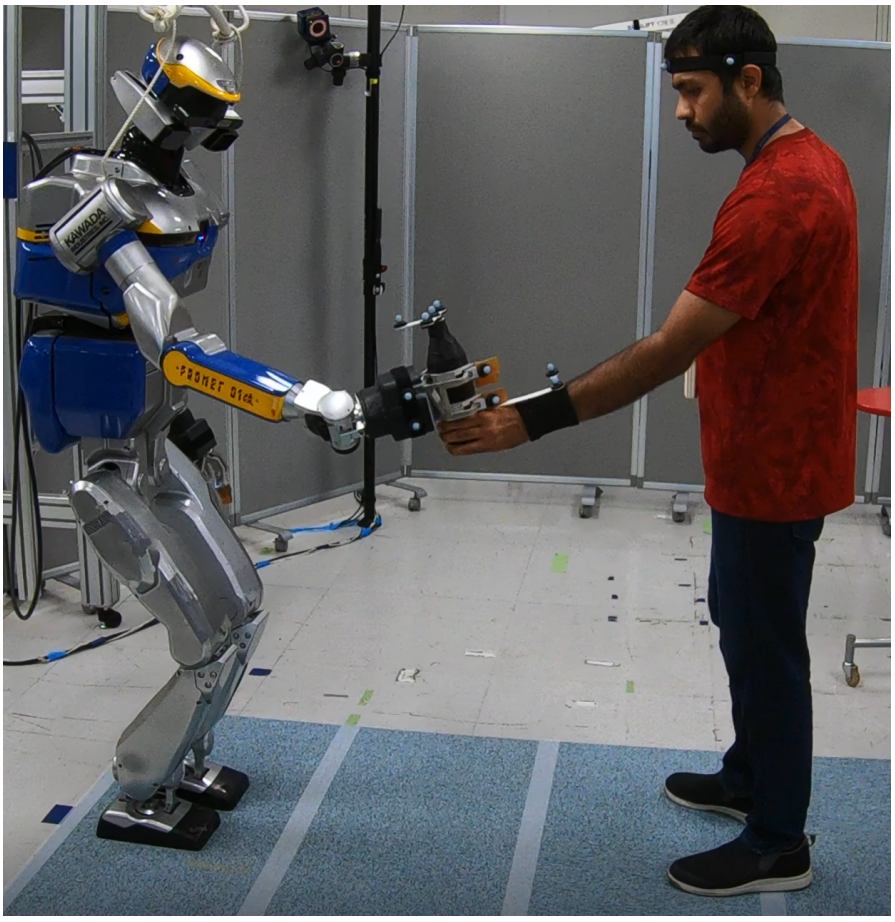

FIGURE 4.11: HRP-2Kai trying to grasp object using right end-effector.

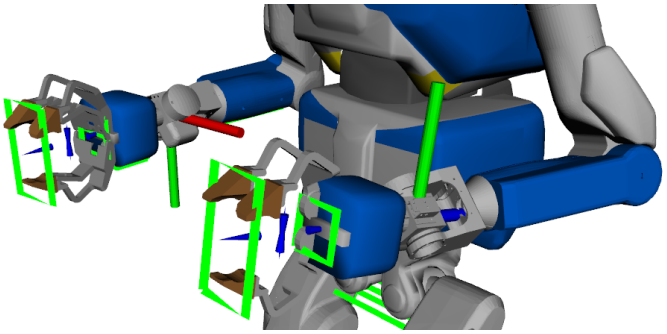

FIGURE 4.12: Virtual intrinsic surfaces (green) on robot wrists.

force vector in the intrinsic surface frame $surf$ of the gripper (see Fig. 4.12). Let ${}^s\vec{f} \in F^6$ denote the *gravity-free* spatial force vector in the local sensor frame s. Note that ${}^s\vec{f}$ has both force and couple components, but we were only interested in the force component. We can easily get the coordinate transformation between the surface frame and force sensor frame, knowing the body at which the force sensor is attached.

$$^{\text{surf}}X_s = {}^{\text{surf}}X_b\, {}^{b}X_s \tag{4.22}$$

where, b denotes the body frame at which the force sensor is attached, in our case force sensor(s) are attached to the wrist(s) of HRP-2Kai.

One can generally obtain the transformation matrix for a force vector as explained in [38] if X is responsible for coordinate transformation on motion vectors then using the equation (4.23), X^* would do the same transformation on force vectors since both are related [38],

$$X^* = X^{-T} \tag{4.23}$$

therefore, force vector in the surface frame $surf$ can be obtained by utilizing equations (4.23) and (4.22), we get

$$^{\text{surf}}\vec{f} = {}^{\text{surf}}X_s^{*s}\vec{f} \tag{4.24}$$

where, $^{\text{surf}}X_s^*$ is the transformation matrix for transformation of force vector from force sensor frame s to gripper intrinsic surface frame $surf$. Finally we measure $\left|^{\text{surf}}\vec{f}\right|$ (after removing initial offset) along the gripper's insertion (z)-axis, during the interaction between object and gripper just prior to handover during 1$^{\text{st}}$ *sequence* and if the measured $\left|^{\text{surf}}\vec{f}\right|$ is greater than 5N along with the outcome of equation (4.20) then it is safe for robot to close the gripper and hence grasp the object. We further explained complete handover *routine* utilizing above discussed methods in the next subsection (Finite state machine).

4.7.3 Finite state machine

The whole handover *routine* is a continuous process but for clarity we have divided it into several transition steps of Finite State Machine (FSM) [58], also (see Fig. 4.14) for graphical implementation and Algorithm (2) of (Appendix: Handover) as well, the transitions between states are set to be continuous upon the success of previous transition. To understand the interaction forces model, let $\vec{\mathcal{F}} \in \mathbb{R}^3$ denote the current *gravity-free* force sensor reading in the robot frame $\mathcal{R}$. During 1$^{\text{st}}$ *sequence* of human to robot handover when human holds the object and starts to approach somewhere with the reachable workspace of robot

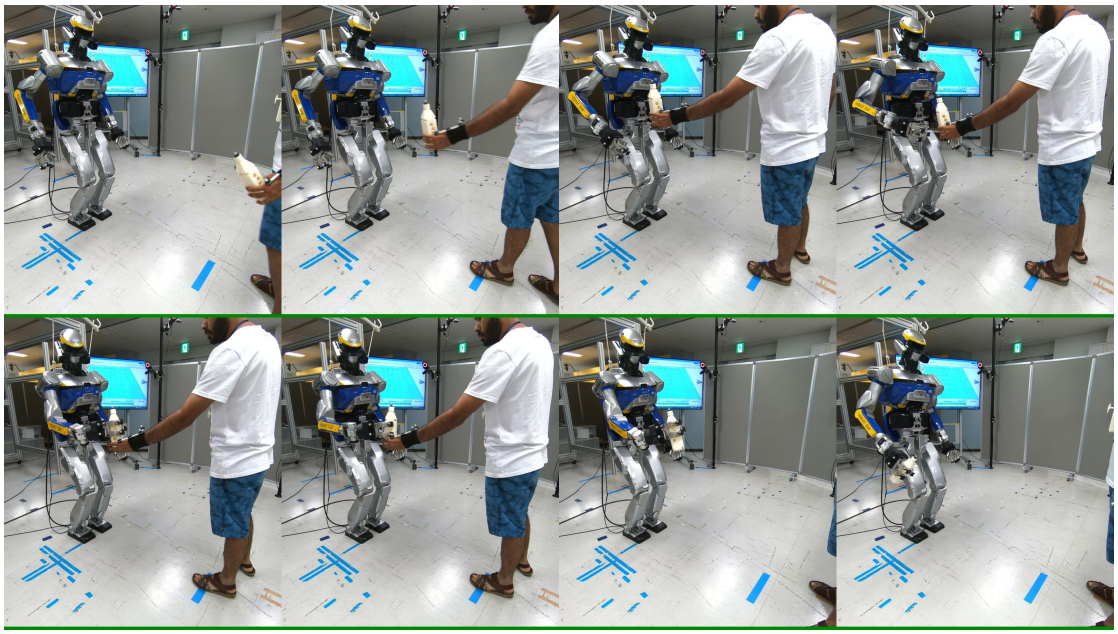

FIGURE 4.13: human to humanoid object handover, t1 to t8 transition states.

to handover the object (see Fig. 4.13), in such a situation due to any acceleration of the robot end-effector while approaching towards the object, a wrist force sensor would only show readings due to the inertial forces [99] that are acting on the robot end-effector, which we termed ${}^{\text{zero}}\vec{\mathcal{F}}$ as force sensor offset reading (see equation 4.25). Let ${}^{\text{obj}}\overline{\mathcal{F}} \in \mathbb{R}^3$ be the average of contact forces between the end-effector (gripper) and the environment (object) during the resting (${}^{\text{ef}}v = 0$) period of robot end-effector along the xyz axes and let ${}^{\text{inert}}\vec{\mathcal{F}}$ be the inertial force acting on the object due to the acceleration (lets call it ${}^{\text{ef}}a$) of robot end-effector when moving towards the predicted pose of human hand during the 2nd *sequence* of handover as shown in (Fig. 4.15). Let ${}^{\text{pull}}\vec{\mathcal{F}}$ be the current *minimum* interaction force exerted on the object by the human co-worker and sensed by the robot wrist force sensor while retreating the object during 2nd *sequence* of robot to human handover and let ${}^{\text{old}}T$, ${}^{\text{new}}T \in \mathbb{R}^3$ be the respective initial default hand-tuned and updated force thresholds. We now explain each state of FSM as shown in (Fig. 4.14).

t0: $\left\| {}^{h}P - {}^{\text{obj}}P \right\| < 0.02$

We start FSM under the assumption that the human co-worker is already grasping the object, and he/she is ready with the intention of handover. ${}^{h}P$ is the position of point A on the **L** shape body as the human hand marker position (see Fig. 4.5).

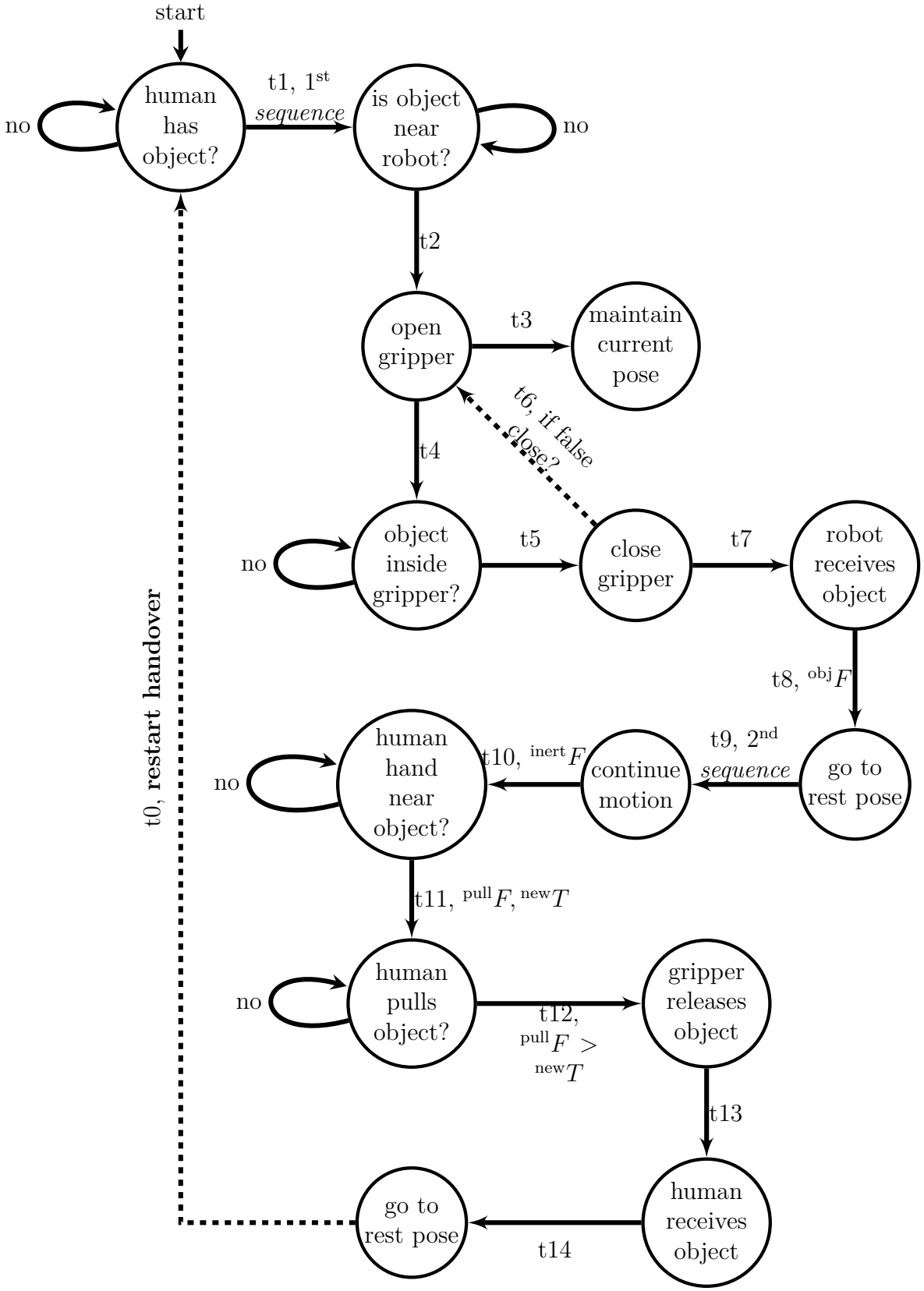

FIGURE 4.14: Overview of human humanoid object handover Finite-State-Machine (FSM)

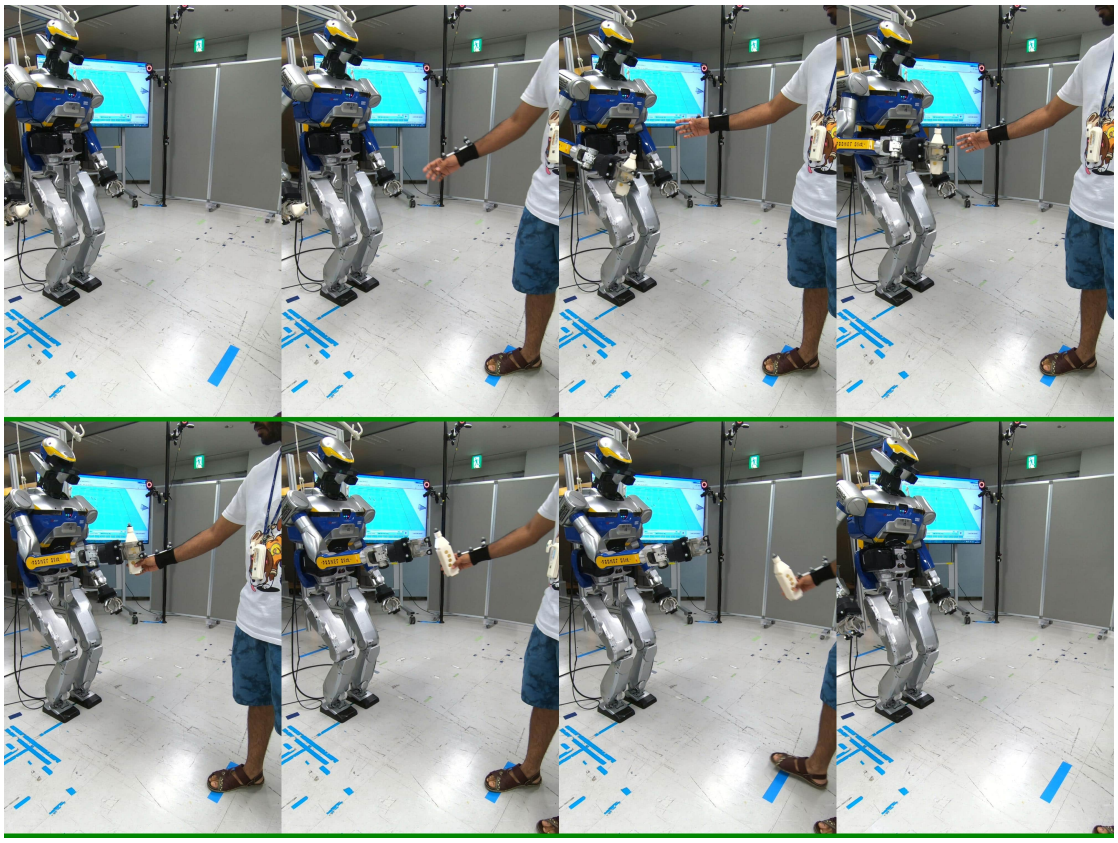

FIGURE 4.15: humanoid to human object handover t9 to t14 transition states.

t1: $\left\| {}^{h}P - {}^{\text{ef}}P \right\| < 0.10$

During 1st *sequence* of handover *routine*, i.e. human to robot object handover. We measure the relative position of human hand and robot end-effector mocap markers, the state transition is successful if the euclidean distance d is less than 0.1 meters, where $d = \left\| {}^{h}P - {}^{\text{ef}}P \right\|$. ${}^{\text{ef}}P$ is the average position of gripper tips marker ${}^{\text{ga}}P, {}^{\text{gb}}P$.

t2: Open Gripper

The robot opens the gripper and presents with its intention to grasp the object.

t3: $\left\| {}^{h}P - {}^{\text{ef}}P \right\| \leq 0.05$, maintain current pose

To avoid collision between robot end-effector and human hand we reduce the end-effector velocity (${}^{\text{ef}}v \simeq 0$) when the interaction distance $d = \left\| {}^{h}P - {}^{\text{ef}}P \right\|$ is less than 0.05 meters. We also measure ${}^{\text{zero}}\vec{\mathcal{F}}$ as force sensor offset during this time.

$$ {}^{\text{zero}}\vec{\mathcal{F}} = \vec{\mathcal{F}} \tag{4.25} $$

t4: $({}^{\text{surf}}\vec{f}(z) \geq 5N) \quad \& \quad (f({}^{\text{obj}}\vec{P}) == 1)$
We declare robot is ready to close the gripper when the object is inside gripper if output of equations (4.21, 4.24) satisfy together.

t5: Close Gripper
Let ${}^{\text{close}}\vec{\mathcal{F}}$ be the measured force reading at the timing of closing gripper.

$$ {}^{\text{close}}\vec{\mathcal{F}} = \vec{\mathcal{F}} \tag{4.26}$$

Robot closes gripper; presumably, the object is grasped as well. However, it is easy to check whether the robot grasps the object or if it is a false close. It is safe to say that its a false close if output of equation (4.21) is 0, along with the condition $\left\| {}^{\text{zero}}\vec{\mathcal{F}} - {}^{\text{close}}\vec{\mathcal{F}} \right\| \simeq 0$, since these are same measured force sensor offsets. Therefore, in such scenario next transition state would be **t6** to open gripper and repeat, otherwise **t7**, as shown in (Fig. 4.14).

t6: Open Gripper due to false close, otherwise,

t7: This transition confirms that the robot receives the object and now the object *mass* can be calculated based on the forces measured during previous states.

$$ {}^{\text{obj}}\overline{\mathcal{F}} = \frac{1}{n}\sum_{i=1}^{i=n} |(|\vec{\mathcal{F}}| - |{}^{\text{zero}}\vec{\mathcal{F}}|)| \tag{4.27}$$

${}^{\text{obj}}\overline{\mathcal{F}}$, is pure force sensor reading when ${}^{\text{ef}}a = 0$ and object is grasped by the robot, n is the low-level controller time-step counter that increments every 5 ms (see subsection Robot QP controller), before transitioning to next state, we intentionally stay on this state for 1 second i.e. until $i == 200$ to measure the average of ${}^{\text{obj}}\vec{\mathcal{F}}$ over 200 samples. Finally, object *mass* can be obtained using equation (4.28).

$$ objMass = \left\| {}^{\text{obj}}\overline{\mathcal{F}} \right\| / 9.80665 \tag{4.28}$$

t8: Go to rest pose
Both human and robot return to their resting posture, with the robot carrying the object. This ends the 1^{st} *sequence* of handover.

t9: 2^{nd} *sequence* begins
Robot to human object handover. The robot continues to predict human

hand position and moves towards it when the human co-worker approaches somewhere within the robot's reachable workspace. During this time, we measure the ${}^{\text{inert}}\vec{\mathcal{F}}$ inertial force acting on the object due to the acceleration of end-effector.

$$ {}^{\text{inert}}\vec{\mathcal{F}} = objMass * {}^{\text{ef}}\overline{a} \tag{4.29} $$

Where, ${}^{\text{ef}}\overline{a}$, is the average acceleration of the robot end-effector.

t10: $\left\| {}^{h}P - {}^{\text{ef}}P \right\| < 0.05$
Once again, we measure the relative position of human hand and robot end-effector mocap markers, the state transition is successful if the euclidean distance $d = \left\| {}^{h}P - {}^{\text{ef}}P \right\|$ is less than 0.05 meters. That means human is ready with the intention to grasp the object.

t11: Human attempts to retrieve the object

$$ {}^{\text{pull}}\vec{\mathcal{F}} = |(|\vec{\mathcal{F}}| - |{}^{\text{inert}}\vec{\mathcal{F}}| - |{}^{\text{zero}}\vec{\mathcal{F}}|)| \tag{4.30} $$

$$ {}^{\text{new}}\vec{T} = {}^{\text{obj}}\overline{\mathcal{F}} + {}^{\text{old}}\vec{T} \tag{4.31} $$

where, ${}^{\text{old}}\vec{T}$ was hand tuned after several attempts with multiple objects. Default ${}^{\text{old}}\vec{T}$ values were set to $[6, 6, 6]$ N, after some preliminary trials.

t12: Open Gripper, human grasps the object if both below conditions satisfy

$$ \begin{cases} \left\| {}^{h}P - {}^{\text{obj}}P \right\| < 0.02 \\ {}^{\text{pull}}\vec{\mathcal{F}} \geq {}^{\text{new}}\vec{T}, \qquad \vee x, \vee y, \vee z \end{cases} \tag{4.32} $$

where, $\left\| {}^{h}P - {}^{\text{obj}}P \right\|$ is again euclidean distance between human hand and object mocap markers.

t13: Object returns to the human co-worker, human retreats.

t14: End of 2$^{\text{nd}}$ *sequence* of handover.
Both human and robot returns to their resting posture, with human carrying the object (see Fig. 4.1).

Finally, this ends the object handover *routine* between human and robot co-workers. Afterwards, we again repeat the handover *routine*, starting with 1st *sequence* of handover.

4.8 Either hand generalized handover

As mentioned in an earlier section (Handover routine), up till now we have discussed human-robot bi-directional object handover under the scenario where robot always uses its left end-effector, and human always uses his/her right hand. However unlike several handover studies in the past [23, 53, 68, 76], we can take the benefit of having a humanoid at our disposal; therefore we further generalize our human-humanoid bi-directional object handover *routine* and extend it by exploiting either human left or right hand and similarly left or right end-effector of robot. Basically we extended our one-handed handover *routine* into four possible scenarios (see Fig. 4.16) such as,

1. robot left end-effector $R_{\text{efl}} \longleftrightarrow$ human right hand H_r
2. robot left end-effector $R_{\text{efl}} \longleftrightarrow$ human left hand H_l
3. robot right end-effector $R_{\text{efr}} \longleftrightarrow$ human left hand H_l
4. robot right end-effector $R_{\text{efr}} \longleftrightarrow$ human right hand H_r

In this section we will only mention changes that need to be incorporated into the previous sections for the generalization and extension of previously stated handover *routine* to cover above four possible scenarios (Fig. 4.16). We mainly modify here parameters of FSM states during transitions **t0, t1** and **t10**, which are already discussed in detail (see subsection Finite state machine). Again we assumed a human is ready to handover the object if he/she is holding it in his/her either hand. We have also assumed that just like many humans, our robot also acts like a *right-handed* 'person', therefore robot right end-effector would get priority over left in case object is at relatively same distance from both end-effectors or in case where the handover predicted position is at or converging towards the centre of robot body. This hand preference is mainly due to a recent study [48], which showed that right-handed people tend to prefer the right over left hand when they have the choice of pointing at a target location that is almost equally distant between both hands.

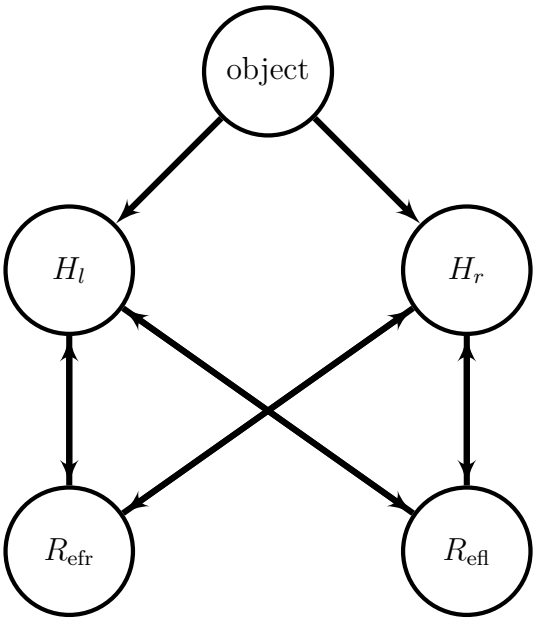

FIGURE 4.16: Possible handover scenarios between human and humanoid.

In this framework, the choice or preference of employing end-effector (either left or right) by the robot co-worker is based on the shortest relative distance of object to either human hand, which can be determined by using equation (4.33) along with together the direction (mainly along y-axis) and shortest relative distance of *that* active human hand with respect to both end-effectors, as per equations (4.34 and 4.35) respectively. For example, if human is holding object in his/her right hand ${}^{\text{hr}}P$ and if the estimated predicted position of his/her hand (see section Position prediction model) is converging somewhere in the negative y-coordinate space, then robot right end-effector ${}^{\text{efr}}P$ would be utilized to receive the object during handover as shown in (Fig. 4.17).

$$\begin{cases} \left\| {}^{\text{hl}}P - {}^{\text{obj}}P \right\| < \left\| {}^{\text{hr}}P - {}^{\text{obj}}P \right\|, & \text{human left hand } ({}^{\text{hl}}P) \\ \\ \left\| {}^{\text{hl}}P - {}^{\text{obj}}P \right\| > \left\| {}^{\text{hr}}P - {}^{\text{obj}}P \right\|, & \text{human right hand } ({}^{\text{hr}}P) \end{cases} \tag{4.33}$$

$$\begin{cases} \left\| {}^{h}P(y) \right\| > 0.1, & \text{robot left end-effector } ({}^{\text{efl}}P) \\ \\ \left\| {}^{h}P(y) \right\| \leq 0.1, & \text{robot right end-effector } ({}^{\text{efr}}P) \end{cases} \tag{4.34}$$

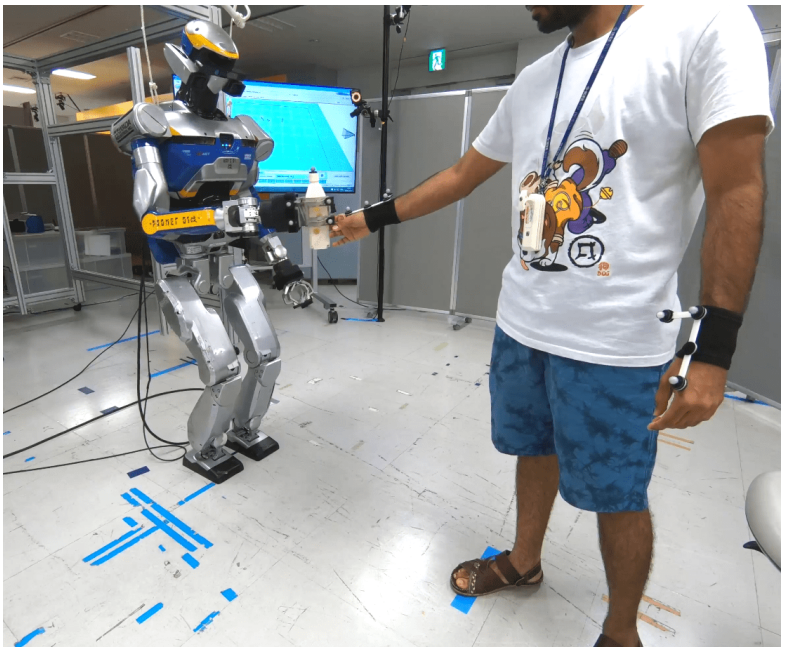

FIGURE 4.17: Object handover between human right hand and HRP-2Kai right end-effector.

$$\begin{cases} \left\| {}^{h}P - {}^{\text{efl}}P \right\| < \left\| {}^{h}P - {}^{\text{efr}}P \right\|, & \text{robot left end-effector } ({}^{\text{efl}}P) \\ \\ \left\| {}^{h}P - {}^{\text{efl}}P \right\| > \left\| {}^{h}P - {}^{\text{efr}}P \right\|, & \text{robot right end-effector } ({}^{\text{efr}}P) \end{cases} \tag{4.35}$$

Where ${}^{h}P$ in equations (4.34 and 4.35) could be either of the human hand position depending upon equation (4.33). However in cases where there is a switching of object in between human hands and within the 1st *sequence* of handover, such as in some rare case human co-worker may decide to move the object from his/her left to right hand or vice-versa for any reasons, under those conditions we rely on the effect of *hysteresis* for robot to decide whether it needs to switch end-effector or continue uninterruptedly. But note that we do not consider the problem of object handover in-between robot end-effectors, therefore once the object is being handed over to the robot co-worker, i.e. during 2nd *sequence*, then the robot would not be able to switch its end-effector, however the human co-worker is still free to choose either of his/her hand to grasp the object back. Using the earlier example where human co-worker right hand has the object, and his/her position is converging somewhere in the negative y-coordinate space. While during the 1st *sequence* of handover if human switches

the object in-between his/her hand —say from right to left hand, then by taking recent history (direction) of human hand into account we further utilize the outputs of equations (4.34 and 4.35) to measure change in the direction of human hand and its shortest relative distance from the end-effectors, and based on these observations robot decides to act accordingly. By exploiting *hysteresis* effect, we make sure that robot does not respond abruptly to changes made by the human.

4.9 Bi-manual handover

It is very natural between humans to use both hands to manipulate a heavy or large shape object to gain confidence and maintain stability during a physical interaction or even while performing a collaborative task. Using both hands together during handing over such an object to one another is no different. Similarly, in scenarios where the use of the single hand is not enough or feasible to perform safe and reliable handover of a large, heavy object between human and humanoid co-workers, then it should also be an obvious choice for the robot as well to use both hands together whenever necessary.

Here, we extend the handover *routine* under the scenario of bi-manual large object transfer between human and humanoid co-workers. We formulate this handover *routine* in a manner such that human co-worker is allowed to use either or both hands to handover/receive the object to/from robot co-worker. However, the robot would always use both hands while receiving and returning of such object, given the physical, structural properties of the object.

4.9.1 Handover object(s)

The object(s) (two of them) we chose to handover between human-humanoid dyads are cylindrical (see Fig. 4.18). We chose these objects purely for simplicity and demonstration purposes in this study. Though our handover model would practically work on several distinguishable objects as long as the object's basic physical, structural properties are known; however, the mass of the object is optional. The cylindrical structures we used are hollow yet quite rigid. The inner r_i and outer r_o radii for those two objects are [0.055, 0.065] m and [0.07, 0.08] m respectively, lengths l are [0.90, 0.12] m, and the mass of objects are [0.40, 1.1] kg, again we don't need to know mass of object in advance as it can be computed

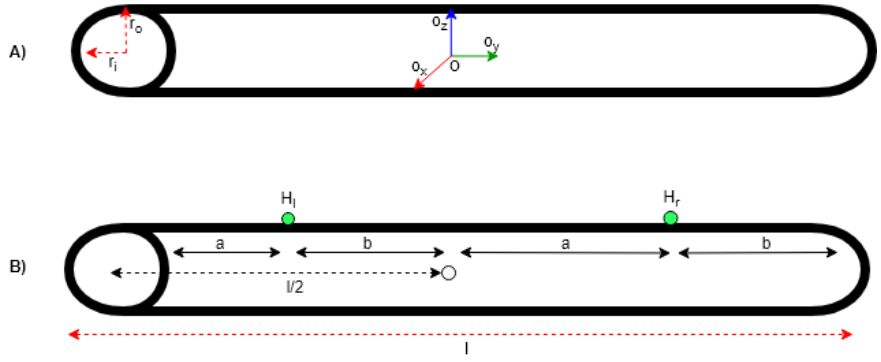

FIGURE 4.18: Hollow cylinder shaft as object for bi-manual handover between human humanoid. Subplot A) shows inner and outer radius of the hollow cylinder and placement of the **L** body shape with *o*. Subplot B) shows representation of our method to get the offset for safe handover location.

during handover *routine* when robot carries the object as already explained earlier in the subsection (Finite state machine).

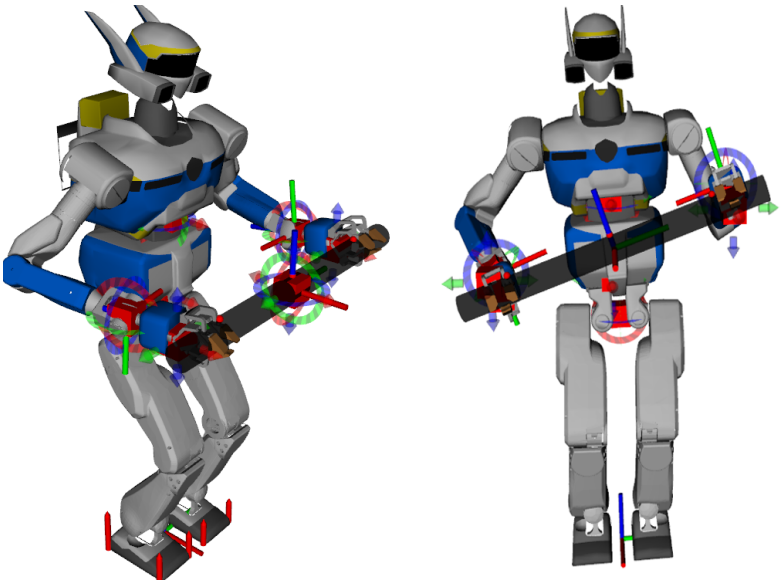

FIGURE 4.19: HRP-2Kai using both end-effectors to manipulate handover object based on the human hand relative orientation.

Here as well we have placed a **L** shape rigid body at the centre of the object as shown in (Fig. 4.18 and Fig. 4.19) with respective xyz local coordinate axes in local frame o and are along the direction of robot frame axes. The object pose (position and orientation) is given by ${}^{o}X_{M}$ (see equation 4.8). Also object orientation can be formulated similarly to human hand orientation, as explained earlier in section (Grasp configuration model).

4.9.2 Constraint motion

Following is an overview of constraint motion during handover *routine* using both hands and end-effectors.

- Human moves with the intention to handover the object.
- Both robot end-effectors approaches towards the object.
- Robot receives the object.
- Contacts are established between robot grippers and object surfaces.
- The contact constraint governs robot end-effectors motion under null velocity.
- Robot end-effectors follows the dominant human hand under the contact constraint.

Here we approach differently during the 1st and 2nd *sequence*s of handover. During the 1st *sequence* of object handover from human to humanoid, we predict and estimate both human hands positions individually along with estimating the object orientation. Specifically, we use unique `position` and `orientation` tasks (see subsection QP tasks) to move each of the robot end-effector to the desired handover location. Once the object is handed over to the robot co-worker and after grasping it using both end-effectors, we remove the `position` and `orientation` tasks on one of the end-effector at the beginning of 2nd *sequence* because of the kinematic contact constraints (see subsection QP constraints) imposed by the object.

Now we would first introduce contact surfaces and kinematic constraints before explaining the simultaneous motion of the robot end-effectors due to constraints imposed by the object during 2nd *sequence* of handover *routine*.

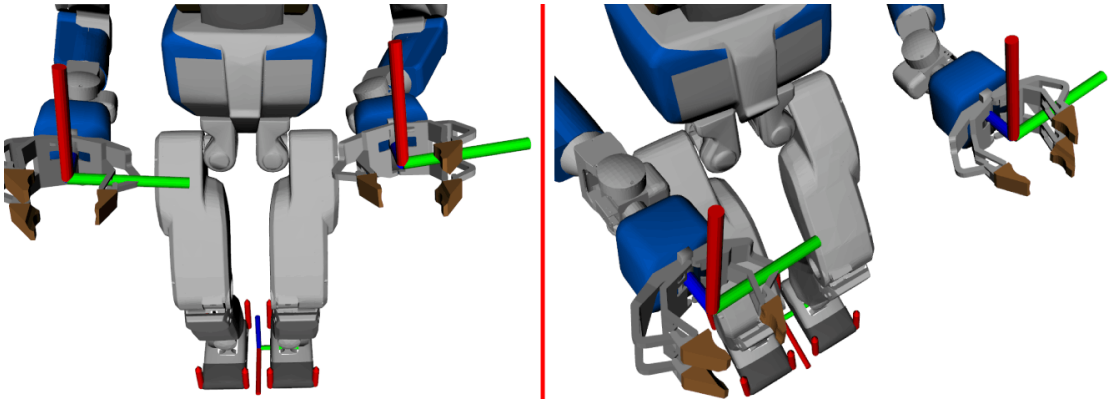

FIGURE 4.20: Robot grippers with graspable internal surfaces.

Contact surface(s) The contact surfaces or surface patches were initially defined on the palm of each gripper in advance. Grippers local frame are shown in (Fig. 4.20). The contacts are established, when during the handover *routine* the robot grasps the object and its grippers internal surface come in contact with the object's graspable surface. These contacts are necessary to move freely or limit the motion of end-effectors in one or more direction (3 `x` translation or 3 `x` rotation) [16]. Thus robot may lose one or more degrees of freedom (DOF) in motion due to the constraints introduced by the object's body.

Contact kinematics and constraint To allow the concurrent motion of the robot end-effectors and the object, contacts are defined as the kinematic constraints in the (Robot QP controller), specifically we used the *fixed* contact mode, as defined by the [9], where all six degrees of freedom are constrained (no translation, no rotation at contact) which restricts and prevents any possibility of sliding motion between the robot end-effectors and the object. Lets consider b_l, b_r and b_o be the respective left, right end-effectors and object bodies and let v_i be the i-th body velocity. Let j_l, and j_r be the two joints under the kinematic constraint between these bodies. Such that, the relative joint velocities v_{jl} and v_{jr} between these bodies in contact would be given by the set of equations (4.36) [37] and therefore the velocity constraints between these bodies would be given by the set of equations (4.37) [83] (see also subsection QP constraints). We later introduce this velocity constraint to the (Robot QP controller).

$$\begin{cases} v_{\mathrm{jl}} = v_{\mathrm{bl}} - v_{\mathrm{bo}} \\ v_{\mathrm{jr}} = v_{\mathrm{br}} - v_{\mathrm{bo}} \end{cases} \tag{4.36}$$

$$\begin{cases} J_{\mathrm{lo}}(v_{\mathrm{bl}} - v_{\mathrm{bo}}) = 0 \\ J_{\mathrm{ro}}(v_{\mathrm{br}} - v_{\mathrm{bo}}) = 0 \end{cases} \tag{4.37}$$

where, J_{ik} is the Jacobian matrix of all points of contact forces between i-th body and k-th body.

1st *sequence*: before object-robot contacts Under the handover *routine* scenarios, we initiate handover 1st *sequence* when human holds the object and start approaching somewhere within the reachable workspace of the robot — assuming that he/she is ready with the intention to handover the object to the robot. The

human can grasp the object with any possible comfortable orientation using either left/right or both hands simultaneously and any place on the object's surface along its length. The only constraint we put while holding/grasping object was not to occlude the **L** shape body and mocap markers on it (see Fig. 4.21 for such possible pose(s)).

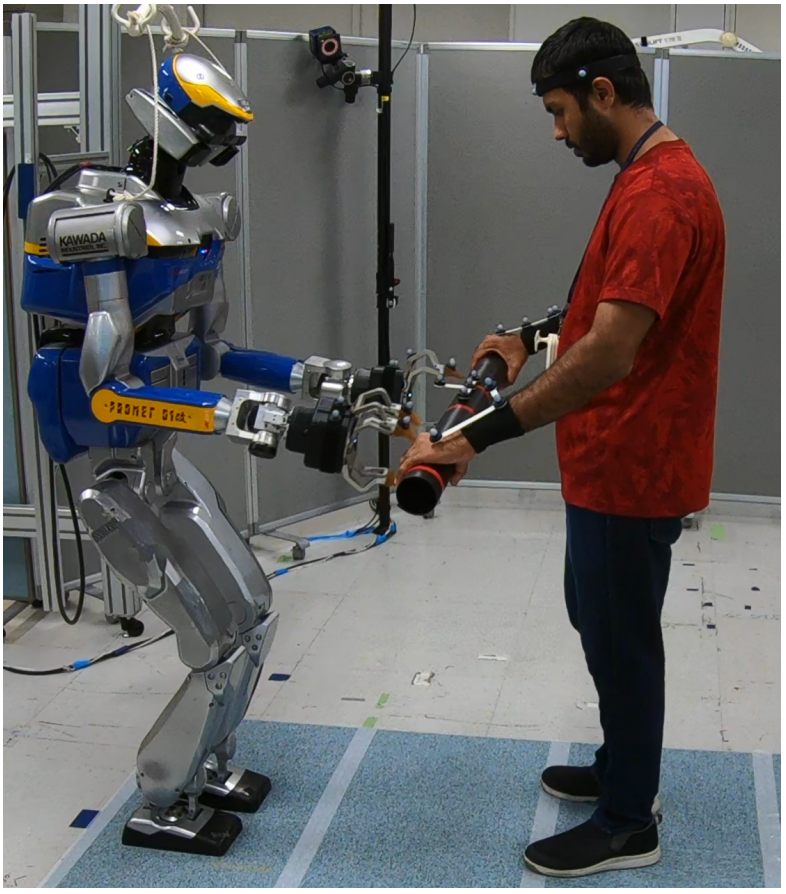

FIGURE 4.21: Bi-manual object handover between human and humanoid using both human hands and both end-effectors.

Compared to the one-handed handover scenario, which was discussed in previous section (Either hand generalized handover), here during human to robot co-worker object handover *sequence* instead of just predicting human hand positions individually like earlier, we also measure the Euclidean distances of each human hand on the object's surface `w.r.t` the object's centre using the following set of equations (4.38). These distances act as an offset correction to the predicted positions of human hands, along the length of the object. These offsets are essential as they allow the robot to find safe and optimum positions on the object's surface to grasp. Also, while making sure end-effectors stay quite away from the human hands occupied the object's surface (see Fig. 4.21).

Moreover, it avoids any possible head-on collision between the end-effectors and the human hands when the robot tries to approach and grasp the object.

Initially, we predict and estimate human hand positions by utilizing previously discussed prediction model from section (Position prediction model). Given the object shape and its structural properties (in our case length of cylindrical shaft), the offsets along object's length can be calculated using set of equations (4.38) in the object local frame o (see Fig. 4.18 B) from the center in both directions. This offset is then further transformed into the robot frame and finally added to the already predicted position of the human hands `w.r.t` robot end-effectors using equation (4.40).

$$\begin{cases} a = \left\| {}^{\text{obj}}P - {}^{h}P \right\| \\ b = |l/2 - a| \\ \\ {}^{\text{off}}d = \pm 2 * a/3 \qquad \text{if } a \geq b \;\; \& \;\; a \leq l/2 \\ {}^{\text{off}}d = \mp 2 * b/3 \qquad \text{if } a < b \;\; \& \;\; a \leq l/2 \end{cases} \tag{4.38}$$

where, ${}^{\text{obj}}P$ is the centre position given by the mocap marker at its centre, a, b and ${}^{\text{off}}d$ are the euclidean distances, which provides grasped location of human hands on the object surface from its centre. Using this crucial information robot can estimate possible points on the object's surface, which are available to be grasped during the handover. Here, h in ${}^{h}P$ represents either left H_l or right H_r human hand and the sign of ${}^{\text{off}}d$ depends on the choice of left or right human hand (see Fig. 4.18 B). Let $\hat{u} = \{0, 1, 0\}$ be the free unit vector along the length of the object, i.e. along the o_y-axis of local frame o, therefore offset position vector in object frame would be given by

$${}^{\text{off}}P_o = {}^{\text{off}}d\,\hat{u} = \{0, {}^{\text{off}}d, 0\} \tag{4.39}$$

We know for sure that without these offsets, robot end-effectors would inevitably collide with the human hands. Since our prediction model is estimating and predicting the positions of both human hands. Therefore, we need to introduce these offsets in the predicted positions of human hands relative to robot end-effectors. We start by measuring these offsets continuously and from the beginning of handover *sequence*. This allowed the robot to adjust while

approaching the object, depending on the human hands grasped location on the object's surface. We can obtain the modified predicted positions based on these offsets using Plücker transformation. We transformed offset position ${}^{\text{off}}P_o$ from object frame to mocap frame ${}^{\text{off}}P_M$ by below equation (4.40). Please note, above offset correction method is also valid during the 2$^{\text{nd}}$ *sequence* of handover when robot holds the object and approaches towards the human decided handover location.

Note here, we considered predicted position of the human hand, but to relatively orient robot end-effectors, we considered the orientation of object but not the human hand(s). In this example of a cylindrical object, the orientation of human hand and object is similar however to generalize this for other possible distinguishable shape objects; it is crucial to consider object's orientation instead of the human hand. As for the other shape objects relative human hand's orientation to grasp the object may not be feasible to perform by the robot.

$$ {}^{\text{off}}X_M = {}^{\text{off}}P_o \begin{bmatrix} {}^{o}\mathcal{O}_M & {}^{h}\mathcal{P}_M(i_{\text{predict}}) \end{bmatrix} \tag{4.40} $$

where, ${}^{o}\mathcal{O}_M$ provides the orientation of object in the mocap frame (see equation 4.8) and ${}^{h}\mathcal{P}_M$ is the predicted position of human hand(s). Finally, using equation (4.40), we can replace translation and orientation components of ${}^{h}X_M$ in the equation (4.13) with ${}^{\text{off}}X_M$, therefore new pose of the handover location relative to the robot end-effectors would be given by

$$ {}^{\text{off}}X_{\text{ef}} = {}^{\mathbf{off}}\mathbf{X_M}\,{}^{M}X_R\,{}^{\text{ef}}X_R{}^{-1} \tag{4.41} $$

Finally, at the handover location, we measure the $\left|{}^{\text{surf}}\vec{f}\right|$ (after removing initial offset) forces along the both gripper's insertion (z)-axes during the interaction between object and gripper just before handover. Handover occurs when $\left|{}^{\text{surf}}\vec{f}\right|$ exceeds 5N on both end-effectors along with the set of following conditions in equation (4.14) satisfy for both robot end-effectors.

2$^{\text{nd}}$ *sequence*: after object-robot contacts So far we have discussed estimating and predicting object handover pose for the robot end-effectors during the 1$^{\text{st}}$ *sequence* of handover *routine*. Up till now, each robot end-effector motion was controlled by its own `position` and `orientation` task. During the 2$^{\text{nd}}$ *sequence* of handover *routine* after the contacts have been established between

the robot grippers and the object surfaces. Also, because of the introduction of kinematic constraints imposed by the object on the end-effectors, the robot cannot move its end-effectors individually. The successive motion of the end-effectors is therefore now governed by the `contact constraint` that we introduce to the robot's low-level QP controller. This constraint maintains the contacts between the object and the robot grippers surfaces all the time and the concurrent motion of the end-effectors is made possible by targeting a null velocity constraint with the target objective $\mathscr{I}_{\text{contact}} = 0$ at the contact joints between the object and the end-effectors, see equation (4.37). The `contact constraint` is already explained at the beginning of this section and also in the subsection (QP constraints).

As already mentioned earlier, the human co-worker is allowed to use either (both) hand(s) to handover/receive the object to/from robot co-worker. Therefore, when the human starts approaching somewhere within the reachable workspace of the robot to receive the object. We utilized equation (4.42) to select the dominant human hand, mainly by measuring the relative distances between the robot end-effectors and the human hands. We check this condition only once at the beginning of the 2$^{\text{nd}}$ *sequence* of handover *routine* after the human hand(s) arrive within the reachable workspace of the robot.

$$\begin{cases} \left\| {}^{\text{hr}}P - {}^{\text{efl}}P \right\| < \left\| {}^{\text{hl}}P - {}^{\text{efr}}P \right\|, & \text{robot left end-effector } ({}^{\text{efl}}P) \\ \\ \left\| {}^{\text{hr}}P - {}^{\text{efl}}P \right\| > \left\| {}^{\text{hl}}P - {}^{\text{efr}}P \right\|, & \text{robot right end-effector } ({}^{\text{efr}}P) \end{cases} \tag{4.42}$$

Where, ${}^{\text{hl}}P$ and ${}^{\text{hr}}P$ are the position vectors of the respective left and right human hand. Depending on the choice of the dominant human hand, for example, if the left human hand is selected then we remove the `position`, and `orientation` tasks of the left end-effector and therefore the motion of this end-effector is now governed using the `contact constraint` by targeting the null velocity. By doing this, the robot right end-effector would lead the motion by predicting and estimating the pose of the dominant human hand. The problem of predicting and estimating human hand pose can now be treated similarly to the one-handed handover *routine* as mentioned in the section (Either hand generalized handover). Please note, set of equations (4.38) is also valid to calculate the offset position of end-effector when robot predicts and approaches

towards the handover location chosen by the dominant human hand. We just need to replace the human hand position vector ${}^{h}P$ with the end-effector position vector ${}^{\text{ef}}P$. Where ef in ${}^{\text{ef}}P$ is either left efl or right efr end-effector.

Finally, a handover occurs when the set of conditions in the equation (4.32) satisfy for both end-effectors (see Finite state machine). Note that the conditions in the equation (4.32) are valid only if a human tries to pull the object from the robot. After the robot grippers release the object, we also remove the null velocity `contact constraint` between the end-effectors and the object surfaces, and add again the previously removed `position` and `orientation` tasks to that end-effector. This completes bi-manual handover *routine*.

4.10 Locomotion and handover

A broad general definition of locomotion describes it as an ability to move from one place to another, that could be achieved either by walking, running, jumping and more. Though we are mainly interested in the walking locomotion of a *floating* base robots such as our HRP-2Kai in the context of the object handover between human and robot co-workers. However, after a thorough search of state-of-the-art research in the related field, none of the previous work on the human-robot dyad considered object handover and 'walking' in a single framework using a *biped* humanoid platform such as HRP-2Kai. Therefore in order for the robot to be sufficiently proactive, we believe it is essential to consider the possibility of a robot taking a step or two to handover or exchange an object with the human co-worker, in scenarios where short-distance travel is required, to eventually extend robot's reachable workspace. Note that we consider the problem of taking a few steps to handover/receive the object rather than motion planning and navigation.

Some previous studies on human-human dyad object handover have demonstrated that we humans are surprisingly able to predict where our partner would handover an object, often without an explicit communication [63, 64]. However we came across one of such study [49], results of which had shown that we humans often handover an object at the middle of our interpersonal distances [47, 101].

Up till now, we formulated our handover problem under the scenario that both human and especially robot co-worker base (feet) are stationary on their respective position in the world frame, such that object handover can happen

just by extending their arms. Next in this section, we further extended our handover problem and added another dimension in which robot takes a step(s) (we call it *step-walk*) to handover or receive the object from the human co-worker based on the interpersonal distance between them. We have tested this scenario during both when human-robot dyad uses either one hand or both hands simultaneously.

4.10.1 Walking pattern generator

Though there are many state-of-the-art methods available to generate walking pattern for humanoids, however in this study for step-walk locomotion, we primarily chose to adopt walking pattern generator (WPG) based on the Linear Inverted Pendulum Mode (LIPM) which was designed and tested in our group [25, 59] along with its native stabilizer [26, 60].

The goal of WPG is to generate the on-line trajectory $P_G(t)$ of the Center of Mass (CoM) of the robot, while all-time maintaining the Zero Momentum Point (ZMP) $P_Z(t)$ of the robot within the support polygon. This support polygon is usually defined by the contact points between the robot (feet) and the environment (floor). During Double Support Phase (DSP) — when both feet are in contact with the ground, the contact surface corresponds to the convex hull of all possible (flat) ground contact points. While During the Single Support Phase (SSP) — when one foot is above the ground (swing state), then this contact surface lies below the robot foot which supports its weight.

In general, WPG provides CoM trajectory $P_G(t)$ and also the trajectory of an angular-momentum $L_c(t)$, however, when considering $L_c = 0$, this model can be reduced to a single output of CoM, and the resulting model is known as Inverted Pendulum Mode. While if walking is under the assumption of a horizontal flat surface (as in our handover problem) such that CoM height remains constant, then this model can be further simplified to Linear Inverted Pendulum Mode, as given by equation (4.43). LIPM establishes a relationship between ZMP and CoM of the pendulum, resulting in a dynamical system with CoM jerk as an input to the system. The desired ZMP trajectory can, therefore, we obtained by appropriately computing CoM jerk. Moreover, to ensure the balance of biped robot while walking, WPG task is to minimize the error between the CoM velocity and a reference velocity (one angular velocity and two translation velocities), also to minimize CoM jerk while respecting the constraints on the robot ZMP.

$$P_Z = P_G - \frac{h}{g}\ddot{P}_G \tag{4.43}$$

where g is gravity, h is the constant height of CoM in equation (4.43).

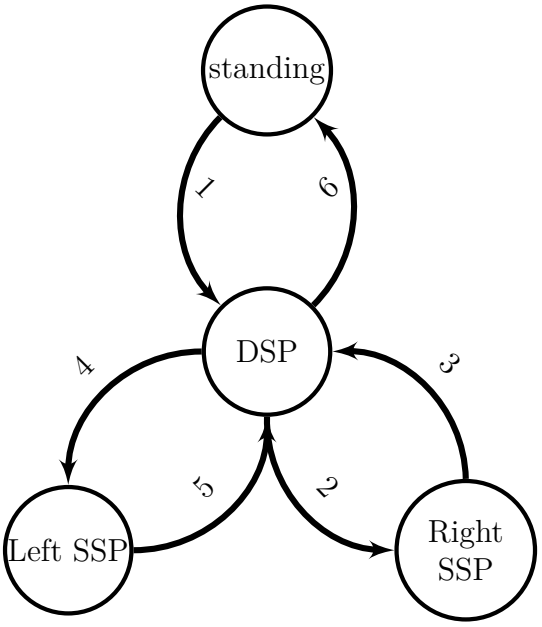

FIGURE 4.22: Walking state machine with standing phase, single support phase (SSP) and double support phase (DSP).

In this study, the number of footsteps (two left and two right), length of footsteps, duration of single support, double support phases and swing height in WPG were predefined for robot during forward and backward step-walk. The WPG can be implemented using three phases of FSM (walking state machine) —standing phase, double support phase and single support phase as illustrated in (Fig. 4.22 and Fig. 4.23). We mentioned the parameters to control WPG in the (Table. 4.1).

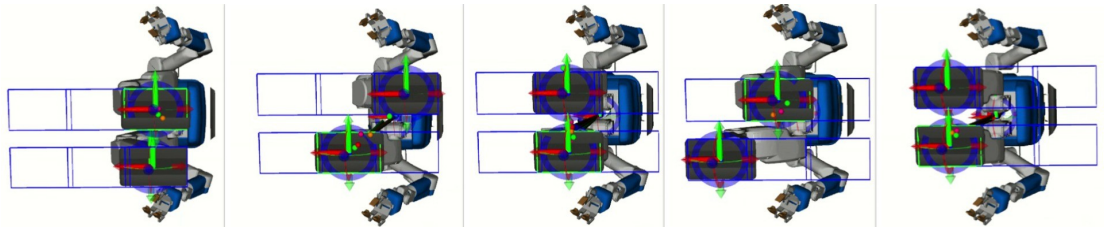

FIGURE 4.23: Bottom view of forward step-walk (4 footsteps) states of WPG: with starting phase Standing —> DSP —> Right SSP —> DSP —> Left SSP —> Standing.

TABLE 4.1: WPG parameters.

Parameters	**Values**
Total footsteps	4
Footstep length	0.2 meters
Swing height	0.05 meters
SSP duration	0.8 seconds
DSP duration	0.2 seconds
Step-walk duration	4.2 seconds

4.10.2 Step-walk

As said above, the moment at which this step-walk should be triggered depends on the interpersonal distance between human and robot co-worker bodies and along with the height of active human hand (${}^{z}H = {}^{h}\mathcal{P}_{M}(z)$) (object carrying/receiving hand). The interpersonal distance D (4.44) is calculated between the human co-worker body position ${}^{b}H$ and the robot co-worker body position ${}^{b}R$ in the **X**-coordinate (walking direction) of world frame. We get the robot body position by using `CoM` task (see QP tasks), and as mentioned earlier, three mocap markers were placed on the head of the human co-worker to get his/her body position. These three markers make up a circle in xy-plane such that the centre of the circle is considered as the human co-worker body position. We remind again that we formulated the problem with a common origin O, therefore $\mathcal{R} \equiv M$ (both frames are located between the feet of robot HRP-2Kai).

$$D = \left| {}^{b}H - {}^{b}R \right| \tag{4.44}$$

Initially, the problem of handover was formulated under the scenario that both human and robot co-worker feet are stationary on their respective position in the world frame; therefore the object handover can happen just by extending their arm(s) and end-effector(s) respectively. However, with an exception that human co-worker is allowed to move nearer to the robot co-worker if needed. The initial interpersonal distance ${}^{i}D$ between the human and robot co-workers bodies were approximately kept 1.2 meters, such that object handover is possible as long as equations (4.1 and 4.45) satisfy,

$$0 <= {}^{i}D <= 1.2 \tag{4.45}$$

Though, now with the possibility of taking few step(s), our previous handover *routine* can be extended further to some possible scenarios (within and beyond its initially defined reachable workspace) where an object handover could occur between human and humanoid, either using one hand or both hands together, even when human co-worker is out of robot's reachable workspace in the direction of **X**-axis.

The key idea here is to trigger the step-walk when human co-worker goes beyond the robot co-worker's reachable workspace (stepping backwards) and presents its intention to handover/receive the object. The intention of human co-worker is established when the condition (4.46) satisfy followed by the condition (4.47) i.e. (4.46) & (4.47).

$$125\%({}^{i}D) <= D <= 150\%({}^{i}D) \tag{4.46}$$

$${}^{z}H >= waistHeight \tag{4.47}$$

where, $waistHeight$ is the height of respective human co-worker. Also note that ${}^{z}H$ is not just any human hand but the active human hand height which either holds the object during 1st *sequence* or approaches towards the object to grasp it during 2nd *sequence* of a handover *routine* as shown in (Fig. 4.24).

4.11 Handover task protocol

The handover task protocol is an emblem of our bi-directional object handover problem between human and humanoid co-workers. It consists of all the models and methods that we have presented so far. (Position prediction model) for predicting and estimating the handover location. (Grasp configuration model) for estimating the orientation of robot end-effector(s), relative to the orientation of an object or active human hand during handover. (Interaction forces model) for minimizing the forces during the handover of an unknown mass object.

Moreover, when considering step-walk, the (Handover routine) can be performed under four possible cases (see Table. 4.2) in which an object handover could occur between human and humanoid, either when during (Either hand generalized handover) or (Bi-manual handover) scenarios.

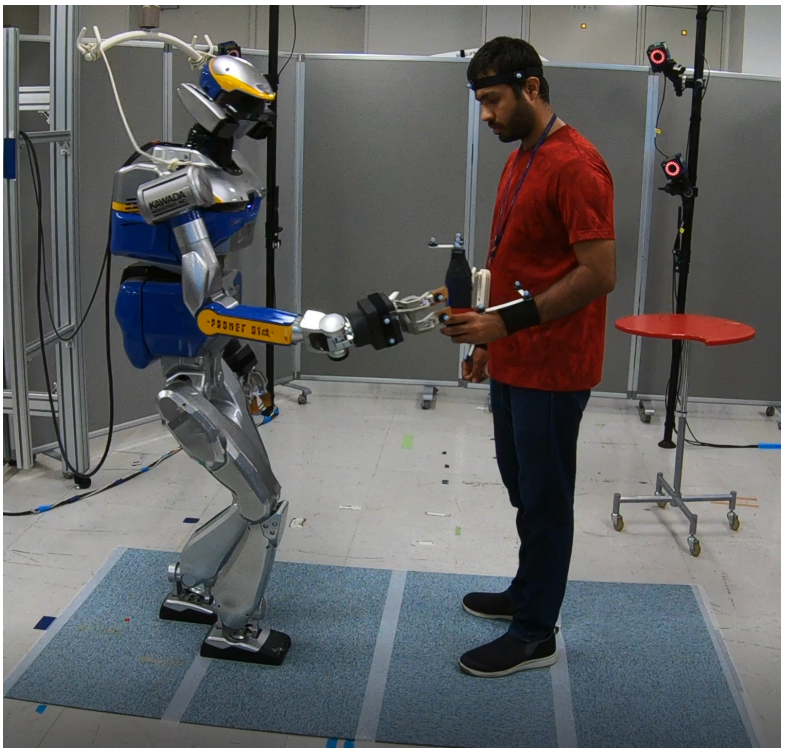

FIGURE 4.24: Object handover between human and humanoid co-worker when robot takes a forward step-walk while attempting to grasp the object.

TABLE 4.2: Possible object exchange cases during the *sequence*s of a handover *routine*.

During both *sequence*s, human co-worker can handover the object while staying at their starting position or first take a step backward and then handover the object.

1st *sequence*	**2nd *sequence***
stays	stays
stays	steps backward
steps backward	stays
steps backward	steps backward

Within the handover task protocol, each trial of handover *routine* starts from an initial posture, standing still with both hands down as shown earlier in (Fig. 4.1), such that it must satisfy the condition (4.48).

$$D > 150\%({}^{i}D) \tag{4.48}$$

Afterwards, the trial begins when the human co-worker moves to a 'starting position' (4.49), from there it is up to human co-worker, whether he/she chooses to exchange (handover/receive) object from that stationary position or take a

step backward, while at the same time raise his/her active hand, which results in signaling the robot to trigger the step-walk and eventually exchange the object with the human co-worker as per the conditions (4.46) & (4.47). Note that we utilize the fundamentals of hysteresis such that robot would trigger forward step-walk only when the conditions are valid in following mentioned order (4.48) & (4.49).

$$0 <= D <= 1.2 \tag{4.49}$$

The step-walk is triggered when $125\%({}^{i}D) <= D <= 150\%({}^{i}D)$, where $\max({}^{i}D) == 1.2$, while at the same time ${}^{z}H$ is above human co-worker's waist. This basically agrees with our assumption that human co-worker is ready with the intention to handover/receive the object.

Finally, once the object handover has occurred, the robot co-worker needs to go back to its initial starting position, such that it requires to take backward step-walk to complete the handover *sequence*. For simplicity, we have coupled the backward step-walk with the forward step-walk; therefore, backward step-walk is triggered only when the robot had taken forward step-walk. We trigger the backward step-walk, once the object is fully grasped by the robot co-worker (1^{st} *sequence*), as stated by the transition states **t7** and **t8** of (Finite state machine) or by the human co-worker at the end of (2^{nd} *sequence*), as stated by the transition states **t12** and **t13**, then the robot safely return its end-effector(s) to a relax/initial posture and walks back to where it started. This lets completion of one trial of a handover *routine*.

4.12 Discussion

To summarize this chapter, we introduced a framework to solve the problem of intuitive and proactive bi-directional object handover between a human and a biped humanoid co-worker dyad using whole-body control and locomotion. This handover framework has been implemented and tested on a real HRP-2Kai. Here we designed models to answer three important questions —when (*timing*), where (*position in space*) and how (*orientation and interaction forces*) of the handover *routine*. By addressing the common key features of object handover between human and robot dyad —the *timing*(s) and overall duration of handover, the *pose*

of handover and the *magnitude* of the interaction forces between human hand(s) and robot end-effector(s).

During the trials of a handover *routine*, we found that our (Position prediction model) is able to predict the human hand position such that robot is able to proactively plan its end-effector's motion and arrive at the human chosen handover location approximately at same time as human co-worker, both during the 1st *sequence*s and 2nd *sequence*s. This lead to an overall reduction in handover trial duration, thanks to the approximate prediction and estimation of handover location in advance. The behaviour of our prediction model can be tuned by two initially required constant time periods, i_{observe} and i_{predict}, though at the moment we did not test its performance thoroughly. The values of i_{observe} and i_{predict} were set to 20 ms and 200 ms respectively in the preliminary tests.

However, predicting handover location alone is not enough when robot co-worker is unaware of the grasp configuration that is required to handover the object. Also to keep in mind the comfort and requirement of the human co-worker [6], it is pivotal for the robot to be able to find the most appropriate configuration to grasp (as *receiver*) or release (as *giver*) the object. Moreover, according to [23], we humans prefer the handover of an object in its default orientation. Therefore, we mainly chose to handover the object in which it is most commonly being grasped hence the default orientation. We proposed a method to get the desired object grasping orientation of robot end-effector either by considering the relative orientation of the active human hand or the object itself in (Grasp configuration model). The only limitation of this model is its dependency on the position of **L** shape mocap markers, that is attached to the object (1st *sequence*) and active human hand wrist (2nd *sequence*). Another thing to note, in this study, we only considered class of rigid basic straight shape objects (bottle or pipe); however, it is possible to further generalize this method to other classes (compound shapes) of objects given the object physical, structural properties in advance. Because by knowing the object shape, **L** body can be placed accordingly and offsets can be created for safer handover between human and robot co-workers as discussed in section (Bi-manual handover). The model is adaptable to objects of different mass within consecutive trials.

Another solution that we proposed here using (Interaction forces model) is related to the *timing* of grasping and releasing the object while at the same time minimizing the *magnitude* of forces during the release of the object in such interactions. We designed a model of interaction forces using (Finite state

machine) which enables the robot end-effector to interact with the object independent of the knowledge of its mass in advance. We proposed two methods within this model, in first method we made sure that robot grasps/releases the object only when active human hand is within its gripper's graspable space using the mocap markers position and in second method we established the intention of the human co-worker to handover/receive the object by measuring the offset free-acting force on the intrinsic surface of the gripper along its insertion (z)-axis at the time of contact. Moreover, during the 2$^{\text{nd}}$ *sequence*, prior to handover the object from robot to human co-worker, the object mass has been calculated in the transition state (**t7**) of FSM, which was later utilized to set the optimal threshold (**t11**) to minimize the interaction force during the release of object. Though this optimal threshold is dependent on the object mass, but it was calculated within this model. We have tested this interaction forces model using a variety of objects with mass ranging from [0.17 to 1.1] kg.

Initially we asked three important questions and we answered them now by utilizing (Position prediction model) to answer **where**, we answered **when** by utilizing (Position prediction model) and (Interaction forces model) and finally answered **how** by using both (Grasp configuration model) and (Interaction forces model), during a handover *routine*.

We started the problem of human-robot bi-directional object handover under the scenario where robot always uses its left end-effector, and human always uses his/her right hand. Later based on above discussed models, we further generalize our bi-directional handover *routine* and extend it into four possible scenarios, robot left end-effector $\longleftrightarrow$ human right hand, robot left end-effector $\longleftrightarrow$ human left hand, robot right end-effector $\longleftrightarrow$ human left hand, robot right end-effector $\longleftrightarrow$ human right hand. In this framework, the choice or preference of employing end-effector (either left or right) by the robot co-worker was based on the shortest relative distance of object to either human hand along with together the direction (mainly along y-axis) and shortest relative distance of active human hand with respect to both end-effectors. During our preliminary tests with HRP-2Kai and based on above-defined conditions, we found that the robot was able to choose its left or right end-effector properly.

Except for a study by [67] which solely focused on grasp planning, we did not find studies on handover which had involved human co-worker during dual-arm object manipulation and handover. Therefore we further extended our handover framework to allow robot co-worker to use both of its end-effectors during object

manipulation and handover with a human co-worker using whole-body control configuration. We chose two hollow cylindrical pipes of slightly distinguishable physical properties for demonstration, however knowing the mass of the object in advance was again optional. Compared to (Either hand generalized handover) scenario, here during 1st *sequence* instead of just predicting human hand positions individually like earlier, we also measured the Euclidean distances of each human hand on the object's surface `w.r.t` the object's centre. These distances acted as an offset correction to the predicted positions of human hands along the length of the object. These offsets were important as they allowed the robot to find safe and optimum positions on the object's surface to grasp. Also, while making sure end-effectors stay quite away from the human hands occupied object's surface. During the 2nd *sequence* after the robot co-worker grasped the object, the successive motion of end-effectors was governed by the kinematic constraint (QP constraints), that was imposed by the object. This constraint maintained the contacts between the object, and the robot grippers surface all the time, and the concurrent motions of the end-effectors were made possible by targeting a null velocity constraint.

Though some studies [105, 109] have adapted object handover and manipulation using dual-arm motion planning but did not consider robot locomotion. Also, in these studies, dual-arm manipulation was limited between robot arms. Therefore in order for the robot to be sufficiently proactive, we believed it was crucial to consider the possibility of the robot taking a step to handover or exchange an object with the human co-worker, in scenarios where short-distance travel is required. Hence we added one final dimension to our handover framework in which we utilized robot's whole-body control along with step-walk locomotion (Locomotion and handover). During the preliminary tests in both (Either hand generalized handover and Bi-manual handover) scenarios, we confirmed that the robot was able to take a step-walk forward while at the same time being able to predict the position of the active human hand to handover the object. In this method, the step-walk was triggered only when the human co-worker moved away (backwards) from the robot and still presented his/her intention to handover the object.

Conclusion

To conclude this thesis, our achieved results contributed in the broad field of human-robot interactions (especially with the humanoid robot) both at a safer distance and in close proximity, namely during a human-robot interaction (HRI) and physical human-robot interaction (pHRI) respectively. The work done in this thesis was about the interactions between human and biped humanoid robot as 'co-workers' in the industrial scenarios. We started with the non-physical human-robot interaction scenario based on an industrially inspired *Pick-n-Place* task example and then advanced towards the physical human-robot interactions with an example of human, humanoid bi-manual bi-directional object handover.

Since the beginning, this thesis was divided into two parts. In the context of *non-physical* human-robot interactions, the studies conducted in 1^{st} part of this thesis (Chapter 2 and Chapter 3) were related to the behavioural effects of motor contagions and motivated by the 'implicit' social interactions between human and humanoid co-workers. While in the context of *physical* human-robot interactions, the 2^{nd} part of this thesis (Chapter 4) was motivated by the physical manipulations of object and handover between nearby human and humanoid using robot whole-body control framework and locomotion.

We examined an empirical repetitive industrial task in which a human participant and a humanoid co-worker near each other. We primarily chose cyclic and repetitive *pick-n-place* task for the experiments in Chapters 2 and 3, as we wanted a task that is simple but rich and could represent several industrial co-worker scenarios. We found that this is one of the most common tasks in current industrial platforms where robots are often employed.

In Chapter 2, our results and findings suggest that *on-line* contagions affect participant's movement frequency while the *off-line* contagions affect their movement velocity. Also, *off-line* motor contagions were mainly notable after observing human co-worker, but the effects of *on-line* contagions were equal with both human and humanoid co-workers. Therefore, perhaps the *off-line* contagion is more sensitive to the nature of the co-worker. These two contagions were also

observed to be sensitive to the behavioural features of both co-workers, but with robot co-worker, these motor contagions were induced only when robot movements were biological. Note that this study did not consider the effects of factors such as age, physical or behavioural characteristics of the partner co-worker. They may have had indirectly affected these two motor contagions, perhaps its an interesting topic of discussion and need to be explored in future research. Finally, the overall observations made in this Chapter emphasize on our hypothesis that distinct motor contagions are induced in human participant's *during* the observation of a co-worker (*on-line* contagions) and as well as *after* the observations of same co-worker (*off-line* contagions).

In Chapter 3, we further explored our findings from Chapter 2 and under the same experimental task and set up along with the addition of a few more conditions. Primarily, our findings suggest that the presence of a humanoid co-worker (or a human co-worker) can influence the performance frequencies of human participants. We observed that participants become slower with a slower co-worker, but also faster with a faster co-worker. We also argued the performance has to be measured considering together, both task speed (or frequency) as well as task accuracy. Some previous studies in motor control have shown that motor noise often constrains human movements, which eventually increases with the enormity of motor commands in the muscles [50]. This consequently leads to the trade-off between the speed and accuracy of ordinary and usual daily life movements [39]. However, by regulating the arm impedance by muscle co-contraction, one can also modulate the movement accuracy [20, 41, 42]. Therefore here we showed how touch accuracy of participants have changed alongside the contagions in their *htp* and hence performance of the human co-worker during the task. We also investigated the effects of physical form, by adding two conditions where both human and robot co-worker's head and torso were covered, and human participants were only able to see visible moving arm of the co-worker. Our findings suggest that the presence of a humanoid co-worker can affect human performance, but only when its humanoid form is visible.

Moreover, this effect was supposedly increased with the human participants having prior robot experience. Finally, our results show that human task frequency, but not task accuracy, is affected by the observation of a humanoid co-worker, provided the robot's head and torso are visible. Note that in Chapter 3, we quantify the participants level of the robot exposure by a

self-perceived robot exposure score by themselves rather than the actual robot exposure. As an actual standard robot exposure questionnaire to measure this effect is currently absent, and the development of one can be useful to understand how this effects, such as the one we highlight here, vary over time.

Overall the findings mentioned and discussed in Chapters 2 and 3 highlights several new features of motor contagions, but also open new questions for future research. One can find these results useful for customizing the design of robot co-workers in industries and sports in future studies by moderating or exploiting these contagions. While if ethically allowed, these contagions could be utilized to improve co-workers performance speed and hence productivity.

In Chapter 4, we designed a framework to handover an object between human and robot co-workers in the context of pHRI. We concentrated our efforts towards developing a simple yet robust and efficient handover framework. We introduced an intuitive bi-directional object handover *routine* between a human-humanoid dyad using whole-body control (WBC) and locomotion. Throughout this chapter, the problem of bi-directional object handover between human and humanoid co-worker was treated as one-shot continuous fluid motion. Initially, we started by designing a general framework and within it developed models to predict human hand position to converge at the handover location (Position prediction model) along with estimating the grasp configuration of an object and active human hand during handover *sequence* (Grasp configuration model). We also designed a model (Interaction forces model) to minimize the interaction forces during the handover of an unknown mass object along with minimizing the overall duration of object handover *routine*. We designed these models to answer three important questions related to human-robot object handover —**when** (*timing*), **where** (*position in space*) and **how** (*orientation and interaction forces*) during a handover *routine*.

Within this handover framework, using HRP-2Kai, we first tested and confirmed the feasibility of these models under the scenario where human and robot co-workers always use their right hand and left end-effector, respectively. Later a generalized framework was presented (Either hand generalized handover) and tested where both human and robot co-workers were able to choose either of their hand to handover or exchange the object. In addition, thanks to the native low-level (Robot QP controller) of our robot HRP-2Kai and by utilizing whole-body control configuration, we were able to extend further our handover framework, which allowed the robot to use both hands simultaneously during the object handover *routine* (Bi-manual handover).

Furthermore, as mentioned earlier, none of the previous work on the human-robot dyad considered object handover and 'walking' in a single framework using a *biped* humanoid platform such as HRP-2Kai. Therefore for a proactive handover of an object between human and robot we believed it was essential to consider the possibility of a robot taking a step to handover or exchange an object with the human co-worker, in scenarios where short-distance travel is required. Hence, we explored the full capabilities of HRP-2Kai and added a scenario where the robot needs to proactively take a few steps in order to handover or exchange the object between its human co-worker. This scenario had been implemented on HRP-2Kai and tested during both when human-robot dyad uses either single or both hands simultaneously.

Finally, to conclude our preliminary testing of the complete handover framework under above-mentioned scenarios, including locomotion. We confirm that our bi-directional object handover framework is intuitive and adaptable to several objects of distinguishable physical properties (shape, size and mass), including industrial tools. It only needs the information of handover object's shape and size, though knowing the mass of the object is not important in the beginning. We confirmed the feasibility of our handover framework under several objects with mass ranges from [0.17 to 1.1] kg, during above-mentioned scenarios. However, over the course of several handover *routine* trials, we report that the calculated object mass is not accurate and has marginal error of $\pm 10\%$ compared to object's actual mass and needs further improvement on better estimation of the inertial forces at play or better ways to remove offsets from force sensors although it didn't affect the optimal threshold which is vital at the time of object handover from robot to human co-worker.

Though overall our method allows us not to stop the motion of end-effector and still being able to handover (both ways) the object (see Finite state machine), however, if the handover occurs while both human and robot end-effectors are moving then this problem of handover would be extended to the problem of object collaboration and manipulation, which is already being studied extensively in our research group [1–4, 21, 22]. Therefore we concentrated solely on the proactive bi-directional handover problem and hence decided to reduce the end-effectors velocity (${}^{\text{ef}}v \simeq 0$) at the time of handover.

By adding a dimension of step-walk locomotion, We did not focus on the problem of motion planning or navigation in a large cluttered environment [67, 74, 105]. However, instead, we concentrated our efforts to solve

and optimize object handover problem which requires immediate shared efforts between human-robot dyad in a small space where few steps are necessary and enough for a comfortable and convenient object handover. Our proposed method is simple but effective to take advantage of the humanoid robot and deal with the problem of bi-directional object handover using robot whole-body control. However, note that in the cases when human co-worker decides to step backwards, then for sometime after the forward step-walk is triggered, the interpersonal distance D would become larger than 1.2 meters (since human is away from the robot), therefore in order for this model to work, the human co-worker shouldn't take more than few steps backward. Though at the moment, step-walk is triggered only when interpersonal distance between the co-workers becomes greater than $125\% <= D <= 150\%$, however more possibilities including the estimation of direction in which human co-worker may wish to move (laterally) and handover the object will be considered in the future scope of this study.

At last, in the near future, a human-user study will be conducted shortly after further improving the performance of the overall proactive handover framework with step-walk locomotion. This handover framework exploits whole-body control of a biped humanoid robot and can be utilized in several possible industrial applications where human and robot co-workers need to work collaboratively.

Appendix: Motor contagion

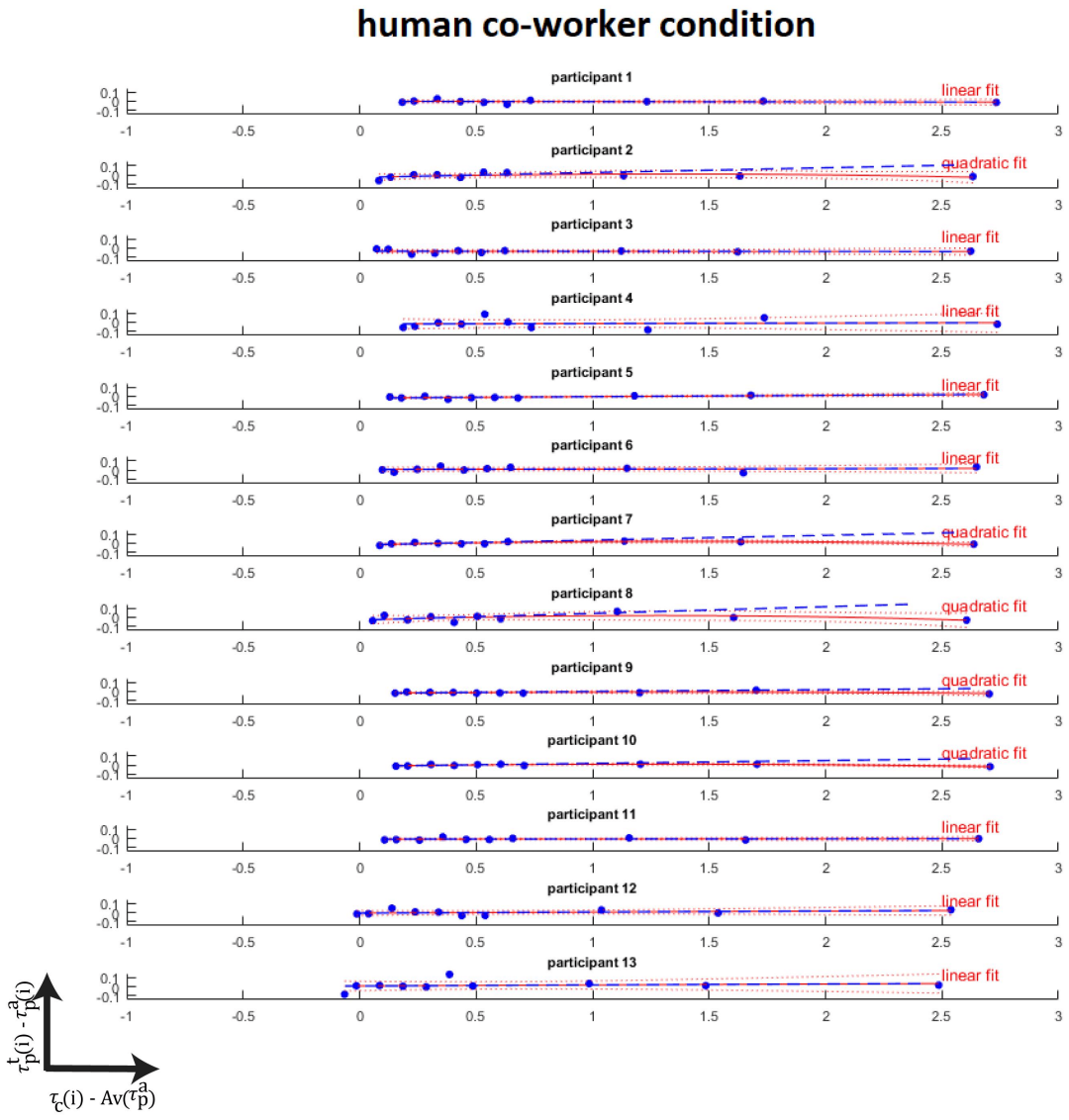

Figure A.1: All participants regression fits in the human co-worker condition. Examples of linear regression fits obtained between the participant's *htp* change between the together and alone conditions (ordinates), as a function of co-worker's *htp*s (abscissa). The positive slopes show that the human co-worker's performance *htp* (hence frequency) influenced the human participants.

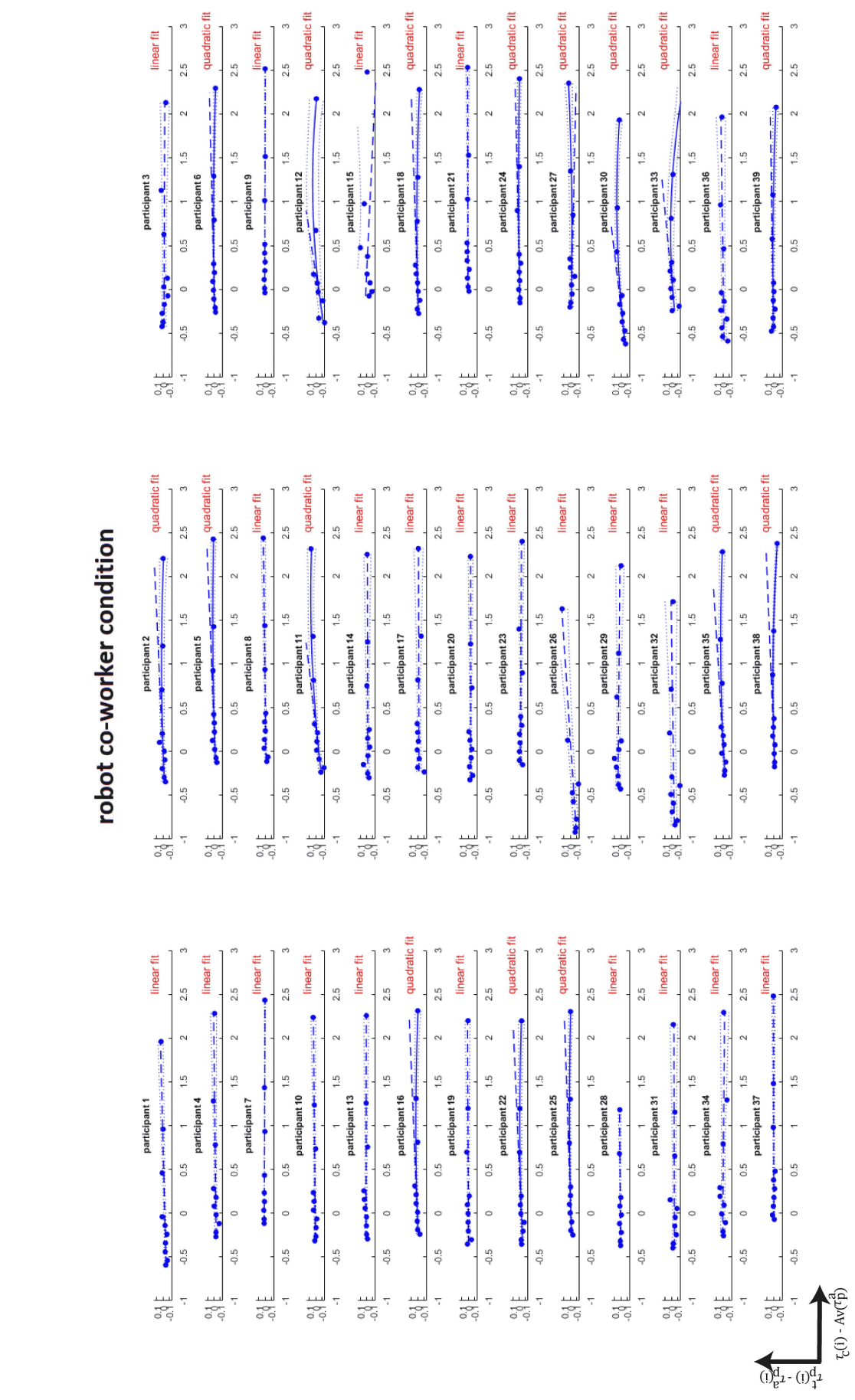

FIGURE A.2: All participants regression fits in the robot co-worker condition. Note that most participant plots show a positive slope indicating that the robot co-worker's performance *htp* (hence frequency) influenced the human participants.

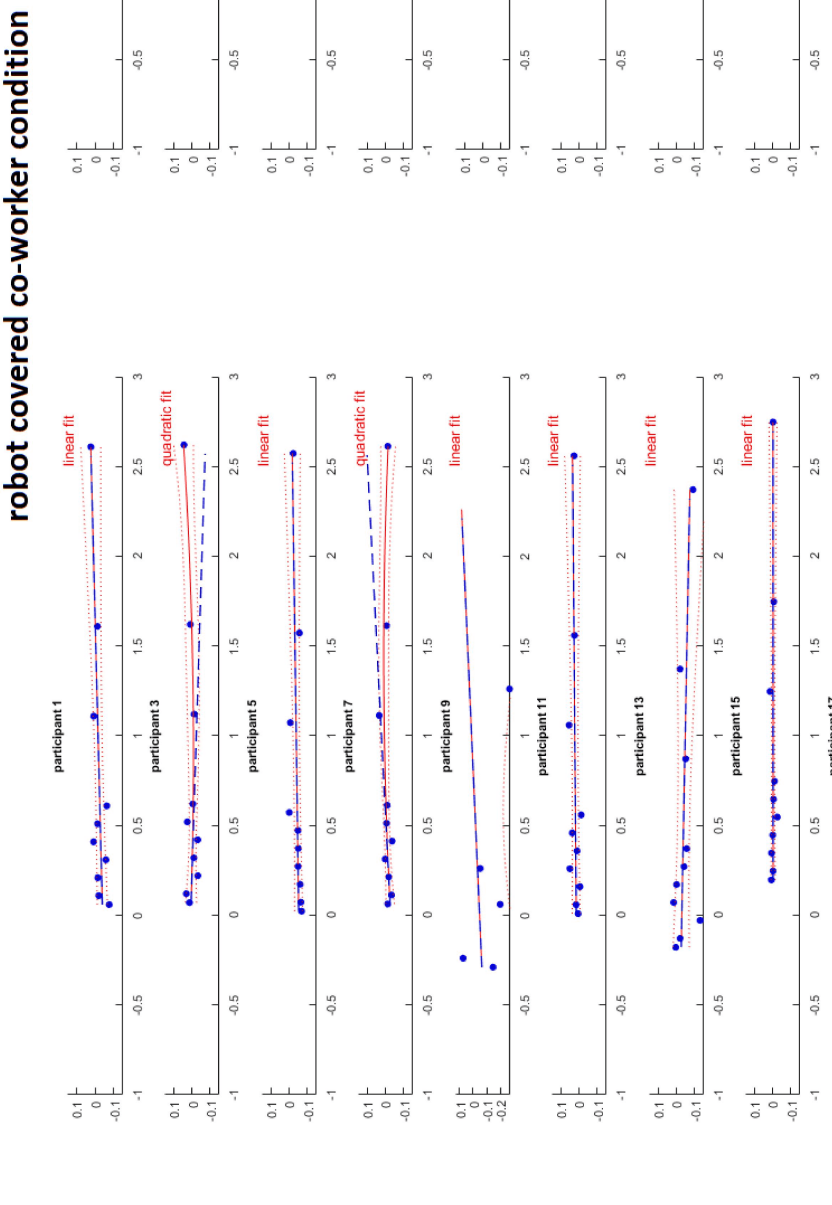

FIGURE A.3: All participants regression fits in the robot covered co-worker condition. Note that there is no trend in slopes across participant —the slopes were in fact observed to be zero across participants (Fig. 3.6), indicating that the participant's *htps* were not affected in the robot covered co-worker condition.

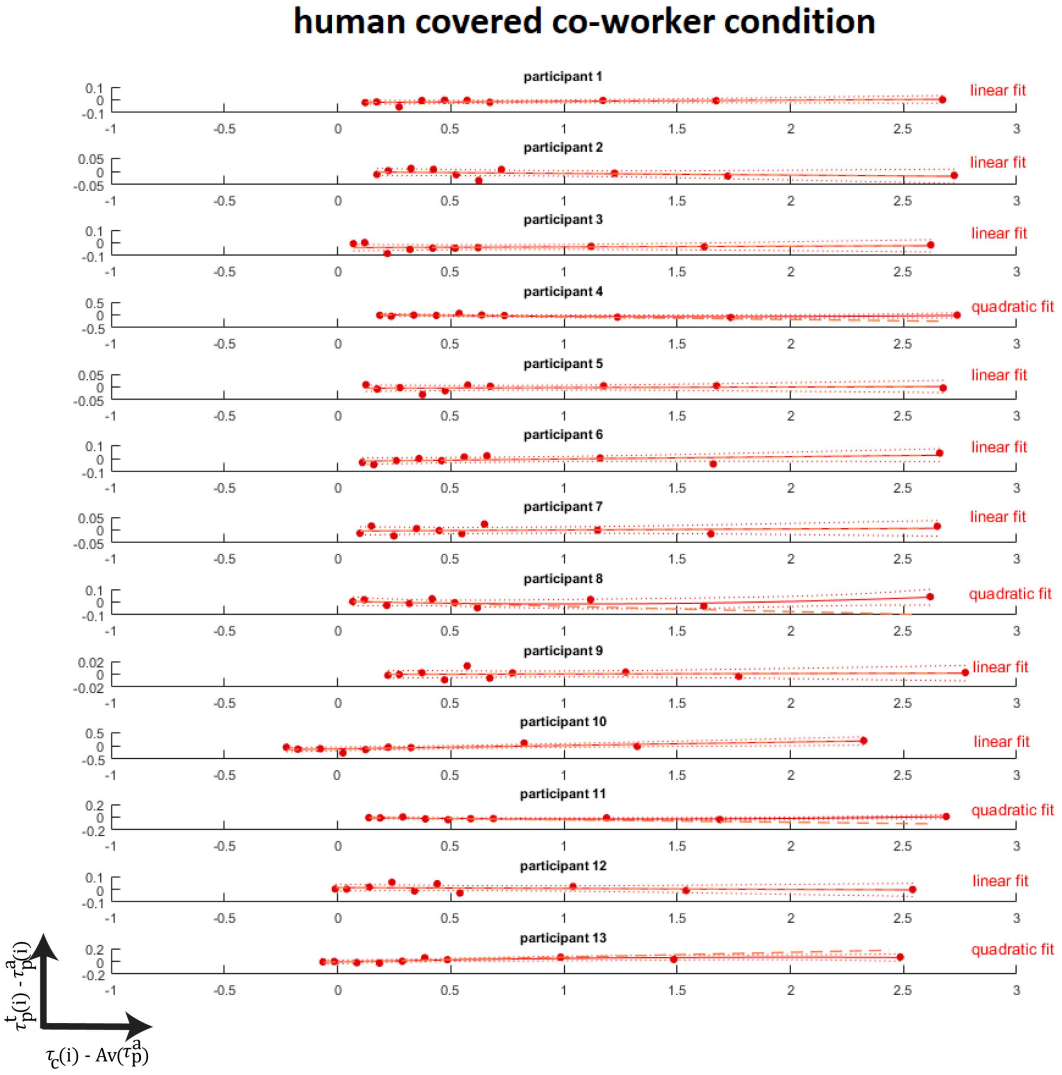

FIGURE A.4: All participants regression fits in the human covered co-worker condition. Like in A.3, the slopes were observed to be zero across participants (Fig. 3.6), indicating that the participant's *htp*s were not affected in the human covered co-worker condition

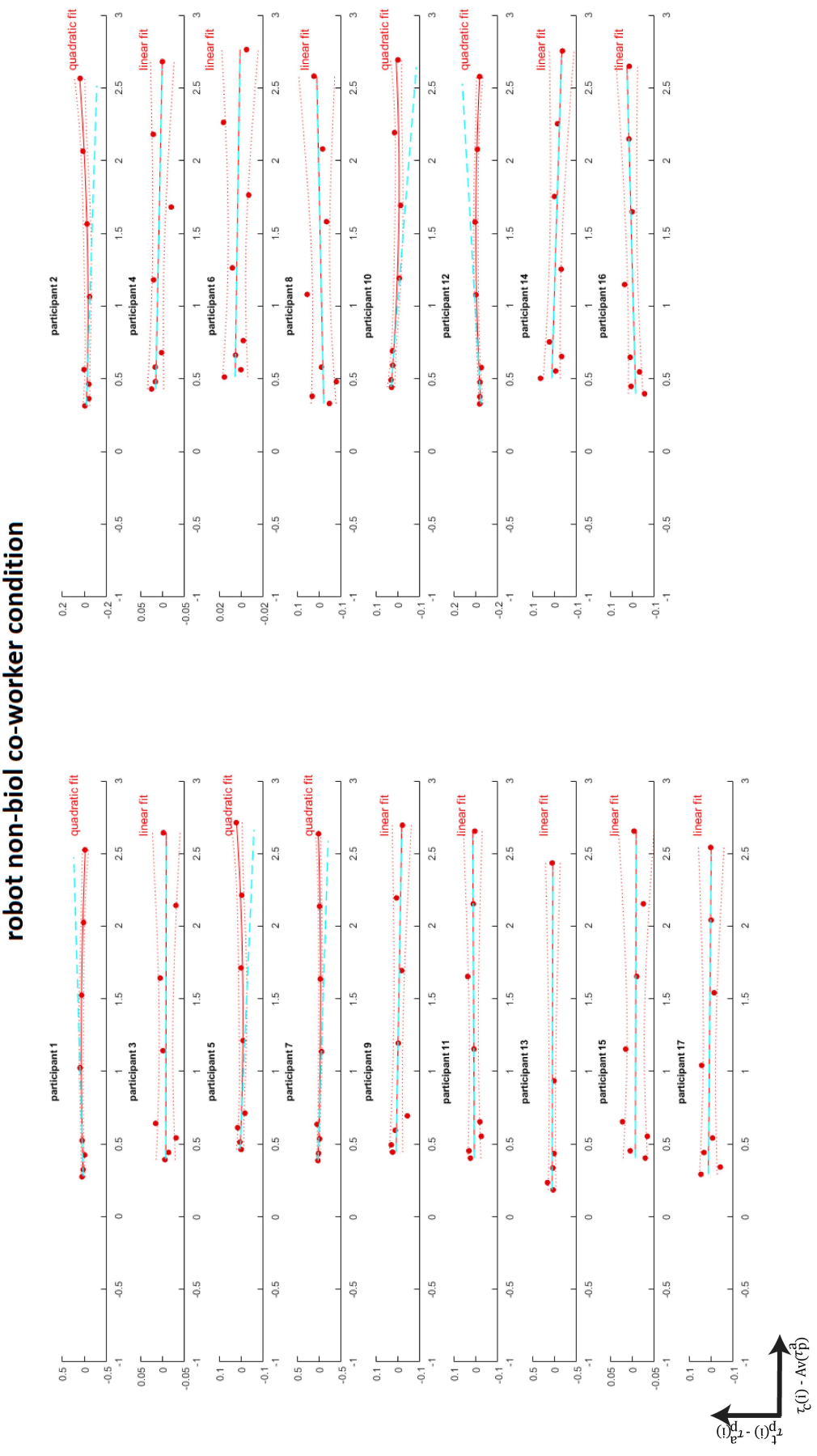

FIGURE A.5: All participants regression fits in the robot non-biol co-worker condition. The plots again show that the participant's *htps* were not affected in the robot non-biol co-worker condition.

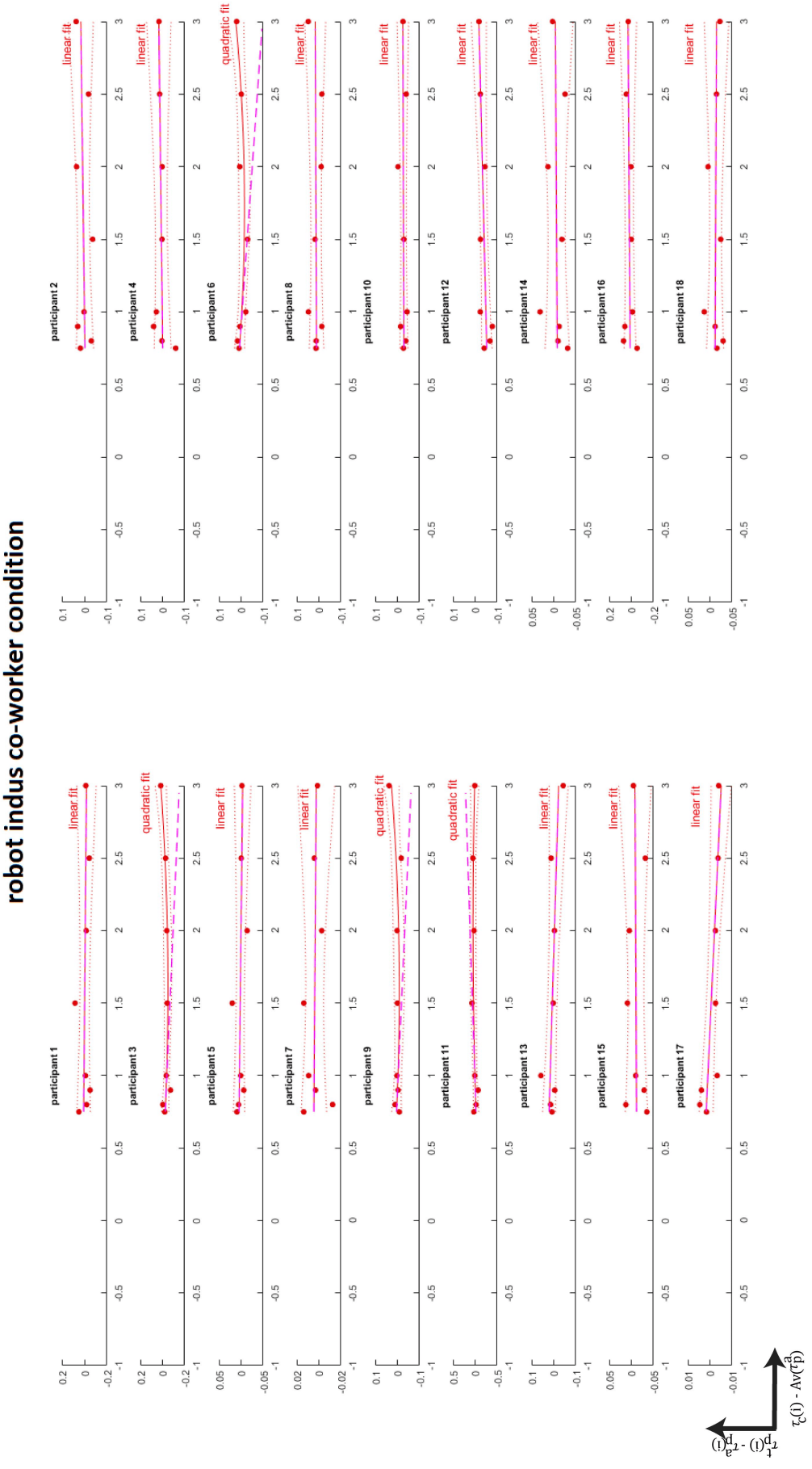

FIGURE A.6: All participants regression fits in the robot indus co-worker condition. Like in A.3 to A.5, we observed no effect in the participants in the robot indus co-worker condition.

Appendix: Handover

Algorithm 1: linear position prediction model

Input: ${}^{M}X_R, {}^{\text{ef}}X_R, mocapData$

Output: ${}^{h}wp_{\text{ef}}$ `// predicted waypoints`

Data: Initial require: $i_{\text{observe}} = 20$ ms, $i_{\text{predict}} = 200$ ms, $i = dt = 5$ ms

i+=dt `// increments as per controller run-time (dt)`

if $(i\%i_{observe}) == 0$ **then**

  for $j = 1$ *to* $i_{observe}$ **do**

    ${}^{h}\mathcal{P}_M = mocapData.handMarker(i - i_{\text{observe}}) + j)$

  ${}^{h}\bar{\mathcal{V}}_M = \frac{1}{i_{\text{observe}}} \sum_{j=1}^{j=i_{\text{observe}}} ({}^{h}\mathcal{P}_M(j) - {}^{h}\mathcal{P}_M(j-1))/dt$

  `/* predict human hand handover position at` i_{predict} `*/`

  ${}^{h}\mathcal{P}_M(i_{\text{predict}}) = {}^{h}\bar{\mathcal{V}}_M \cdot (i_{\text{predict}} - i_{\text{observe}}) \cdot dt + {}^{h}\mathcal{P}_M(i_{\text{observe}})$

  ${}^{h}X_M = \begin{bmatrix} {}^{h}\mathcal{O}_M & {}^{h}\mathcal{P}_M \end{bmatrix}$

  `/* transform handover position relative to robot end-effector */`

  ${}^{h}X_{\text{ef}}(i_{\text{predict}}) = {}^{h}X_M {}^{M}X_R {}^{\text{ef}}X_R{}^{-1}$

  `/* way points between human hand and robot end-effector handover location */`

  Function `generateWp(`${}^{ef}\mathcal{P}_R, {}^{h}\mathcal{P}_{ef}(i_{predict}), i_{predict}$`):`

    for $k = 0$ *to* $i_{predict}$ **do**

      ${}^{h}wp_{\text{ef}}(k) = [{}^{h}\mathcal{P}_{\text{ef}}(i_{\text{predict}}) - {}^{\text{ef}}\mathcal{P}_R].(\frac{k}{i_{\text{predict}}}) + {}^{\text{ef}}\mathcal{P}_R$

    return ${}^{h}wp_{\text{ef}}$

Algorithm 2: Interaction Forces

Input: $\mathcal{F}$ `// EF wrist worldWrenchWithoutGravity`

Output: ${}^{\text{pull}}\mathcal{F}, {}^{\text{new}}T$ `// Pull force, new threshold based on object mass`

if *human hand is near robot* **then**

`/* when human holds the object */`

if $\left\| {}^{h}P - {}^{ef}P \right\| < 0.05$ `// gripper is empty`

then

Open Gripper

${}^{\text{zero}}F = \mathcal{F}$ `// wrench offset`

`/* when robot holds the object */`

${}^{\text{obj}}\overline{\mathcal{F}} = \frac{1}{n}\sum_{i=1}^{i=n} |(|\mathcal{F}| - |{}^{\text{zero}}\mathcal{F}|)|$

$objectMass = \left\| {}^{\text{obj}}\overline{\mathcal{F}} \right\| / 9.80665$ `// get object mass`

${}^{\text{inert}}\mathcal{F} = objectMass * efAce$ `// efAce - avg end-effector acceleration`

${}^{\text{new}}T = {}^{\text{obj}}\overline{\mathcal{F}} + {}^{\text{old}}T$ `// T_old set to [5,5,5]`

Function `CheckPullForce`$(\vee x, \vee y, \vee z)$**:**

${}^{\text{pull}}\mathcal{F} = |(|\mathcal{F}| - |{}^{\text{inert}}\mathcal{F}| - |{}^{\text{zero}}\mathcal{F}|)|$

if ${}^{pull}\mathcal{F} > {}^{new}T \vee x, \vee y, \vee z$ **then**

release object `// release object`

Bibliography

[1] D. J. Agravante, A. Cherubini, A. Sherikov, P. Wieber, and A. Kheddar. Human-humanoid collaborative carrying. *IEEE Transactions on Robotics*, 35(4):833–846, Aug 2019. doi: 10.1109/TRO.2019.2914350.

[2] Don Joven Agravante, Andrea Cherubini, Antoine Bussy, and Abderrahmane Kheddar. Human-humanoid joint haptic table carrying task with height stabilization using vision. In *2013 IEEE/RSJ International Conference on Intelligent Robots and Systems*, pages 4609–4614. IEEE, 2013.

[3] Don Joven Agravante, Andrea Cherubini, Antoine Bussy, Pierre Gergondet, and Abderrahmane Kheddar. Collaborative human-humanoid carrying using vision and haptic sensing. In *2014 IEEE international conference on robotics and automation (ICRA)*, pages 607–612. IEEE, 2014.

[4] Don Joven Agravante, Alexander Sherikov, Pierre-Brice Wieber, Andrea Cherubini, and Abderrahmane Kheddar. Walking pattern generators designed for physical collaboration. In *2016 IEEE International conference on Robotics and Automation (ICRA)*, pages 1573–1578. IEEE, 2016.

[5] Hirotogu Akaike. Information theory and an extension of the maximum likelihood principle. In *Selected Papers of Hirotugu Akaike*, pages 199–213. Springer, 1998.

[6] Jacopo Aleotti, Vincenzo Micelli, and Stefano Caselli. Comfortable robot to human object hand-over. In *2012 IEEE RO-MAN: The 21st IEEE International Symposium on Robot and Human Interactive Communication*, pages 771–776. IEEE, 2012.

[7] Simon L Altmann. *Rotations, quaternions, and double groups*. Courier Corporation, 2005.

[8] Emil Artin. *Geometric algebra*. Courier Dover Publications, 2016.

[9] Devin J Balkcom and Jeffrey C Trinkle. Computing wrench cones for planar rigid body contact tasks. *The International Journal of Robotics Research*, 21(12):1053–1066, 2002.

[10] Cristina Becchio, Andrea Pierno, Morena Mari, Dean Lusher, and Umberto Castiello. Motor contagion from gaze: The case of autism. *Brain*, 130(9): 2401–2411, 2007.

[11] Luigi Biagiotti and Claudio Melchiorri. *Trajectory planning for automatic machines and robots*. Springer Science & Business Media, 2008.

[12] Ambra Bisio, Natale Stucchi, Marco Jacono, Luciano Fadiga, and Thierry Pozzo. Automatic versus voluntary motor imitation: effect of visual context and stimulus velocity. *PLoS One*, 5(10):e13506, 2010.

[13] Ambra Bisio, Alessandra Sciutti, Francesco Nori, Giorgio Metta, Luciano Fadiga, Giulio Sandini, and Thierry Pozzo. Motor contagion during human-human and human-robot interaction. *PloS one*, 9(8):e106172, 2014.

[14] Sarah-Jayne Blakemore and Chris Frith. The role of motor contagion in the prediction of action. *Neuropsychologia*, 43(2):260–267, 2005.

[15] Karim Bouyarmane and Abderrahmane Kheddar. Using a multi-objective controller to synthesize simulated humanoid robot motion with changing contact configurations. In *2011 IEEE/RSJ international conference on intelligent robots and systems*, pages 4414–4419. IEEE, 2011.

[16] Karim Bouyarmane, Stéphane Caron, Adrien Escande, and Abderrahmane Kheddar. *Multi-contact Motion Planning and Control*. Springer Netherlands, Dordrecht, January 2018. ISBN 978-94-007-7194-9. doi: 10.1007/978-94-007-7194-9_32-1.

[17] Karim Bouyarmane, Kevin Chappellet, Joris Vaillant, and Abderrahmane Kheddar. Quadratic programming for multirobot and task-space force control. *IEEE Transactions on Robotics*, 35(1):64–77, 2018.

[18] Louis Brand. *Vector and tensor analysis*. Wiley, 1947.

[19] Marcel Brass, Harold Bekkering, and Wolfgang Prinz. Movement observation affects movement execution in a simple response task. *Acta psychologica*, 106 (1-2):3–22, 2001.

[20] Etienne Burdet, Rieko Osu, David W Franklin, Theodore E Milner, and Mitsuo Kawato. The central nervous system stabilizes unstable dynamics by learning optimal impedance. *Nature*, 414(6862):446, 2001.

[21] Antoine Bussy, Pierre Gergondet, Abderrahmane Kheddar, François Keith, and André Crosnier. Proactive behavior of a humanoid robot in a haptic transportation task with a human partner. In *2012 IEEE RO-MAN: The 21st IEEE International Symposium on Robot and Human Interactive Communication*, pages 962–967. IEEE, 2012.

[22] Antoine Bussy, Abderrahmane Kheddar, André Crosnier, and François Keith. Human-humanoid haptic joint object transportation case study. In *2012 IEEE/RSJ International Conference on Intelligent Robots and Systems*, pages 3633–3638. IEEE, 2012.

[23] Maya Cakmak, Siddhartha S Srinivasa, Min Kyung Lee, Jodi Forlizzi, and Sara Kiesler. Human preferences for robot-human hand-over configurations. In *2011 IEEE/RSJ International Conference on Intelligent Robots and Systems*, pages 1986–1993. IEEE, 2011.

[24] Maya Cakmak, Siddhartha S Srinivasa, Min Kyung Lee, Sara Kiesler, and Jodi Forlizzi. Using spatial and temporal contrast for fluent robot-human hand-overs. In *2011 6th ACM/IEEE International Conference on Human-Robot Interaction (HRI)*, pages 489–496. IEEE, 2011.

[25] Stéphane Caron and Abderrahmane Kheddar. Multi-contact walking pattern generation based on model preview control of 3d com accelerations. In *IEEE-RAS International Conference on Humanoid Robots*, November 2016. doi: 10.1109/HUMANOIDS.2016.7803329.

[26] Stéphane Caron, Abderrahmane Kheddar, and Olivier Tempier. Stair climbing stabilization of the hrp-4 humanoid robot using whole-body admittance control. *arXiv preprint arXiv:1809.07073*, 2018.

[27] Thierry Chaminade and Gordon Cheng. Social cognitive neuroscience and humanoid robotics. *Journal of Physiology-Paris*, 103(3-5):286–295, 2009.

[28] Thierry Chaminade, Erhan Oztop, Gordon Cheng, and Mitsuo Kawato. From self-observation to imitation: Visuomotor association on a robotic hand. *Brain research bulletin*, 75(6):775–784, 2008.

[29] Wesley P Chan, Chris Ac Parker, Hf Machiel Van Der Loos, and Elizabeth A Croft. A human-inspired object handover controller. *The International Journal of Robotics Research*, 32(8):971–983, 2013.

[30] Wesley P Chan, Iori Kumagai, Shunichi Nozawa, Yohei Kakiuchi, Kei Okada, and Masayuki Inaba. Implementation of a robot-human object handover controller on a compliant underactuated hand using joint position error measurements for grip force and load force estimations. In *2014 IEEE International Conference on Robotics and Automation (ICRA)*, pages 1190–1195. IEEE, 2014.

[31] Michael J Crowe. *A history of vector analysis: The evolution of the idea of a vectorial system*. Courier Corporation, 1994.

[32] Martin G Edwards, Glyn W Humphreys, and Umberto Castiello. Motor facilitation following action observation: A behavioural study in prehensile action. *Brain and cognition*, 53(3):495–502, 2003.

[33] Edgar Erdfelder, Franz Faul, and Axel Buchner. Gpower: A general power analysis program. *Behavior research methods, instruments, & computers*, 28 (1):1–11, 1996.

[34] Philip R Evans. Rotations and rotation matrices. *Acta Crystallographica Section D: Biological Crystallography*, 57(10):1355–1359, 2001.

[35] Luciano Fadiga, Leonardo Fogassi, Giovanni Pavesi, and Giacomo Rizzolatti. Motor facilitation during action observation: a magnetic stimulation study. *Journal of neurophysiology*, 73(6):2608–2611, 1995.

[36] Juan Fasola and Maja J Matarić. Robot motivator: Increasing user enjoyment and performance on a physical/cognitive task. In *2010 IEEE 9th International Conference on Development and Learning (ICDL)*, pages 274–279. IEEE, 2010.

[37] Roy Featherstone. *Robot Dynamics Algorithm*. Kluwer Academic Publishers, Norwell, MA, USA, 1987. ISBN 0898382300.

[38] Roy Featherstone. *Rigid body dynamics algorithms*. Springer, 2014.

[39] Paul M Fitts. The information capacity of the human motor system in controlling the amplitude of movement. *Journal of experimental psychology*, 47(6):381, 1954.

[40] Tamar Flash and Neville Hogan. The coordination of arm movements: an experimentally confirmed mathematical model. *Journal of neuroscience*, 5 (7):1688–1703, 1985.

[41] David W Franklin, Etienne Burdet, Keng Peng Tee, Rieko Osu, Chee-Meng Chew, Theodore E Milner, and Mitsuo Kawato. Cns learns stable, accurate, and efficient movements using a simple algorithm. *Journal of neuroscience*, 28(44):11165–11173, 2008.

[42] Gowrishankar Ganesh and Etienne Burdet. Motor planning explains human behaviour in tasks with multiple solutions. *Robotics and Autonomous Systems*, 61(4):362–368, 2013.

[43] Gowrishankar Ganesh and Tsuyoshi Ikegami. Beyond watching: Action understanding by humans and implications for motion planning by interacting robots. In *Dance Notations and Robot Motion*, pages 139–167. Springer, 2016.

[44] PE Gill, SJ Hammarling, W Murray, MA Saunders, and MH Wright. Fortran package for constrained linear least-squares and convex quadratic programming. user's guide for lssol (version 1. 0). Technical report, Stanford Univ., CA (USA). Systems Optimization Lab., 1986.

[45] Michael A Goodrich, Alan C Schultz, et al. Human–robot interaction: a survey. *Foundations and Trends® in Human–Computer Interaction*, 1(3): 203–275, 2008.

[46] Rob Gray and Sian L Beilock. Hitting is contagious: Experience and action induction. *Journal of Experimental Psychology: Applied*, 17(1):49, 2011.

[47] ET Hall. Proxemic theory. *Theory of Communication*, pages 60–67, 1966.

[48] Cheol E Han, Sujin Kim, Shuya Chen, Yi-Hsuan Lai, Jeong-Yoon Lee, Rieko Osu, Carolee J Winstein, and Nicolas Schweighofer. Quantifying arm nonuse in individuals poststroke. *Neurorehabilitation and neural repair*, 27(5):439–447, 2013.

[49] Clint Hansen, Paula Arambel, Khalil Ben Mansour, Veronique Perdereau, and Frederic Marin. Human–human handover tasks and how distance and object mass matter. *Perceptual and motor skills*, 124(1):182–199, 2017.

[50] Christopher M Harris and Daniel M Wolpert. Signal-dependent noise determines motor planning. *Nature*, 394(6695):780, 1998.

[51] Cecilia Heyes. Automatic imitation. *Psychological bulletin*, 137(3):463, 2011.

[52] Hauke Hillebrandt, Karl J Friston, and Sarah-Jayne Blakemore. Effective connectivity during animacy perception–dynamic causal modelling of human connectome project data. *Scientific reports*, 4:6240, 2014.

[53] Markus Huber, Claus Lenz, Markus Rickert, Alois Knoll, Thomas Brandt, and Stefan Glasauer. Human preferences in industrial human-robot interactions. In *Proceedings of the international workshop on cognition for technical systems*, 2008.

[54] Markus Huber, Markus Rickert, Alois Knoll, Thomas Brandt, and Stefan Glasauer. Human-robot interaction in handing-over tasks. In *RO-MAN 2008-The 17th IEEE International Symposium on Robot and Human Interactive Communication*, pages 107–112. IEEE, 2008.

[55] Tsuyoshi Ikegami and Gowrishankar Ganesh. Watching novice action degrades expert motor performance: causation between action production and outcome prediction of observed actions by humans. *Scientific reports*, 4:6989, 2014.

[56] Tsuyoshi Ikegami, Gowrishankar Ganesh, Tatsuya Takeuchi, and Hiroki Nakamoto. Prediction error induced motor contagions in human behaviors. *Elife*, 7:e33392, 2018.

[57] Yan-Bin Jia. Rotation in the space. *Iowa State University Computer Science*, 477:577, 2017.

[58] Walter L Johnson, James H Porter, Stephanie I Ackley, and Douglas T Ross. Automatic generation of efficient lexical processors using finite state techniques. *Communications of the ACM*, 11(12):805–813, 1968.

[59] Shuuji Kajita, Fumio Kanehiro, Kenji Kaneko, Kazuhito Yokoi, and Hirohisa Hirukawa. The 3d linear inverted pendulum mode: A simple modeling for a biped walking pattern generation. In *Proceedings 2001 IEEE/RSJ International Conference on Intelligent Robots and Systems. Expanding the Societal Role of Robotics in the the Next Millennium (Cat. No. 01CH37180)*, volume 1, pages 239–246. IEEE, 2001.

[60] Shuuji Kajita, Mitsuharu Morisawa, Kanako Miura, Shin'ichiro Nakaoka, Kensuke Harada, Kenji Kaneko, Fumio Kanehiro, and Kazuhito Yokoi. Biped walking stabilization based on linear inverted pendulum tracking. In *2010 IEEE/RSJ International Conference on Intelligent Robots and Systems*, pages 4489–4496. IEEE, 2010.

[61] Kenji Kaneko, Mitsuharu Morisawa, Shuuji Kajita, Shin'ichiro Nakaoka, Takeshi Sakaguchi, Rafael Cisneros, and Fumio Kanehiro. Humanoid robot hrp-2kai improvement of hrp-2 towards disaster response tasks. In *Humanoid Robots (Humanoids), 2015 IEEE-RAS 15th International Conference on*, pages 132–139. IEEE, 2015.

[62] Kenji Kaneko, Mitsuharu Morisawa, Shuuji Kajita, Shin'ichiro Nakaoka, Takeshi Sakaguchi, Rafael Cisneros, and Fumio Kanehiro. Humanoid robot hrp-2kai—improvement of hrp-2 towards disaster response tasks. In *2015 IEEE-RAS 15th International Conference on Humanoid Robots (Humanoids)*, pages 132–139. IEEE, 2015.

[63] Saki Kato, Natsuki Yamanobe, Gentiane Venture, and Gowrishankar Ganesh. Humans can predict where their partner would make a handover. In *Companion of the 2018 ACM/IEEE International Conference on Human-Robot Interaction*, pages 145–146. ACM, 2018.

[64] Saki Kato, Natsuki Yamanobe, Gentiane Venture, Eiichi Yoshida, and Gowrishankar Ganesh. The where of handovers by humans: Effect of partner characteristics, distance and visual feedback. *PloS one*, 14(6):e0217129, 2019.

[65] James Kilner, Antonia F de C Hamilton, and Sarah-Jayne Blakemore. Interference effect of observed human movement on action is due to velocity profile of biological motion. *Social neuroscience*, 2(3-4):158–166, 2007.

[66] James M Kilner, Yves Paulignan, and Sarah-Jayne Blakemore. An interference effect of observed biological movement on action. *Current biology*, 13(6):522–525, 2003.

[67] Jinsul Kim, Jihwan Park, Yong K Hwang, and Manjai Lee. Advanced grasp planning for handover operation between human and robot. In *2nd international conference on autonomous robots and agents*, pages 13–15, 2004.

[68] Andras Kupcsik, David Hsu, and Wee Sun Lee. Learning dynamic robot-to-human object handover from human feedback. *arXiv preprint arXiv:1603.06390*, 2016.

[69] Aleksandra Kupferberg, Stefan Glasauer, Markus Huber, Markus Rickert, Alois Knoll, and Thomas Brandt. Video observation of humanoid robot movements elicits motor interference. In *Proceedings of the Symposium on New Frontiers in Human-Robot Interaction, Adaptive and Emergent Behaviour and Complex Systems Convention (AISB)*, 2009.

[70] Aleksandra Kupferberg, Markus Huber, Bartosz Helfer, Claus Lenz, Alois Knoll, and Stefan Glasauer. Moving just like you: motor interference depends on similar motility of agent and observer. *PloS one*, 7(6):e39637, 2012.

[71] Zhi Li and Kris Hauser. Predicting object transfer position and timing in human-robot handover tasks. *Science and Systems*, 2015.

[72] Efrain Lopez-Damian, Daniel Sidobre, Stephane DeLaTour, and Rachid Alami. Grasp planning for interactive object manipulation. In *Proc. of the Intl. Symp. on Robotics and Automation*, 2006.

[73] Jim Mainprice, Emrah Akin Sisbot, Thierry Siméon, and Rachid Alami. Planning safe and legible hand-over motions for human-robot interaction. 2010.

[74] Jim Mainprice, Mamoun Gharbi, Thierry Siméon, and Rachid Alami. Sharing effort in planning human-robot handover tasks. In *2012 IEEE RO-MAN: The 21st IEEE International Symposium on Robot and Human Interactive Communication*, pages 764–770. IEEE, 2012.

[75] Andrea H Mason and Christine L MacKenzie. Grip forces when passing an object to a partner. *Experimental brain research*, 163(2):173–187, 2005.

[76] José R Medina, Felix Duvallet, Murali Karnam, and Aude Billard. A human-inspired controller for fluid human-robot handovers. In *2016 IEEE-RAS 16th International Conference on Humanoid Robots (Humanoids)*, pages 324–331. IEEE, 2016.

[77] Vincenzo Micelli, Kyle Strabala, and Siddhartha Srinivasa. Perception and control challenges for effective human-robot handoffs. In *Robotics: Science and systems workshop on rgb-d cameras*, 2011.

[78] Richard M Murray. *A mathematical introduction to robotic manipulation*. CRC press, 2017.

[79] Kazuyuki Nagata, Youhei Oosaki, Masayoshi Kakikura, and Hideo Tsukune. Delivery by hand between human and robot based on fingertip force-torque information. In *Proceedings. 1998 IEEE/RSJ International Conference on Intelligent Robots and Systems. Innovations in Theory, Practice and Applications (Cat. No. 98CH36190)*, volume 2, pages 750–757. IEEE, 1998.

[80] Heramb Nemlekar, Dharini Dutia, and Zhi Li. Object transfer point estimation for fluent human-robot handovers. In *2018 IEEE International Conference on Robotics and Automation (ICRA). IEEE*, 2019.

[81] Heramb Nemlekar, Dharini Dutia, and Zhi Li. Prompt human to robot handovers by estimation of object transfer point based on human partner's motion. 2019.

[82] Lior Noy, Raffaella Ida Rumiati, and Tamar Flash. Simple movement imitation: Are kinematic features sufficient to map perceptions into actions? *Brain and cognition*, 69(2):360–368, 2009.

[83] Morgan S Ohwovoriole. *An Externsion of Screw Theory and Its Application to the Automation of Industrial Assemblies*. PhD thesis, 1980.

[84] Erhan Oztop, David W Franklin, Thierry Chaminade, and Gordon Cheng. Human-humanoid interaction: is a humanoid robot perceived as a human? *International Journal of Humanoid Robotics*, 2(04):537–559, 2005.

[85] Sina Parastegari, Ehsan Noohi, Bahareh Abbasi, and Miloš Žefran. Failure recovery in robot–human object handover. *IEEE Transactions on Robotics*, 34(3):660–673, 2018.

[86] Claudia Pérez-D'Arpino and Julie A Shah. Fast target prediction of human reaching motion for cooperative human-robot manipulation tasks using time series classification. In *2015 IEEE international conference on robotics and automation (ICRA)*, pages 6175–6182. IEEE, 2015.

[87] Clare Press, Geoffrey Bird, Rüdiger Flach, and Cecilia Heyes. Robotic movement elicits automatic imitation. *Cognitive Brain Research*, 25(3):632–640, 2005.

[88] Wolfgang Prinz. Perception and action planning. *European journal of cognitive psychology*, 9(2):129–154, 1997.

[89] Janine Robinson. Edinburgh handedness inventory. *Encyclopedia of autism spectrum disorders*, pages 1051–1054, 2013.

[90] Mohamad Jafar Sadigh and Habib Ahmadi. Safe grasping with multi-link fingers based on force sensing. In *2009 IEEE International Conference on Robotics and Biomimetics (ROBIO)*, pages 1796–1802. IEEE, 2009.

[91] Vincent Samy, Karim Bouyarmane, and Abderrahmane Kheddar. Qp-based adaptive-gains compliance control in humanoid falls. In *2017 IEEE International Conference on Robotics and Automation (ICRA)*, pages 4762–4767. IEEE, 2017.

[92] Stefan Schaal, Dagmar Sternad, Rieko Osu, and Mitsuo Kawato. Rhythmic arm movement is not discrete. *Nature neuroscience*, 7(10):1136, 2004.

[93] Adena Schachner, Timothy F Brady, Irene M Pepperberg, and Marc D Hauser. Spontaneous motor entrainment to music in multiple vocal mimicking species. *Current Biology*, 19(10):831–836, 2009.

[94] Alessandra Sciutti, Ambra Bisio, Francesco Nori, Giorgio Metta, Luciano Fadiga, Thierry Pozzo, and Giulio Sandini. Measuring human-robot interaction through motor resonance. *International Journal of Social Robotics*, 4(3):223–234, 2012.

[95] Luis Sentis and Oussama Khatib. A whole-body control framework for humanoids operating in human environments. In *Proceedings 2006 IEEE International Conference on Robotics and Automation, 2006. ICRA 2006.*, pages 2641–2648. IEEE, 2006.

[96] Sara Sheikholeslami, Justin W Hart, Wesley P Chan, Camilo P Quintero, and Elizabeth A Croft. Prediction and production of human reaching trajectories for human-robot interaction. In *Companion of the 2018 ACM/IEEE International Conference on Human-Robot Interaction*, pages 321–322. ACM, 2018.

[97] Satoru Shibata, Kanya Tanaka, and Akira Shimizu. Experimental analysis of handing over. In *Proceedings 4th IEEE international workshop on robot and human communication*, pages 53–58. IEEE, 1995.

[98] Dan Song, Nikolaos Kyriazis, Iason Oikonomidis, Chavdar Papazov, Antonis Argyros, Darius Burschka, and Danica Kragic. Predicting human intention in visual observations of hand/object interactions. In *2013 IEEE International Conference on Robotics and Automation*, pages 1608–1615. IEEE, 2013.

[99] Mark W Spong and Mathukumalli Vidyasagar. *Robot dynamics and control*. John Wiley & Sons, 2008.

[100] Olivier Stasse and Thomas Flayols. An overview of humanoid robots technologies. In *Biomechanics of Anthropomorphic Systems*, pages 281–310. Springer, 2019.

[101] Kyle Strabala, Min Kyung Lee, Anca Dragan, Jodi Forlizzi, Siddhartha S Srinivasa, Maya Cakmak, and Vincenzo Micelli. Toward seamless human-robot handovers. *Journal of Human-Robot Interaction*, 2(1):112–132, 2013.

[102] Atsushi Takagi, Gowrishankar Ganesh, Toshinori Yoshioka, Mitsuo Kawato, and Etienne Burdet. Physically interacting individuals estimate the partner's goal to enhance their movements. *Nature Human Behaviour*, 1(3):0054, 2017.

[103] Adam Tierney and Nina Kraus. Auditory-motor entrainment and phonological skills: precise auditory timing hypothesis (path). *Frontiers in Human Neuroscience*, 8:949, 2014.

[104] Spyros G Tzafestas. Human-robot social interaction. In *Sociorobot World*, pages 53–69. Springer, 2016.

[105] Nikolaus Vahrenkamp, Dmitry Berenson, Tamim Asfour, James Kuffner, and Rüdiger Dillmann. Humanoid motion planning for dual-arm manipulation and re-grasping tasks. In *2009 IEEE/RSJ International Conference on Intelligent Robots and Systems*, pages 2464–2470. IEEE, 2009.

[106] Joris Vaillant, Abderrahmane Kheddar, Hervé Audren, François Keith, Stanislas Brossette, Adrien Escande, Karim Bouyarmane, Kenji Kaneko, Mitsuharu Morisawa, Pierre Gergondet, et al. Multi-contact vertical ladder climbing with an hrp-2 humanoid. *Autonomous Robots*, 40(3):561–580, 2016.

[107] Fabio Vannucci, Alessandra Sciutti, Marco Jacono, Giulio Sandini, and Francesco Rea. Adaptation to a humanoid robot in a collaborative joint task. In *International Conference on Robot and Human Interactive Communication (RO-MAN)*. IEEE, 2017.

[108] JP Verma and P Verma. *Determination of Sample Size and Power Analysis with G*Power Software: Step-wise Illustrated Manual for Research Scholars.* Independently published on Amazon, 2017.

[109] Giulia Vezzani, Massimo Regoli, Ugo Pattacini, and Lorenzo Natale. A novel pipeline for bi-manual handover task. *Advanced Robotics*, 31(23-24): 1267–1280, 2017.

[110] David Vogt, Simon Stepputtis, Steve Grehl, Bernhard Jung, and Heni Ben Amor. A system for learning continuous human-robot interactions from human-human demonstrations. In *2017 IEEE International Conference on Robotics and Automation (ICRA)*, pages 2882–2889. IEEE, 2017.

[111] David Vogt, Simon Stepputtis, Bernhard Jung, and Heni Ben Amor. One-shot learning of human–robot handovers with triadic interaction meshes. *Autonomous Robots*, 42(5):1053–1065, 2018.

[112] Jules Waldhart, Mamoun Gharbi, and Rachid Alami. Planning handovers involving humans and robots in constrained environment. In *2015 IEEE/RSJ International Conference on Intelligent Robots and Systems (IROS)*, pages 6473–6478. IEEE, 2015.